General Disclaimer

One or more of the Following Statements may affect this Document

- This document has been reproduced from the best copy furnished by the organizational source. It is being released in the interest of making available as much information as possible.

- This document may contain data, which exceeds the sheet parameters. It was furnished in this condition by the organizational source and is the best copy available.

- This document may contain tone-on-tone or color graphs, charts and/or pictures, which have been reproduced in black and white.

- This document is paginated as submitted by the original source.

- Portions of this document are not fully legible due to the historical nature of some of the material. However, it is the best reproduction available from the original submission.

Produced by the NASA Center for Aerospace Information (CASI)

NASA CR-
160125

(NASA-CR-160125) RANGING AND TRACKING SYSTEM FOR PROXIMITY OPERATIONS, PHASE 1 Final Report (Axiomatix, Los Angeles, Calif.) 172 p HC A08/MF A01 CSCL 17I

N79-19188

Unclas
G3/32 16393

Axiomatix

APR 1979
RECEIVED
NASA STI FACILITY
ACCESS DEPT.

RANGING AND TRACKING SYSTEM FOR PROXIMITY OPERATIONS

FINAL REPORT
FOR PHASE I

Contract No. NAS 9-15666

Prepared for

NASA Lyndon B. Johnson Space Center
Houston, Texas 77058

Prepared by

Sergei Udalov
Peter Nilsen

Contributions by

T. Nessibou
C. L. Weber
J. L. Aker (Kustom Electronics)

Axiomatix Report No. R7901-5
January 30, 1979

TABLE OF CONTENTS

	Page
LIST OF TABLES	iv
LIST OF FIGURES	v
1.0 INTRODUCTION AND OVERVIEW	1
1.1 Phase I Objectives	1
1.2 Phase I Feasibility Study Methods	1
1.3 System Parameters Summary	2
1.4 Functional Description of the Proposed Radar Sensor System	5
1.4.1 Block Diagram Description	5
1.4.2 System Controller Flow Chart Description	8
1.5 The Report Overview	11
2.0 SYSTEM DESCRIPTION AND PARAMETER DEFINITION	14
2.1 System Block Diagram and Modulation Formats	14
2.1.1 Functional Block Diagram and Modulation Formats	14
2.1.2 Modulation Formats	16
2.1.3 Parameter Scales Definition	23
2.2 System Range Equation	25
2.2.1 The Range Equation	25
2.2.2 System Noise Considerations	30
2.3 Measurements Geometry and System Parameters	40
2.3.1 Geometrical Considerations for Target Acquisition	40
2.3.2 Target Velocity and FM Slope Requirement	42
2.4 Target Range and Velocity Acquisition	44
2.4.1 Overview of the Target Acquisition Strategy	44
2.4.2 Detailed Acquisition Sequence Description	50
2.5 Target Tracking	63
2.5.1 Tracker Design Philosophy	63
2.5.2 Tracker Performance Estimate	66
2.6 System Error Budget Estimate	70
2.6.1 Ranging Errors	70
2.6.2 Velocity Errors	75
2.6.3 Range and Velocity Error Summary	79

Page

2.7 Implementation Details 82

2.7.1 Frequency Modulation Synthesis 82
2.7.2 FM Sweep Waveform Generator 92
2.7.3 Baseband Amplifier/Filter and AGC Unit 92
2.7.4 Frequency/Phase Tracker 95

2.8 Special Problems 97

2.8.1 Near-Zero Velocity Measurement 97
2.8.2 Near-Zero Range Measurement 98

3.0 CONCLUSIONS AND RECOMMENDATIONS 99

REFERENCES 100

Appendixes

A. The Effect of Phase Noise on CW Radar Performance

B. Beat Note Analysis in an FM-CW Radar

C. Transient Analysis of Phase Locked Gunn Oscillator Frequency Source

D. The Frequency Sweep Linearity Requirements for a Linearly-Modulated FM-CW Range Measuring Radar

E. Phase Noise of a Phase-Locked Gunn Oscillator Frequency Source

F. Experimental Verification of Low-Velocity Measurement With CW K-Band Radar

G. Performance Goal Specification for Phase II Breadboard

H. Bibliography

LIST OF TABLES

		Page
1.	Ranging/Tracking System Parameters Summary	3
2.	Comparison of Specified and Predicted System Performance With an Ideal 10 m^2 Target	4
3.	Power Budget for a K-Band FM-CW Radar	28
4.	Power Budget for an X-Band FM-CW Radar	28
5.	Power Budget for a V-Band FM-CW Radar	28
6.	Summary of Target Acquisition Performance for K-Band Radar Sensor System	51
7.	Range Measurement Errors	80
8.	Velocity Measurement Errors	81

LIST OF FIGURES

		Page
1.	Radar Sensor Functional Block Diagram	6
2.	Radar Sensor System Controller Flow Chart	9
3.	Functional Block Diagram of Radar Ranging and Tracking System	15
4.	Frequency-Time Pattern in FM-CW Radar for a Linear Triangular Modulation and a Stationary Target	17
5.	Frequency-Time Pattern in FM-CW Radar When the Received Signal Return Frequency Includes Doppler Shift (Target Approaching)	20
6.	Frequency-Time Pattern in FM-CW Radar for a Sawtooth Modulation	22
7.	Doppler Shift Frequency versus Target Velocity for a 24 GHz Radar	26
8.	Simplified Block Diagram of Crystal Mixer Front-End Receiver	32
9.	The Crystal Mixer Receiver Noise Figure Performance; Circa 1959 Technology	34
10.	Latest (Circa 1978) Mixer Technology Provides Considerable Improvement in Flicker Noise Performance at Audio and Subaudio Frequencies	35
11.	Plots of $P_r/N_0(f)$ for the K-Band Homodyne Radar	37
12.	Transmitter FM Noise Spectrum Superimposed on the Baseband Tone Frequency Estimate f_b	39
13.	Radar and Target Geometry During Moving Target Acquisition	41
14.	Plot of T_C and T_C versus Target Range for Maximum Values of V_{RA} and V_{TR}	43
15.	Minimum Slope Required to Prevent Range/Velocity Tone Ambiguity	45
16	Target Range and Velocity Acquisition Sequence Algorithm	47
17.	Target Range and Velocity Acquisition Functional Block Diagram (Receiver Portion Only)	48

18. Short-Range/Velocity Acquisition Algorithm 52

19. Range/Frequency Plot for Short-Range Target Acquisition 53

20. Short- and Long-Range/Velocity Acquisition Algorithm 55

21. Range Frequency Plot for the Medium-Range Target Acquisition 56

22. Upper and Lower Trackers Provide for Search and Acquisition of the Moving Target Spectral Lines 58

23. Range/Frequency Plot for the Long-Range Target Acquisition 62

24. Generic Block Diagram of a Frequency Search and Track Unit 65

25. RMS Frequency Tracking Error σ_f versus P_r/N_0 and Tracker Bandwidth ($T_{av} = 0.5$ seconds) 68

26. Timing and Carrier Frequency Deviation are the Potential Causes of the Modulation Format (Slope) Error 74

27. Originally Proposed Implementation of FM-Ramp CW Modulation 83

28. Model of Frequency Stepper 84

29. Desired Approximation of Linear Frequency Sweep with Phase-Locked Loop 85

30. Time History of Divider Index for "Sawtooth" Sweep 86

31. Alternate Sweep Generation Technique 88

32. Frequency Tracker Characteristics for Sweeping Gunn Oscillator 90

33. Sweep Modulation with Precision Measurement of Actual Slope 91

34. Sweep Generator Detail 93

35. Baseband Amplifier/Filter and AGC 94

36. Phase-Locked Loop (PLL) Implementation of the Frequency Tracker 96

1.0 INTRODUCTION AND OVERVIEW

This is the final report for Phase I of a study task directed towards developing a conceptual design of a small, lightweight range and range rate radar sensor system to meet NASA's requirements for accurate short-range and velocity measurements in an orbital environment [1]. Within the context of the requirements, the "short" range implies system operation at 0 m to 1850 m (6000 ft) and "accurate" implies a range measurement to within 1σ accuracy of 0.20 m (0.67 ft) and a range rate (velocity) measurement to within 1σ accuracy of 0.01 m/sec (0.033 ft/sec).

1.1 Phase I Objectives

Phase I of this program is the first phase of a two-phase contractual effort. The objectives of Phase I were fourfold:

(1) To evaluate various sensor concepts

(2) To make feasibility investigations

(3) To perform trade-off assessments, and

(4) Based on the findings of (1), (2) and (3), to provide a technical recommendation for a baseline system.

As indicated by the contents of this report, all of these objectives have been met and, consequently, the Phase II task dealing with the actual fabrication of a breadboard model can continue along the proposed schedule. The major portion of the Phase I effort was performed by Axiomatix with support from Kustom Electronics. Phase II of this program will be carried out primarily by Kustom Electronics, with partial support from Axiomatix

1.2 Phase I Feasibility Study Methods

To accomplish the objectives of Phase I, the Axiomatix technical staff used a combination of several methods available to them. These included:

(1) Literature search and vendor contact

(2) Mathematical analysis, and

(3) Design trade-off evaluation.

The primary purpose of the literature search was to determine if any of the state of the art techniques are applicable to the design of

the sensor system. A secondary purpose was to eliminate from consideration the techniques which were incompatible with either the specifications or a cost-effective approach towards achieving these specifications. Vendor contact provided the necessary inputs for assessing the state of the art of the microwave sensor technology.

Mathematical analysis was one of the most powerful tools in determining quantitatively the impact of various system parameters upon the system performance goals. The scope of the analysis ranged from such system performance-oriented problems as the effect of phase noise on the CW radar performance to such specific implementation-oriented tasks as an analysis of a phase-locked loop response to a frequency step input.

Of the greatest importance for accomplishing Phase I objectives was the the system design trade-off evaluation. This evaluation was based on the results of the literature survey, examination of the analysis data, and expertise of AXiomatix and Kustom Electronics personnel in the area of radar sensor development and design. The synergetic interaction between the scientists and engineers of the two companies resulted in a baseline design compatible with state of the art technology.

1.3 System Parameters Summary

The baseline system which resulted from the efforts of Phase I is a K-band FM-CW radar system utilizing an all solid-state design. A summary of the salient system parameters is presented in Table 1. Table 2 provides a comparison between the measurement accuracies specified by NASA and those estimated for the breadboard performance. It is important to point out that all system performance parameters and, specifically, the measurement accuracies (NASA and predicted) are based on radar performance with an idealized 10 m^2 (107.7 ft^2) target.

From the data presented in Table 2, it appears that the velocity accuracy requirement can be met at the maximum system range of 1850 m (6000 ft). The detailed breakdown of velocity error contributions to the total velocity error is given in Table 8. Paragraph 2.6.2 provides a detailed description of the sources of velocity error.

Estimates of the range measurement accuracy indicate that, at the maximum range (1850 m), the specified accuracy cannot be met.

Table 1. Ranging/Tracking System Parameters Summary

Performance Characteristics	
Detection Range ($P_D = 0.90$ for 10 m^2 ideal target):	1850 m (6000 ft)
Velocity Capability:	±6.1 m/sec (±20 ft/sec)
Acquisition Time:	<30 sec
Accuracy (3σ)	
Range (Table 7):	0.80 m (2.62 ft) at 1850 m (6000 ft) 0.61 m (2 ft) at 1240 m (4067 ft)
Velocity (Table 8):	0.02 cm/sec (0.62 ft/sec) at 1850 m (6000 ft) and V = ±6.1 m/sec (20 ft/sec)
Readout Update Range:	
Range	One per second
Range Rate	One per second [$V \geq 0.1$ m/sec (0.33 ft/sec)] One per 10 seconds ($V < 0.1$ m/sec)
System Characteristics	
Operating Frequency:	24 GHz
Polarization:	Circular
Antenna:	
Type	Horn
Beamwidth (conical angle, 3 dB)	12°
Gain	25 dB
Scan	Manual
Transmitter Characteristics	
Average Power:	200 mW
Frequency Stability	$\pm 2.5 \times 10^{-3}$
(Long-term and temperature):	($\Delta f = \pm 50$ MHz at 24 GHz)
Receiver Characteristics	
Receiver Type:	Homodyne (Zero IF)
Receiver Noise Figure: (For details, see Figure 10)	22 dB at 1 kHz
Frequency Modulation Program	
Modulation Format:	Linear FM-CW
Deviation (ΔF):	100 MHz p-p
Repetition Frequency:	
$R < 500$ m	12 Hz
$500 \text{ m} < R < 1850$ m	3 Hz
Modulation Slope:	
$R < 500$ m	2400 MHz/sec
$500 \text{ m} < R < 1850$ m	600 MHz/sec

Table 2. Comparison of Specified and Predicted System Performance With an Ideal 10 m^2 Target

Parameter	Specified (3σ)	Predicted for Breadboard (3σ)	Comments
Range Accuracy	0.61 m (2 ft)	0.80 m (2.62 ft)	At R = 1850 m (6000 ft), i.e., maximum range
		0.61 m (2 ft)	At R = 1240 m (4067 ft)
Velocity Accuracy	0.03 m/sec (0.1 ft/sec)	0.02 m (0.62 ft/sec)	At R = 1850 m (6000 ft) and ±V = 6.1 m/sec (20 ft/sec), i.e., maximum velocity

NOTE: Both range and velocity predicted accuracies are based on 0.5 sec averaging time interval and an update rate of one per second.

The major contribution to the excessive error is the random fluctuation caused by mixer flicker noise; in other words, this is a signal-to-noise ratio limitation. As shown in Table 2, the required range accuracy can be met at a closer range of 1240 m (4067 ft). Considering that the range measurement error generally is proportional to range, such range error behavior is not uncommon. A detailed discussion of the range error contributions is given in Paragraph 2.6.1.

1.4 Functional Description of the Proposed Radar Sensor System

1.4.1 Block Diagram Description

Figure 1 shows a functional block diagram of the proposed radar sensor system. Basically, the system is an FM-CW solid-state K-band (24 GHz) radar which extracts both the range and velocity information from the baseband signals (i.e., tones) appearing at the output of a homodyne (i.e., 0 IF) receiver. Generation of all the timing signals, as well as processing of the raw received data, is performed by a microprocessor which forms the System Controller and Data Processing (SCDP) unit.

The transmitter portion of the radar sensor system is comprised of a modulation waveform generator, two Gunn K-band oscillators, a microwave mixer and a counter. The modulation waveform generator provides the waveform required for varying the frequency of the radar transmitter. The waveform is a triangular function whose frequency is selected according to the mode of the radar operation. This waveform is applied to the frequency control terminal of a K-band voltage-controlled oscillator (VCO), thus resulting in a frequency modulation of the oscillator's output.

The frequency-modulated K-band carrier is then applied via a turnstile diplexer to the radar antenna. The nominal (unmodulated) RF frequency of the K-band transmitter is 24 GHz and the baseline output power is 200 mW.

To provide for accurate control of the transmitter frequency deviation ΔF (nominal $\Delta F = 100$ MHz), the RF output of the transmitter VCO is sampled and mixed with an RF signal developed by a stable, high-Q Gunn-type lock local oscillator (LO). The frequency of the LO is such

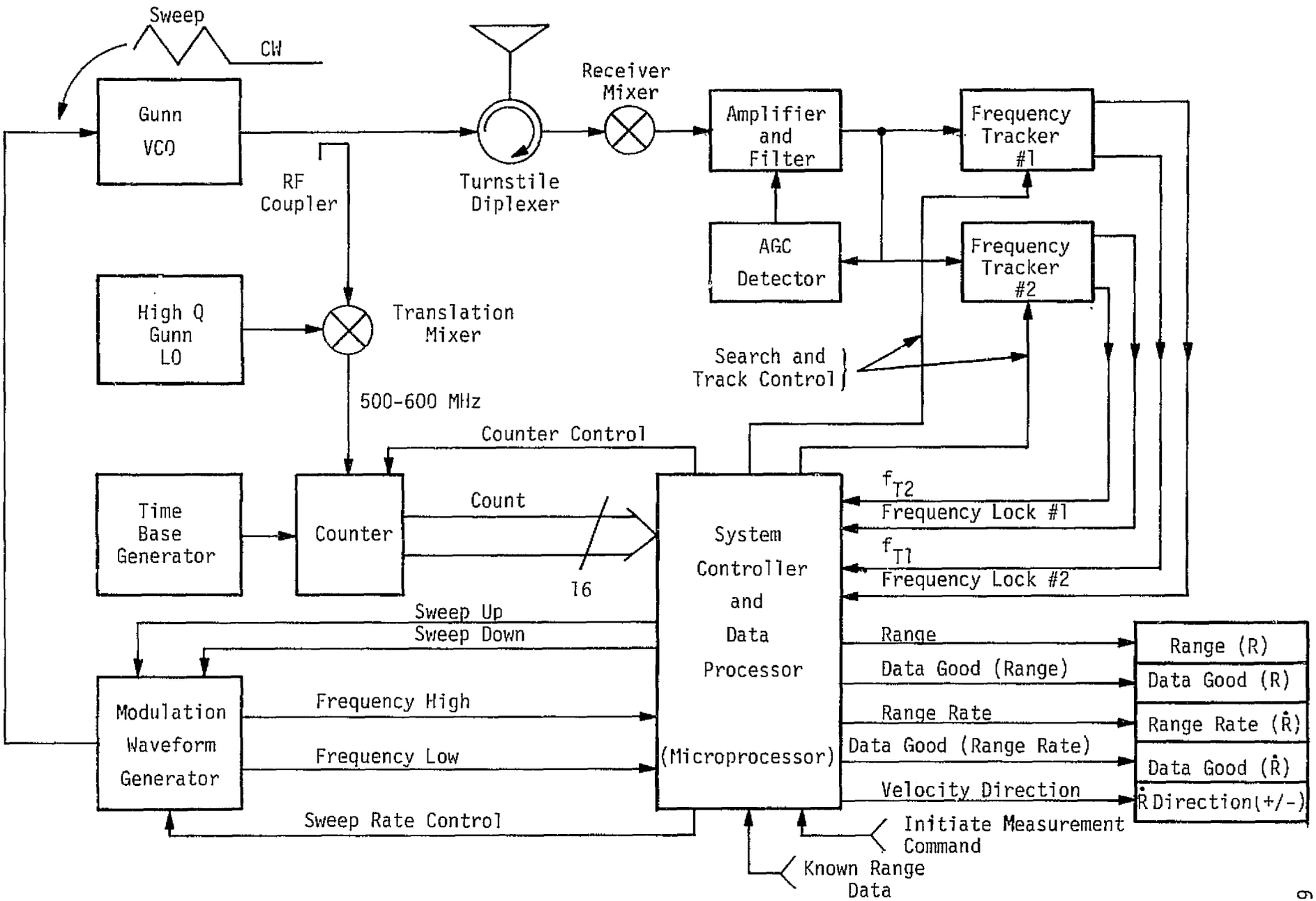

Figure 1. Radar Sensor Functional Block Diagram

that the lower difference frequency between it and the frequency-modulated VCO varies between 500 and 600 MHz, approximately. The difference frequency is applied to a 16-bit counter which determines the lower and upper extremes of the frequency excursion of the transmitted signal. The frequency counts corresponding to the lower and upper extremes are performed upon the "Frequency High" and "Frequency Low" commands developed by the modulation waveform generator. These commands are delivered to the system controller which, in turn, commands the modulator to either continue the frequency sweep in the opposite direction or hold the transmitter in either high- or low-frequency extremes. By such control of the transmitter modulation waveform, either an FM-CW or a simple CW signal can be provided by the transmitter. As explained in Paragraph 2.5.2, the CW signal can be used to provide accurate velocity readings at moderately short ranges.

The exact time duration measurement of both the frequency up and frequency down swings is provided by counting the number of pulses developed by a time-base generator during the frequency sweep interval. This number is measured by time-sharing a single 16-bit counter between the RF frequency and the time-reference pulse counts. The purpose of the precise time interval measurement is to obtain an accurate value of Δt_m which, combined with an accurately measured value of ΔF, can provide the data processor with all the information required to calculate the frequency sweep slope S in MHz/sec, the latter being defined as $\Delta F/\Delta t_m$. Because the slope plays an important role in determining the accuracy of the proposed system, such "dynamic" determination of the slope eliminates the major bias inaccuracies associated with component value changes in the FM-CW transmitter circuitry. This is explained in more detail in Paragraph 2.6.1.3.

The receiver of the proposed radar sensor system is a homodyne receiver, also known as a "0 IF" receiver. As shown in the block diagram, the receiver consists of a mixer followed by an amplifier. The amplifier also includes the required filtering and an Automatic Gain Control (AGC) function. A particular set of modulation formats and the range of doppler frequencies encountered with a 24 GHz radar system places the range of the filtering requirement of the receiver amplifier at near-zero Hz to about 9000 Hz.

As shown in Figure 1, the receiver mixer has only one RF input. This is because the second signal, i.e., the local oscillator, is an attenuated fraction of the transmitted signal itself. The controlled degree of the transmitted signal attenuation is provided by the turnstile diplexer unit. This unit delivers the VCO output to the antenna and couples only a small fraction of the transmitted signal to the receiver mixer. There this local reference is mixed with the signal received from the target, thus resulting in the baseband tones which are applied to the receiver amplifier and filter.

The initial acquisition of the baseband tones (or a single tone, as the case may be) is performed by the two frequency tracking units. These tracker units are under the control of the microprocessor and, upon completion of target acquisition, output to the processor the frequencies of the target tones being tracked. As described in Section 2.1, the output of the receiver may be either a single tone for the case of a stationary target or two tones for the case of a moving target. With CW modulation, a single tone indicates a moving target.

The frequency information obtained by the frequency trackers is analyzed by the microprocessor for the signal quality and, if the latter exceeds a preset criterion, the frequency information is converted into the range (R) and range rate ($\dot{R}$) signals. These processed and scaled signals are then applied to the display, which permits viewing of the R and $\dot{R}$ information along with the direction indication for $\dot{R}$. The "Data Good" indicators are also included as a part of the display.

Note that, except for the "Initiate Measurement" command and the "Known Range" data, the sensor system does not require any external commands. This is because all the system timing and data processing is performed by a microprocessor-based System Controller and Data Processing unit. The algorithm controlling the operation of this unit is described below.

1.4.2 System Controller Flow Chart Description

Figure 2 shows the simplified flow chart for the system controller algorithm. As shown in the figure, the first step of the algorithm deals with the system power turn-on procedure and initialization. This is carried out before any other information, such as the "Initiate

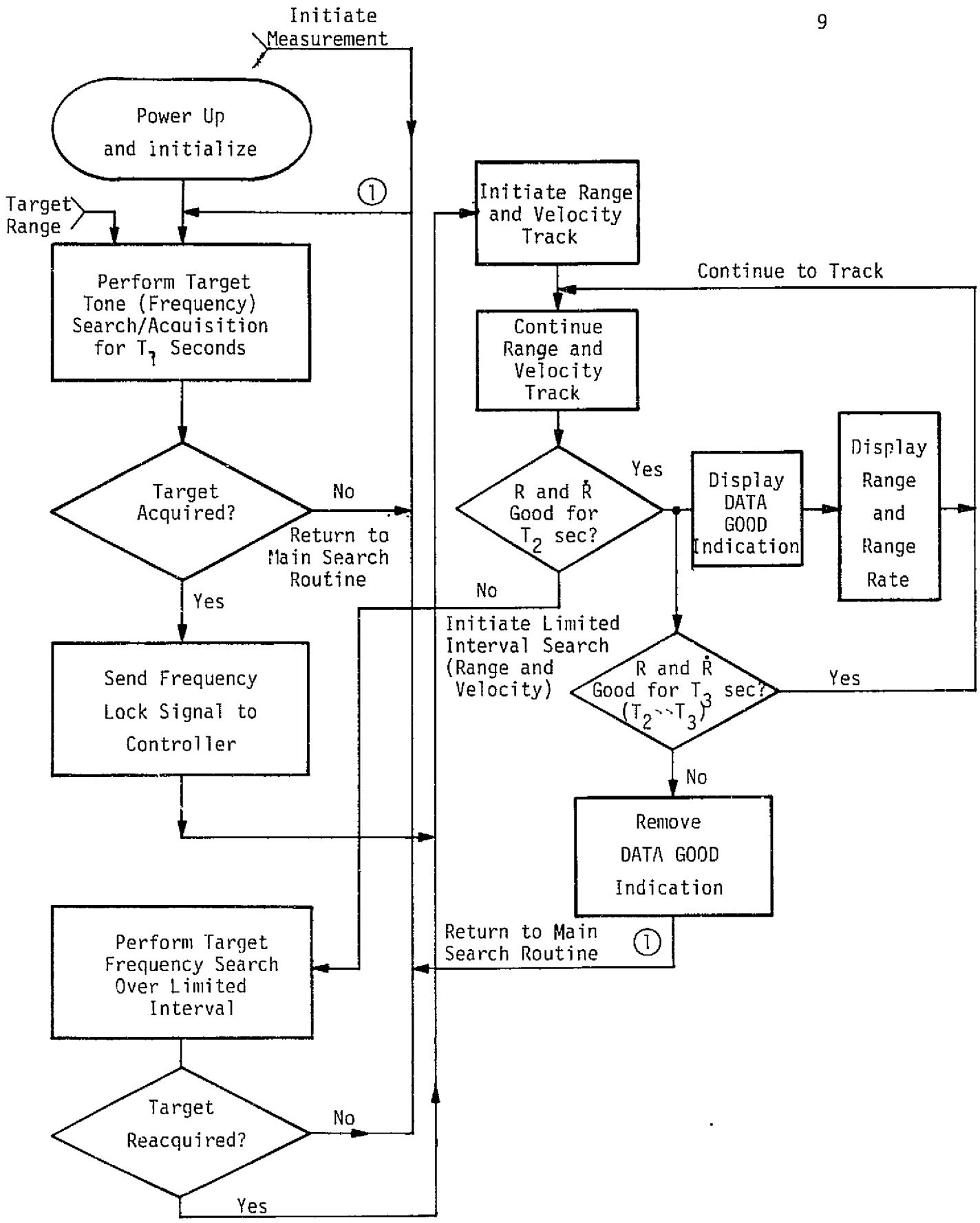

Figure 2. Radar Sensor System Controller Flow Chart

Measurement" (IM) command and the "Target Range" (TR) data (if known a priori), can be entered into the controller.

Following initialization, the system controller is ready to accept the external commands and/or data. Specifically, upon receipt of the IM command, the system performs an automatic range search for the target signal. As described in Section 2.4, in the absence of a priori target range information, the radar system automatically searches for targets over a range interval from 0 m to 1850 m (6000 ft), the latter being the maximum specified range of the system. This search is performed sequentially over the following three range intervals:

(1) 0 - 50 m (164 ft)

(2) 50 m - 500 m (1640 ft)

(3) 500 m - 1850 m (6000 ft).

For each of these intervals, an optimum modulation format is selected by the controller and an optimum search strategy is used. The total search time (T_1) is less than 30 seconds.

If the target is not detected on the first pass of the multistep search, the entire search routine is repeated as long as the IM command is present.* When the target is detected, the frequency trackers deliver a Frequency Lock signal to the controller. The controller, in turn, sets the parameters of the trackers to the TRACK mode, thus initiating the range rate (velocity) tracking. Meanwhile, the data processor analyzes the tracked data for consistency (i.e., "quality") over a period of T_2 seconds.

If the data is consistent over each consecutive one-second data update interval, the data processor makes a "Data Good" decision and presents the computed range and range rate information, along with the corresponding "Data Good" flags, to the display. If the data good criterion is not met after the transition to the tracking mode, a signal search is initiated over a limited frequency region surrounding the frequency at which the initial target detection took place.

Reacquisition of the target within a preset interval of time

---

*One can visualize the IM command as a signal generated by an operator pushing on or holding down a trigger-like switch, while the operator aims the antenna at the target.

returns the system to the track initiate phase with the subsequent test for data quality and presentation to the display. Conversely, a failure to reacquire the target brings the system to the beginning of the main search routine.

In addition to the short-term data-good test for T_2 seconds (one second), a longer test of the quality of the data is performed. The time constant, T_3, of this test is nominally 5 seconds and is chosen to eliminate display responses to operator movements which may accidentally result in a loss of signal strength due to considerable antenna miss-pointing. In other words, this additional time constant prevents the fluctuation of the display during momentary short-term signal fades. If the "data good" criterion fails for more than 5 seconds and if the IM signal is still present, the system is returned to the starting point (Point 1) of the main search routine and the entire search procedure is repeated.

Again, it must be emphasized that the acquisition of the target is predicated upon the availability of angular (i.e., direction) information to the target. This means that either an operator points the antenna at the target and generates the IM signal or the vehicle on which the sensor is mounted is oriented so that the antenna is directed at the target and the IM signal is generated remotely.

In comparison, the other target information, such as range and range rate, is not required by the system for the purpose of target acquisition. However, if a priori range information is available for target acquisition, the system controller algorithm will make use of such information to shorten the initial acquisition search sequence. The degree of such reduction of the acqusition time will depend, of course, on the actual range to the target.

1.5 The Report Overview

Section 2.0 which follows contains the major portion of the detailed technical material of this report. Section 2.1 presents a discussion of the modulation formats selected for the sensor breadboard. Various parameters associated with the linear FM-CW radar are defined and their relative significance with respect to the system operation is explained.

Section 2.2 presents the system range equation and corresponding power budget estimates for system operation at various RF frequencies ranging from X-band (≈10 GHz) to V-band (≈70 MHz). The advantages of operating the proposed breadboard at a K-band frequency (≈24 GHz) are described. Also included in Section 2.2 is a detailed discussion of the various noise mechanisms affecting FM-CW homodyne radar. There it is explained why the mixer flicker noise is the dominant limiting factor rather than thermal noise. The estimated values of the power received (P_r) over the flicker noise density [$N_0(t)$] are computed and plotted for the purpose of modulation format optimization.

This geometrical aspect of the range and range rate measurement configuration involving the radar sensor and a target are described in Section 2.3. From the postulated geometry, the order of magnitude of the time available to acquire a moving target and to output the range and range rate estimates is determined.

Section 2.4 contains a detailed description of the techniques used for detecting a moving target and for locking on to the appropriate spectral components (i.e., the range and velocity tones) present at the receiver output. The target detection and acquisition algorithm is explained in terms of the three-step range search procedure proposed for the radar sensor breadboard. The estimates of the times required to complete each of the steps are derived and, from these estimates, the total search time of about 30 seconds is calculated.

The target tracking, which follows the target detection and acquisition phase, is described in Section 2.5. Specifically, the target design philosophy is explained and the tracker performance estimates are presented.

Section 2.6 describes the various system errors which affect the accuracy of the range and range rate (velocity) measurements. Proposed methods for minimizing these errors are outlined and explained. A tabular summary of these errors is presented.

The system implementation details are presented in Section 2.7. Specifically, the implementation of such critical subunits as the transmitter and modulator, receiver amplifiers and filters, and frequency/phase tracker are described.

Section 2.8 addresses the special problem areas unique to the

proposed system. The specific areas requiring particular attention are the near-zero velocity and near-zero range measurements. Methods for resolving these problem areas are presented.

Section 3.0 of this report contains the conclusions and recommendations based upon the findings of the study.

In addition to the main body of the report, several appendices are provided. These appendices contain the detailed analysis used for the support of the proposed radar sensor design philosophy. Appendix A contains the analysis of the effects of phase noise on the performance of an FM-CW radar. Appendix B presents a mathematical development for analyzing spectral components of the FM-CW radar signal. The response of a phase-locked loop to a frequency step is analyzed in Appendix C. Appendix D presents the analysis of the linearity requirements for the frequency modulation ramp waveform. The phase noise of a phase-locked Gunn oscillator is given in Appendix E. Appendix F describes an experimental test conducted by Axiomatix to verify the low velocity measurement potential of a CW K-band radar. A recommended specification for the performance of the Phase II breadboard is given in Appendix G. Finally, Appendix H provides the bibliography of the literature sources examined by Axiomatix personnel during the literature survey of the program.

2.0 SYSTEM DESCRIPTION AND PARAMETER DEFINITION

2.1 System Block Diagram and Modulation Formats

2.1.1 Functional Block Diagram Description

The proposed baseline system for ranging and tracking is a radar which utilizes a linear FM-CW signal as the basic modulation format. Figure 3 shows a functional block diagram of the proposed system. As indicated in the block diagram, the frequency of a tunable transmitter is modulated in accordance with a baseband waveform $f_i(t)$, the latter being generated by the transmitter modulator unit. The FM-CW output, T(t), of the transmitter is applied via a circulator to a common transmit/receive antenna. Also, a portion of the transmitted signal, r(t), is attenuated by an RF coupler and is applied to a mixer, where it is utilized as the Local Oscillator (LO) signal.

The signal radiated by the antenna reaches the target, which scatters and reflects it. The small portion of the reflected signal reaches the transmit/receive antenna and is applied, via the circulator, to the mixer. In the mixer, this received signal, y(t), is multiplied by the relatively strong LO signal, f(t). The result of this multiplication, or mixing, is a baseband signal* whose frequency components extend from 0 Hz to some higher frequency defined by the modulation waveform, the target range and the target velocity. Because the LO frequency (with the exception of the doppler shift and the shift due to the target round trip time) is equal to the transmitter frequency, this type of receiver is known as a "homodyne," or a "zero IF" receiver. The latter descriptor implies that no intermediate frequency (i.e., IF) is used for the recovery and amplification of the received signal.

The baseband output, X(t), of the mixer is lowpass filtered to remove the out-of-band noise and is applied to the range and velocity (i.e., range rate) estimators. The estimators extract the range and velocity information from the baseband spectrum and output the processed estimates of these parameters to a display. Both the transmitter signal and the estimators are controlled by the system timing unit which provides the required modulation format for the detection and tracking of targets at the various ranges.

---

*The double RF frequency term is filtered from the output of the mixer.

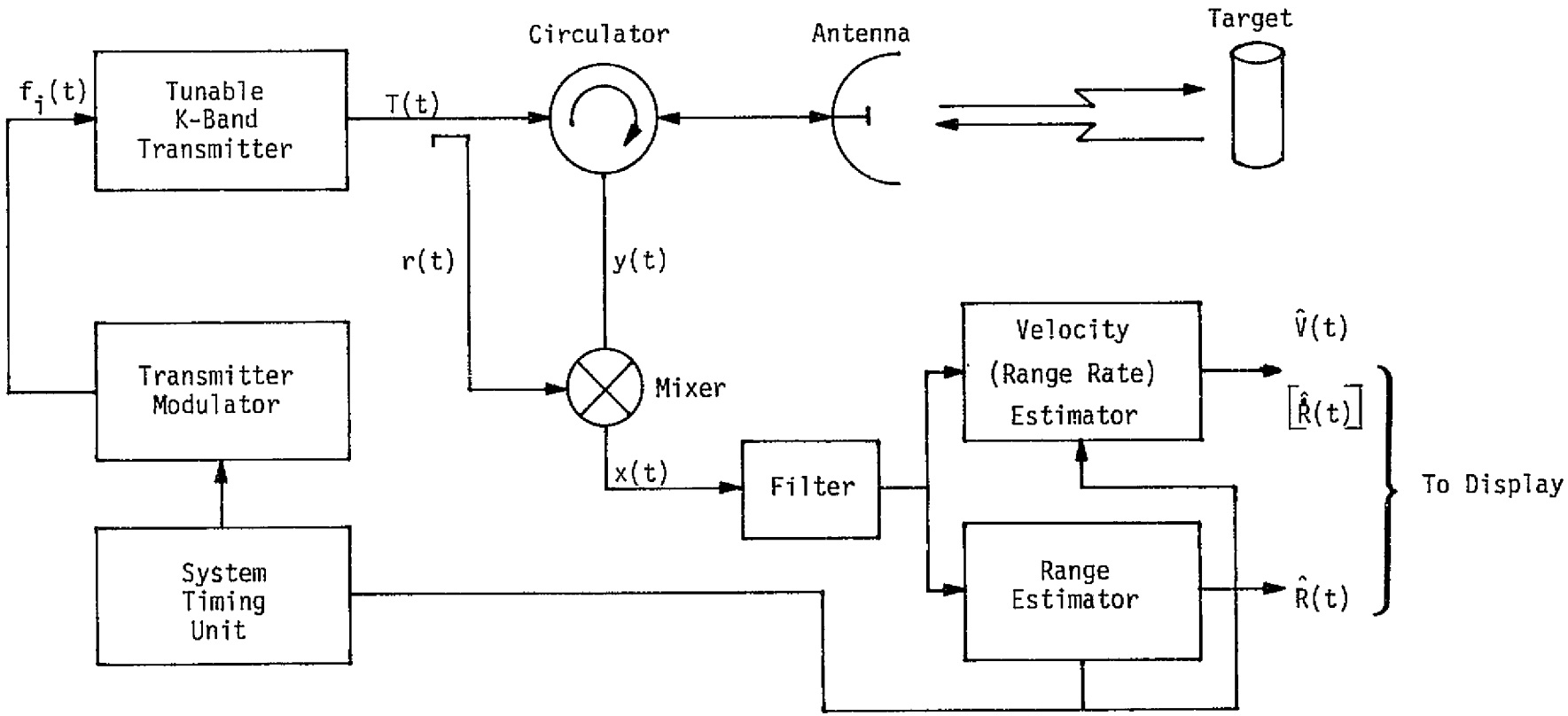

Figure 3. Functional Block Diagram of Radar Ranging and Tracking System

2.1.2 Modulation Formats

Consider, now, the modulation formats to be used with the proposed radar sensor. These formats belong to the general class of linearly varying FM-CW signals. The use of a sinusoidal modulation waveform is not being considered for this system because of a potential difficulty in resolving and tracking multiple targets [2].

2.1.2.1 Linear Triangular Modulation

Figure 4 shows the frequency-time pattern in an FM-CW radar which uses the linear triangular modulation. Part (a) shows the relationship between the transmitter and the received signals. Because of the homodyne configuration of the proposed system, the transmitted and the local oscillator signals are the same (except for the power level) and, therefore, the time-frequency relationship shown in part (a) also applies to the LO signal/received signal pattern.

As a result of the mixer action, a beat note appears at the baseband output of the mixer. For the case of a stationary target, such as the case being illustrated in Figure 4, the frequency of this beat note is proportional to the slope of the transmitter frequency modulation waveform and to the round-trip time to the target. Expressed quantitatively, this relationship is

$$f_r = \frac{\Delta F}{1/2f_m}\left(\frac{2R}{c}\right) = \frac{4Rf_m\Delta F}{c} \tag{1a}$$

$$= ST_d \tag{1b}$$

where

f_r = frequency of the baseband beat note proportional to target range, henceforth referred to as "range frequency" or "range tone"

f_m = modulation waveform repetition frequency

R = target range in meters

$c = 3 \times 10^8$ meters/sec.

T_d = target round-trip delay time

ΔF = peak-to-peak frequency deviation, Hz

S = linear FM modulation slope, Hz/sec.

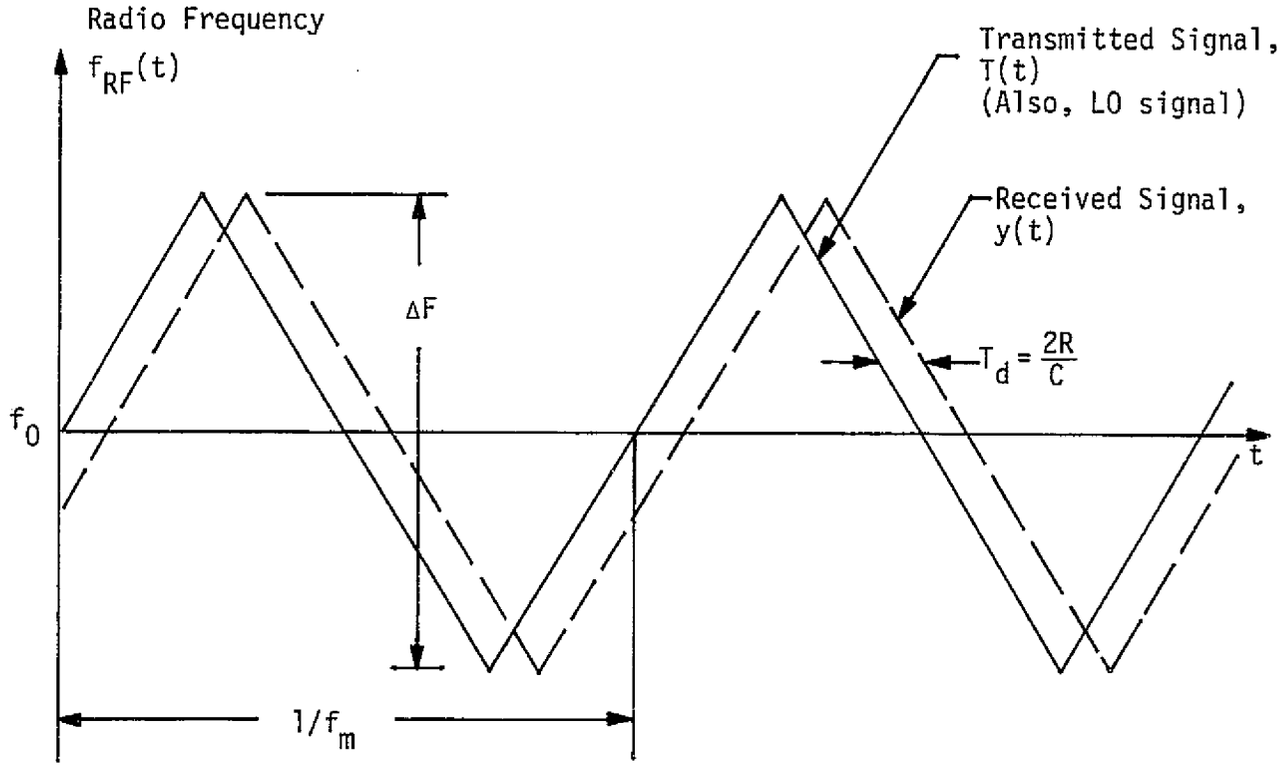

(a) Transmitted and Received RF Signals

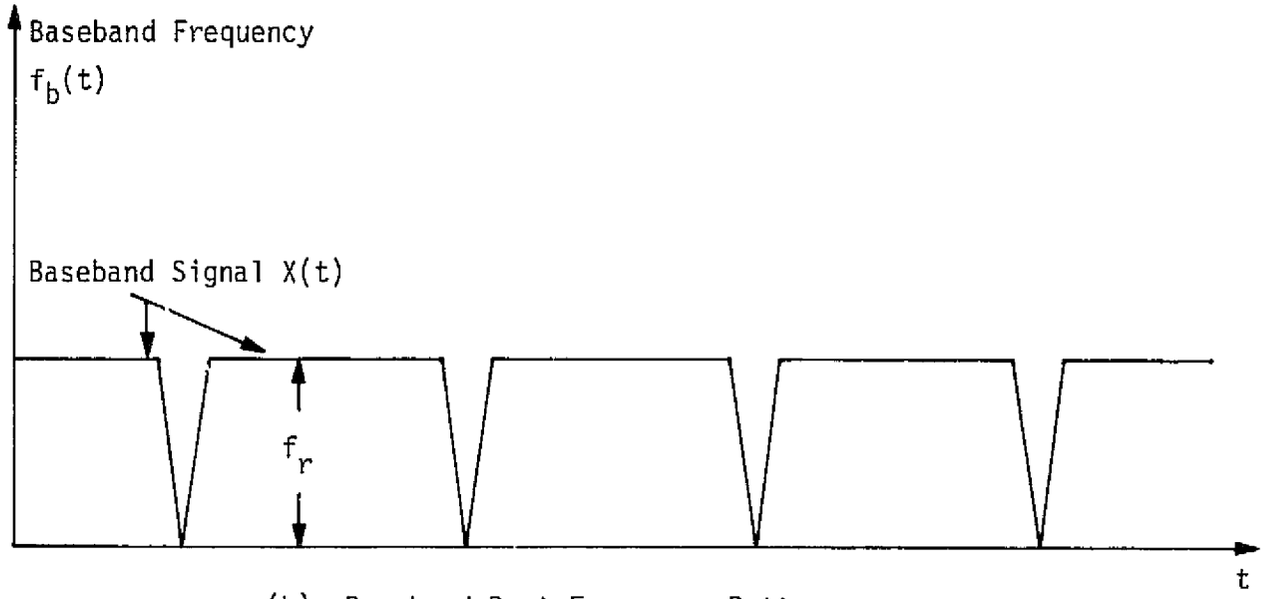

(b) Baseband Beat Frequency Pattern

Figure 4. Frequency-Time Pattern in FM-CW Radar for a Linear Triangular Modulation and a Stationary Target

It must be noted that, because of the periodicity of the linear modulation waveforms shown in part (a) of the figure, the beat note has two discontinuities for each full cycle of modulation. These periodicity-related discontinuities in the time domain result in a discrete line spectrum for the beat note in the frequency domain. Such a discrete line structure of the target return spectrum ([3], also analyzed in Appendix B) gives rise to what is generally referred to as the "quantization error" of a linear modulation FM radar. The effect of this quantization error on the system accuracy is discussed in paragraphs 2.6.1.2 and 2.6.2.2 of this report.

When the target is moving and its motion has a radial component along the direction towards the radar, the reflected signal will be shifted in frequency by the amount quantitatively defined by the following expression:

$$f_d = \frac{2V}{\lambda} + \frac{2Vf_0}{c} \tag{2}$$

where f_d is the apparent shift in target velocity, V is the target velocity in m/sec (along a radial to the radar) and f_0 is the transmitter frequency. The frequency shift f_d is commonly referred to as the "doppler shift" and, depending on the direction of the velocity, this shift can cause either an apparent increase or a decrease in the received signal.

When the target is approaching the radar, the frequency of the received signal is higher than the transmitted frequency. Therefore, the output of the mixer, which is the difference frequency between the transmitted signal and the received signal, contains a component proportional to the doppler shift. Thus, for an approaching target and during the positive-slope portion of the angle, the output of the mixer is

$$\begin{aligned} f_L &= \left| St - \left[S(t-T_d) + \frac{2Vf_0}{c} \right] \right| \\ &= ST_d - \frac{2Vf_0}{c} \qquad \text{for V and S positive} \qquad (3) \\ &= f_r - f_d \, . \end{aligned}$$

The absolute brackets are used to indicate that, with a zero IF receiver,

all the RF shifts appear only as positive frequencies at the baseband.

During the negative-slope portion of the cycle, the beat note frequency for an approaching target is:

$$
\begin{aligned}
f_U &= \left| -St - \left[-S(t-T_d) + \frac{2Vf_0}{c} \right] \right| \\
&= \left| -ST_d - \frac{2Vf_0}{c} \right| \qquad \text{for V positive and S negative} \\
&= ST_d + \frac{2Vf_0}{c} \\
&= f_r + f_d \,. \qquad (4)
\end{aligned}
$$

The situation defined by (3) and (4) is shown in Figure 5. Part (b) of that figure is particularly indicative of this time-frequency relationship at baseband. As shown there, the frequencies f_U and F_L refer to the upper and lower frequencies observed for a particular target situation.

For a receding target, the frequency-time relationship at baseband is the reverse of that for an approaching target. Specifically, the higher beat note will be developed during the positive-slope portion of the cycle and the lower beat note will appear at the output of the mixer during the negative slope. This "role reversal" relationship between f_U, f_L, and the positive and negative slopes of the modulation cycle provides the information required to determine the direction of the target motion.

The range and doppler frequencies are extracted from f_U and f_L in the following manner:

$$f_r = \frac{f_U + f_L}{2} \qquad (5a)$$

and

$$f_d = \frac{f_U - f_L}{2} \qquad (5b)$$

The above equations indicate that some form of processing must be performed on the output of the mixer prior to display of the range and the velocity information. From part (b) of Figure 5, it is also evident that f_r and f_U do not appear simultaneously, a fact which permits a time-multiplexed estimate of these two frequencies to be carried out.

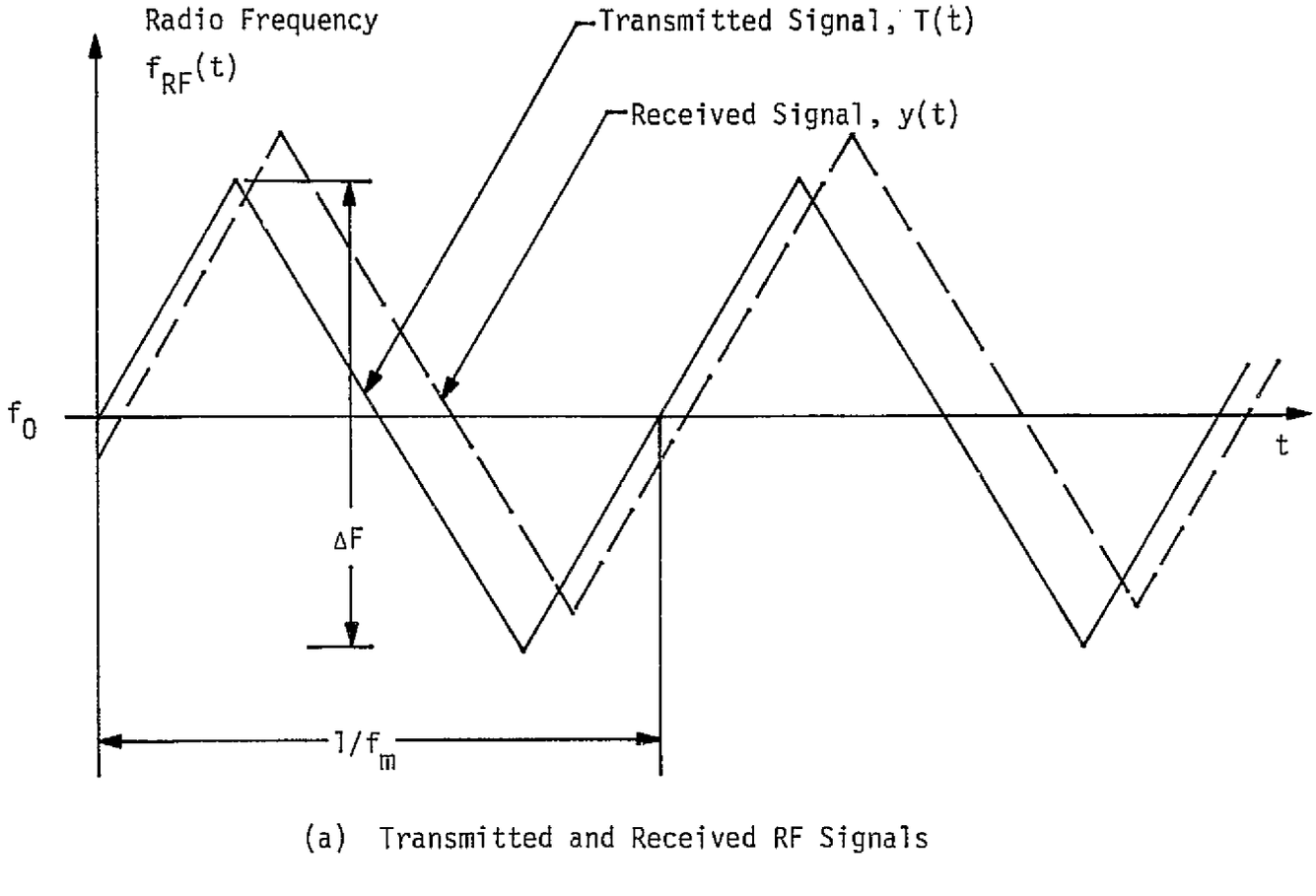

(a) Transmitted and Received RF Signals

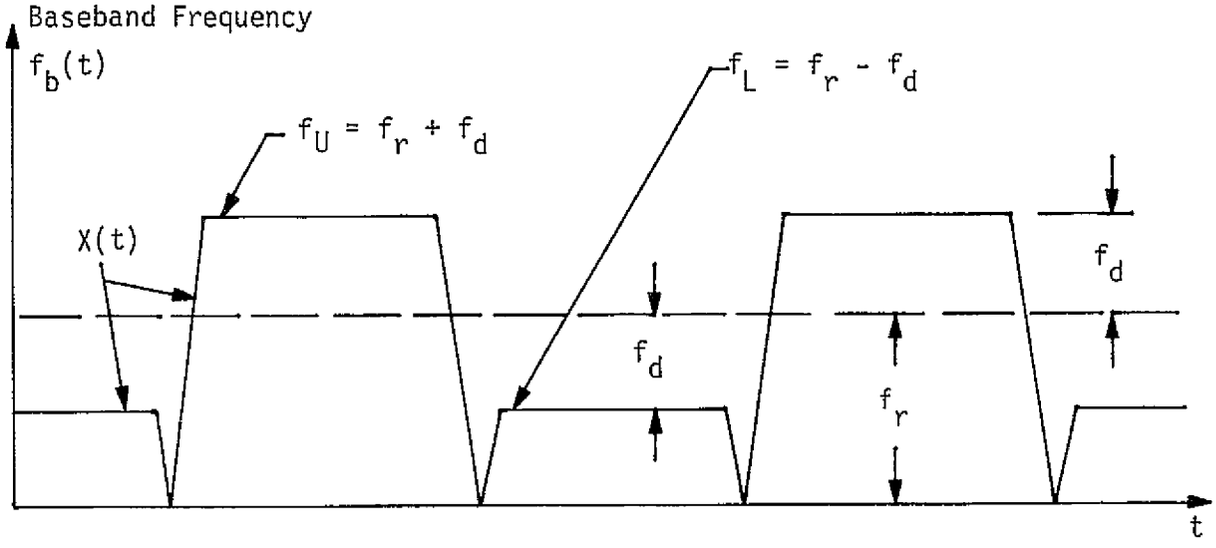

(b) Baseband Beat Frequency Pattern

Figure 5. Frequency-Time Pattern in FM-CW Radar When the Received Signal Return Frequency Includes Doppler Shift (Target Approaching)

The estimate of the required f_r and f_d can then be performed at the end of the allowed averaging period.

For the system considered here, the range and velocity estimates must be presented once every second during the actual ranging and tracking. This implies that about 0.5 second is available for determining f_L and f_U. During the acquisition, however, the measurement intervals may be longer due to the requirement to search out the initial range and the doppler uncertainties. The subject of acquisition is described in detail in Section 2.4.

Another modulation waveform which is commonly used with the linear FM-CW radar is shown in part (a) of Figure 6. This waveform is usually referred to as a "sawtooth" and it is characterized by a relatively fast retrace cycle during which no valid data measurement is performed. With the direction of the frequency deviation being one-sided, the doppler shift cannot be separated from the composite range/velocity tone output by the mixer. Consequently, to obtain the doppler tone, per se, the sawtooth FM waveform is supplemented by periods of pure CW transmissions. During these periods, the radar system reads only the frequency shift due to target velocity. This shift is then either added to or subtracted from the composite tone measured during the sawtooth-modulated periods of radar system operation.

Note that the operation of either an addition or subtraction implies a priori knowledge of the direction of target motion. Because of this requirement, the sawtooth modulation is generally used for target tracking in the cases where the target motion is either known or has been determined by means other than a unidirectional sawtooth modulation.

Among the advantages of the linear sawtooth waveform are the ease of generation and of slope control as well as certain unique spectral characteristics of the target return tone signal. Because of these advantages, the linear sawtooth modulation may be considered for use in the Ranging and Tracking System to perform specialized functions, as described elsewhere in this report.

To make the description of the sawtooth modulation complete, one must explain the significance of the "flyback tone" indicated in part (b) of Figure 6. As shown in the figure, this tone is generated right after the retrace portion of the waveform, and is due to the mixing action of

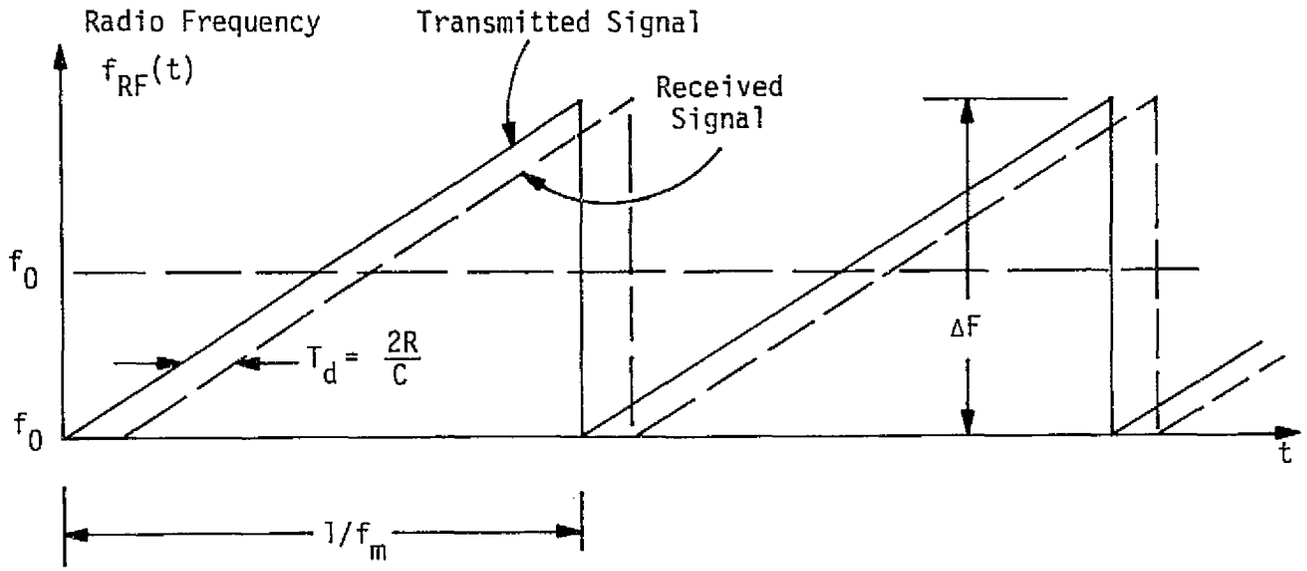

(a) Transmitted and Received RF Signals

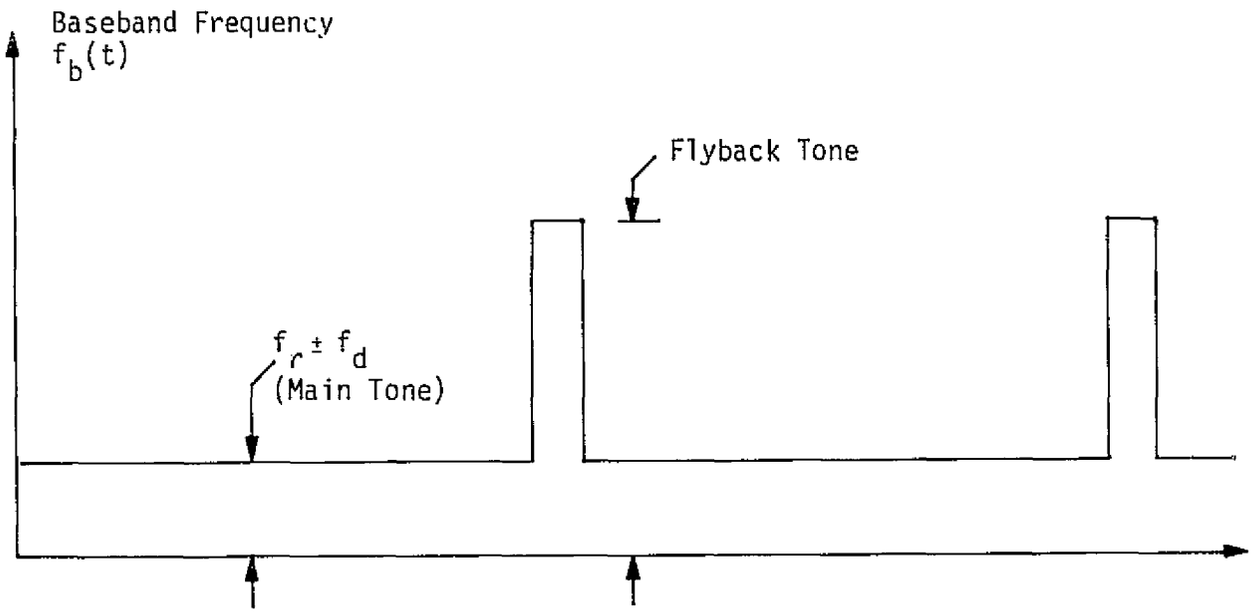

(b) Baseband Beat Frequency Pattern

Figure 6. Frequency-Time Pattern in FM-CW Radar for a Sawtooth Modulation

the "new" transmit cycle waveform and the target return due to the "old" transmit cycle. For the system considered in this report, however, the duration of the flyback tone cycle will be on the order of a few microseconds ($R \leq 2000$ m), while the duration of the modulation cycle T_m (i.e., $1/f_m$) will be on the order of a few milliseconds (i.e., $f_m < 1000$ Hz). Consequently, during the period over which the flyback tone occurs, the range and velocity estimators must be disconnected from the mixer output to prevent spurious readouts.

2.1.3 Parameter Scales Definition

In the preceding paragraph, the operation of a linear FM-CW radar system was described. It was specifically pointed out that, with such a system, both the range and the velocity information are contained in the frequency of the baseband tone(s) which appears at the output of the homodyne mixer. Consequently, to extract the necessary range and velocity information, one must define the scales associated with both the range and velocity tones.

2.1.3.1 Target Range Scale Considerations

For the target range tone, the scale is expressed in Hz/meter and is obtained by multiplying the slope factor S by the round-trip time required to travel to a target located at a 1 meter normalized distance. Thus,

$$\text{Range Scale} = S\,\frac{2R}{c} = S\,\frac{(2)(1)}{3\times 10^{8}}$$

$$= S \times 6.7 \times 10^{-9}\ \text{(Hz/m)} \qquad (6)$$

where S is the FM slope in Hz/sec. Note that one can also define the inverse range scale which is expressed in meters/Hz. In the design of a linear FM ranging system, the scale is generally selected first, then the appropriate slope is determined to provide the required range scale. For example, let us determine the slope required to provide a range scale of 4 Hz/m. Rearranging (6), we obtain

$$S = \frac{\text{Range Scale*}}{6.7 \times 10^{-9}} = \frac{A_R}{6.7 \times 10^{-9}} = \frac{4}{6.7 \times 10^{-9}}$$

$$= 5.97 \times 10^{-8} \text{ Hz/sec}$$

$$= 597 \text{ MHz/sec.} \tag{7}$$

Once the required slope is calculated, the minimum modulation frequency can be determined by considering the practical limitations of the transmitter. Of particular importance is the maximum frequency deviation capability of the transmitting device.

In general, for the purpose of reducing the quantization error, the total frequency deviation ΔF must be made as wide as possible and the duration of the ramp as long as is practical. But, with a finite ΔF capability of the transmitting device, these requirements can be met only with restrictions. For example, let us consider the case where the transmitter deviation is limited to $\Delta F = 100$ MHz. This may be typical of solid-state Gunn oscillators [4], such as those considered for the proposed system. Also, let us assume that we wish to operate the radar with the aforementioned range scale of 4 Hz/m** which requires a slope of 597 MHz/sec. Referring to part (a) of Figure 4, one writes the expression for the lowest modulation frequency:

$$S = \frac{\Delta F}{1/2f_m} = 2f_m \, \Delta F$$

or

$$f_m = \frac{S}{2\Delta F} = \frac{597 \text{ MHz/sec}}{2 \times 100 \text{ MHz}} \tag{8}$$

$$= 2.985 \text{ Hz.}$$

Thus, the minimum repetition frequency would be about 3 Hz. Note that this is a lowest frequency, for there is no restriction on the higher rates except that of the quantization error. Specifically, the range scale could still be maintained with the higher repetition rates and the same slope. The maximum deviation ΔF, however, would be reduced accordingly.

---

*In this report, the range and velocity scales are represented by symbols A_R and A_V, respectively.

**The corresponding inverse scale is 0.25 meter/Hz.

2.1.3.2 Target Velocity Scale

The velocity scale for the radar system is determined by the operating frequency of the radar as defined by (2). For the radar system described in this report, the nominal operating frequency is at 24.0 GHz. Thus, the velocity scale is

$$\text{Velocity scale} = \frac{2Vf_0}{c} = \frac{2(1\text{m/sec})\ 2.4\times10^{10}\text{Hz}}{3\times10^{8}\ \text{m/sec}}$$

$$= 160\ \frac{\text{Hz}}{\text{m/sec}} = A_V \qquad (9)$$

The corresponding inverse velocity scale, i.e., $(A_V)^{-1}$, is 0.00625 (m/sec)/Hz.

It must be noted here that, with the exception of the carrier frequency, which is generally determined by many other factors in addition to the velocity scale, the designer does not have a simple control over the velocity scale as he has over the range scale. This forces the designer to pay particular attention to the absolute values of the doppler shift tones generated by the receiver mixer. For the system considered here, the maximum target velocity is $\pm$6.1 m/sec. Therefore, the relationship between the target velocities and the corresponding doppler velocities is as shown in Figure 7. Note that, because of the homodyne mixing, the positive and negative velocities appear on the same (i.e., positive) side of the velocity axis. Consequently, determination of the direction of the target motion must be performed by means other than the simple doppler velocity measurement. Such means are described elsewhere in the report.

2.2 System Range Equation

2.2.1 The Range Equation

The range equation is the starting point of the design of a radar system. Into this equation are entered all of the known or well-predicted parameters. From this equation, the available received power, P_r, is determined as a function of the range and it is compared to the estimated level of the system noise density, N_0. The overall ratio P_r/N_0 is then used to characterize all other pertinent system performance predictions.

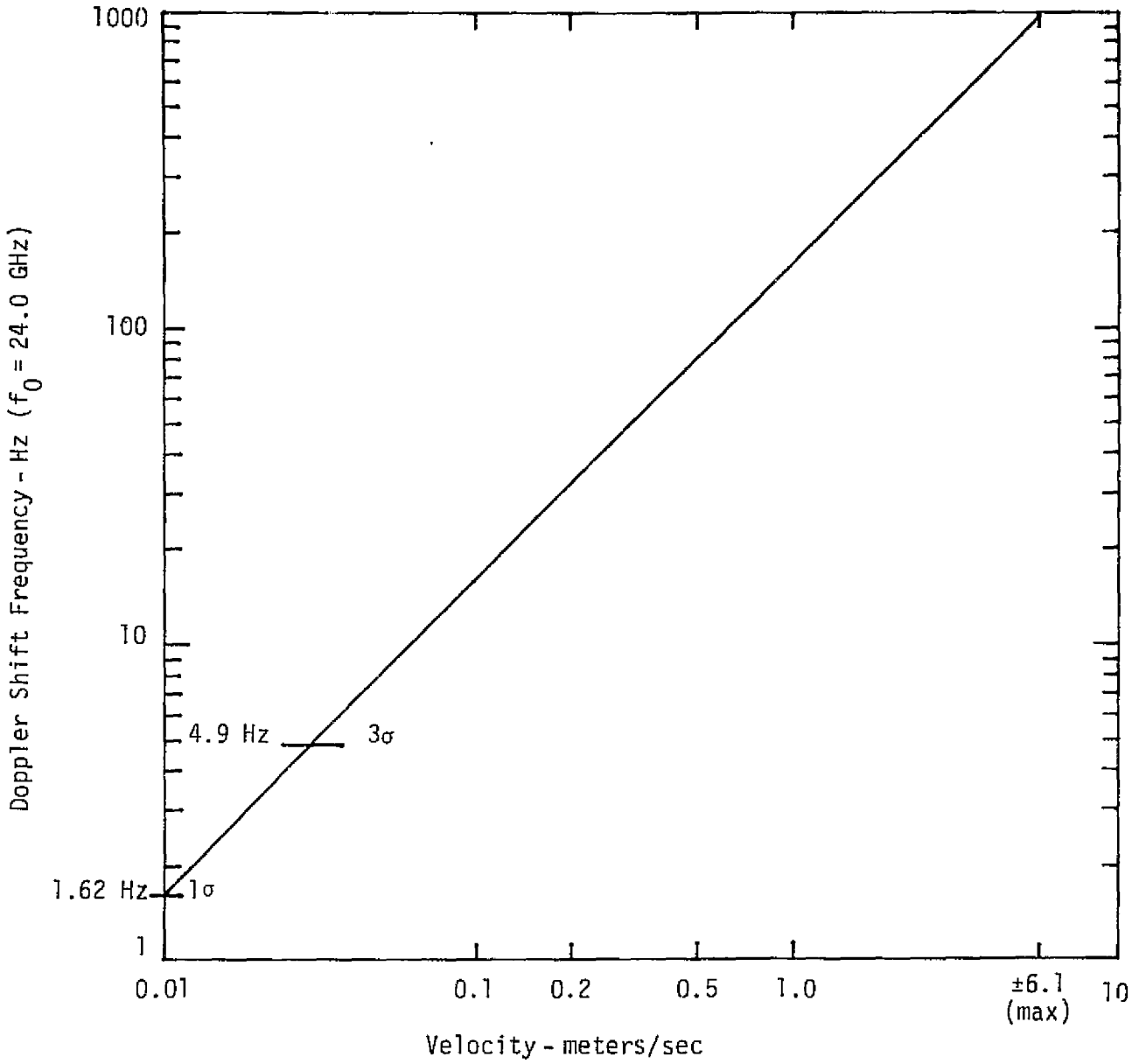

Figure 7. Doppler Shift Frequency versus Target Velocity for a 24 GHz Radar

The basic form of the range equation is given below:

$$P_{rec} = \frac{P G^2 \lambda^2 \sigma L}{(4\pi)^3 R^4}$$

where

P_{rec} = received power (dBm)

P = transmitter output power (dBm)

λ = carrier wavelength (m)

R = range (one-way, m)

σ = target radar cross-section (m^2)

L = RF losses (dB)

From this basic range equation, the power budgets for the radar system operation can be prepared in terms of the pertinent factors. Tables 3, 4, and 5 show the power budgets for a radar system operating at the K, X, and V bands, respectively.

Although the K-band system is the primary candidate for the proposed radar sensor system, the sample power budgets for the other bands are included for comparison. In all three tables, the gain of the antenna is assumed to be 23 dB, which corresponds approximately to a 12° beamwidth, i.e., the beamwidth used by the existing K-band equipment which will be utilized for the breadboard construction. Also, all power budgets shown are for the maximum radar operating range of ≈1853 m, i.e., 1.0 nmi.

Although, from the standpoint of the received power, the X-band system (Table 5) appears favorable, its dimensions are about 2.5 times greater than those of the K-band system. Furthermore, the X-band doppler velocities are 0.4 the value of those for the K-band and, thus, they are subject to about 4 dB more flicker noise*.

At the other extreme, the 70 GHz V-band power budget estimate shows at least a 17 dB disadvantage with respect to the K-band operation. The major portion of the apparent V-band disadvantage is that, for an identical beamwidth, the V-band antenna has a much smaller receive aperture than that of an equivalent beamwidth (and gain) antenna at a lower

*For discussion of the flicker noise, see paragraph 2.2.2.2.

Table 3. Power Budget for a K-Band FM-CW Radar

Parameter	Value	Budget Entry
P	200 mW	+ 23 dBm
G	23 dB	+ 46 dB
λ	0.0125 m (24 GHz)	- 38.1 dB-m^2
R	1853 m	-130.8 dB-m^4
$(4\pi)^3$	Constant	- 33 dB
σ	10 m^2	+ 10 dB
L	1.5 dB	- 1.5 dB
P_{rec}	Power at input to mixer	-124.3 dBm

Table 4. Power Budget for an X-Band FM-CW Radar

Parameter	Value	Budget Entry
P	500 mW	+ 27 dBm
G	23 dB	+ 46 dB
λ	0.0286 m (10.5 GHz)	- 30.9 dB-m^2
R	1853 m	-137.7 dB-m^4
$(4\pi)^3$	Constant	- 33.0 dB
σ	10 m^2	+ 10.0 dB
L	1.0 dB	- 1.0 dB
P_{rec}	Power at input to mixer	-112.6 dBm

Table 5. Power Budget for a V-Band FM-CW Radar

Parameter	Value	Budget Entry
P	50 mW	+ 17 dBm
G	23 dB	+ 46 dB
λ	0.0043 m (70 GHz)	- 47.4 dBm-^{2}
R	1853 m	-130.8 dB-m^4
$(4\pi)^3$	Constant	- 33 dB
σ	10 m^2	+ 10 dB
L	3 dB	- 3 dB
P_{rec}	Power at input to mixer	-141.2 dBm

IF frequency. The restriction of keeping the same beamwidth of ≈12° for all bands is due to requirements for the manual angular acquisition of the target. Narrower beamwidth (and higher gains) would make the manual pointing of the radar beam rather difficult. In addition to this, the cost of V-band equipment is considerably higher than that of the K-band system. Therefore, it appears that, for the breadboard, the K-band system offers the most cost-effective approach to feasibility demonstration.

In addition to the estimate of the received signal level, the calculation of the noise level is required to predict the performance of the system at the maximum range. As discussed in the paragraphs which follow, there are several types of noise which contribute to the composite "noise floor" of the radar receiver. Thus, one proceeds to determine this composite noise floor in terms of an equivalent dBm-Hz level, then one computes the P_r/N_0 value accordingly. For example, if the overall receiver noise figure (NF) is 10 dB, then the P_r/N_0 can be computed using the K-band system power budget (i.e., Table 3) as follows:

$$\begin{aligned} \frac{P_r}{N_0}\,(\text{dB-Hz}) &= P_r\,(\text{dBm}) - [-174\,(\text{dBm-Hz}) + \text{NF}\,(\text{dB})] \\ &= -124.3\,(\text{dBm}) + 174\,(\text{dBm-Hz}) - \text{NF}\,(\text{dB}) \\ &= +39.7\ \text{dB-Hz} \end{aligned} \tag{11}$$

To determine the actual signal-to-noise ratio (SNR) in a bandwidth of a particular device (say, a range tracker), one uses the available P_r/N_0 to obtain the SNR value:

$$\text{SNR (dB)} = \frac{P_r}{N_0}\,(\text{dB-Hz}) - 10 \log_{10} B \tag{12}$$

where B is the noise bandwidth in Hz of the device under consideration. Thus, for example, a tracker of a noise bandwidth B = 200 Hz has the SNR of

$$\begin{aligned} \text{SNR} &= +39.7\ \text{dB-Hz} - 10 \log_{10} (200) \\ &= +39.7\ \text{dB-Hz} - 23\ \text{dB-Hz} \\ &= +16.7\ \text{dB} \end{aligned} \tag{13}$$

Calculations such as shown above, although numerically rather simple, form the basis for the prediction of the system performance during the

various phases of its operation. Consequently, these equations appear frequently throughout this report. All of them, however, involve the received power value P_r, estimated as shown in Tables 3 through 5, and the system noise floor N_0. The estimate of the N_0 value for the proposed system is described below.

2.2.2 System Noise Considerations

For the homodyne radar system as described in this report, the following three sources of system noise must be considered: (1) thermal noise, (2) mixer flicker noise, and (3) self-noise. The nature of these noise sources and their relative significance in determining the overall noise floor of the system are presented in the following paragraphs.

2.2.2.1 Thermal Noise

The thermal noise is generally considered the fundamental limiting factor of most radar and communication systems. This is particularly true of the systems which utilize preamplifiers and several stages of nonzero frequency IF amplification. For these systems, the receiver thermal noise density N_0 is determined primarily by the noise figure of the preamplifier; thus,

$$N_0 = -174 \text{ (dBm-Hz)} + NF \text{ (dB)} \tag{14}$$

where -174 dBm-Hz is the reference noise floor of a 0 dB noise figure front-end at 290°K, and NF is the noise figure of the preamplifier which precedes the mixer.

With a preamplifier of noise figure NF_A and gain G_A placed ahead of the mixer, the contribution of the noise figure of the mixer is reduced considerably:

$$NF_0 = NF_A + \frac{NF_M - 1}{G_A} \tag{15}$$

where NF_0 is the overall system noise figure and NF_M is the noise figure of the mixer. Thus, with the receiver having a preamplifier $NF_A = 3.0$ dB and $G_A = 20$ dB, a mixer noise figure of 10 dB degrades the overall noise figure NF_0 by only 0.2 dB.

The use of a low-noise, high-gain preamplifier to reduce the mixer noise is generally reserved for large, relatively complex and expensive

systems. In our case, however, the requirement for portability and cost-effectiveness precludes the use of a preamplifier. Consequently, we must consider the noise figure of a crystal mixer type receiver front-end, such as represented by the simplified block diagram of Figure 8. As shown in this figure, the RF signal received by the antenna is applied directly to the mixer (assuming negligible receiver RF losses) where it is converted to an intermediate frequency which, for a homodyne receiver, may be as low as 0 Hz. The mixer introduces a conversion loss, L_c, and is characterized by a noise temperature ratio, t_r. Also, the amplifier following the mixer is characterized by a noise figure, NF_A. The corresponding expression for the overall noise figure of a mixer front-end receiver is

$$F_0 = L_c (t_r + NF_A - 1) \tag{16}$$

Note that the temperature ratio t_r plays an important role in determining the overall noise figure of a crystal mixer receiver. The temperature ratio is related to the flicker noise, which is generally referred to as "1/f" noise of a mixer. At mixer output frequencies above 100 kHz, the value of t_r is constant and is typically between 1.2 and 2.0. Thus, with a 1.5 dB noise figure amplifier, $t_r = 1.4$ (ratio, not dB), and the mixer loss of 6 dB, the overall noise figure of the crystal receiver would be 8.6 dB, provided that all of the received signal components, or the IF amplifier, are centered above 100 kHz. In this case, the receiver performance is generally referred to as "thermal noise limited" and the mixer noise temperature ratio, although appearing in (16), is not considered a determining factor. This is because most practical amplifiers have a noise figure on the order of 2 dB to 3 dB, thus introducing a dominant term into (16).

Crystal mixer RF reception with mixer output frequencies lower than 100 kHz is therefore considered "flicker noise limited." Consequently, the flicker noise characteristics of a crystal mixer receiver are of great importance for estimating the performance of the homodyne radar system described in this report.

2.2.2.2 Mixer Flicker Noise

The homodyne receivers operate with the RF signal components mixed

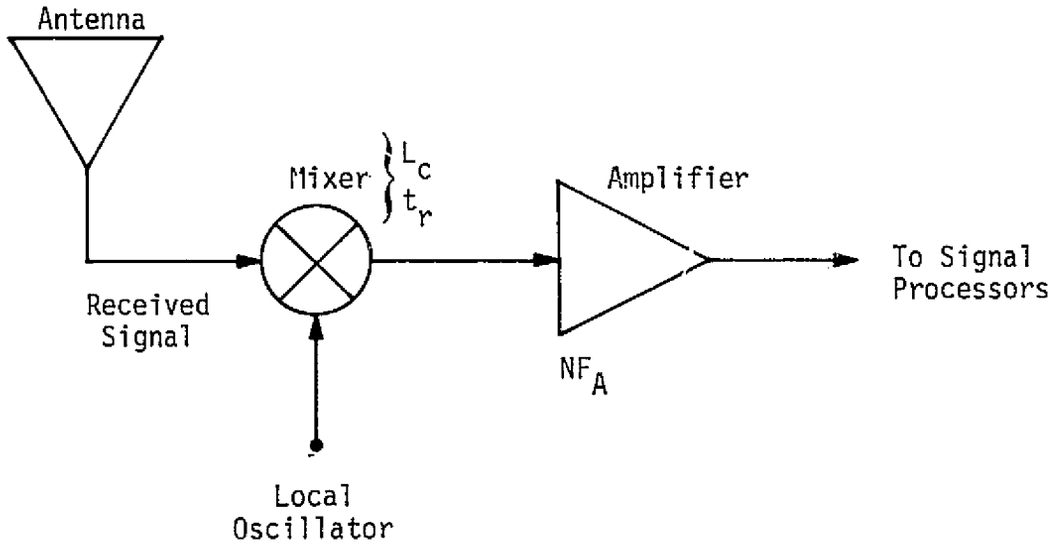

Figure 8. Simplified Block Diagram of Crystal Mixer Front-End Receiver

down to a low frequency range which, in most cases, is confined to the region from 0 Hz to less than 100 kHz, and quite often to an even narrower region with the upper frequency on the order of 10 kHz. Consequently, the output of a crystal mixer homodyne receiver is essentially confined to what is usually referred to as the "audio" frequency range.

The initial investigations (conducted in the early 1940's and throughout the 1950's) of the flicker noise performance of the crystal mixers indicated that the flicker noise increases below 100 kHz at a rate proportional to 1/f. Consequently, if a noise figure for a signal component above 100 kHz was measured to about 8 dB to 9 dB, it was observed to increase to about 25 dB at 10 kHz, 35 dB at 1 kHz, and to 50-60 dB in the 100 Hz to 10 Hz range [2]. Such behavior, experimentally verified [5] for a typical X-band mixer is shown in Figure 9. This 1/f behavior of the flicker noise below about 100 kHz presented a formidable obstacle to obtaining high sensitivity performance for the homodyne receivers.

However, with the advent of police radars in the late 1950's, considerable interest was generated in the improvement of the flicker noise performance in the audio range, i.e., at frequencies in the 1 kHz to 10 kHz range. Consequently, the mixer technology has followed suit, and advances were made in reducing the mixer flicker noise at the audio frequencies. Another strong impetus for improving the flicker noise performance of the microwave mixers was provided during the late 1960's by the ever-increasing use of the personnel motion detectors, i.e., the intrusion alarms. These homodyne systems require low-noise performance in the subaudio frequency range (5 Hz to 100 Hz, typically) to detect slowly moving or crawling intruders.

Figure 10 shows the typical flicker noise performance of a contemporary (circa 1978) microwave mixer operating in the RF frequency range from 13 GHz to 25 GHz. For purposes of comparison, the 1/f portion of the curve shown in Figure 9 is also included. From these two curves, it is evident that, for the modern mixer, the so-called 1/f "break point" has been moved down from about 100 kHz to approximately 1 kHz. Such a two-orders-of-magnitude break point frequency reduction results in the lowering of the noise figure in the subaudio range (5 Hz to 100 Hz) by 15 dB to 18 dB. Furthermore, at 1 kHz, the improvement is about 13 dB

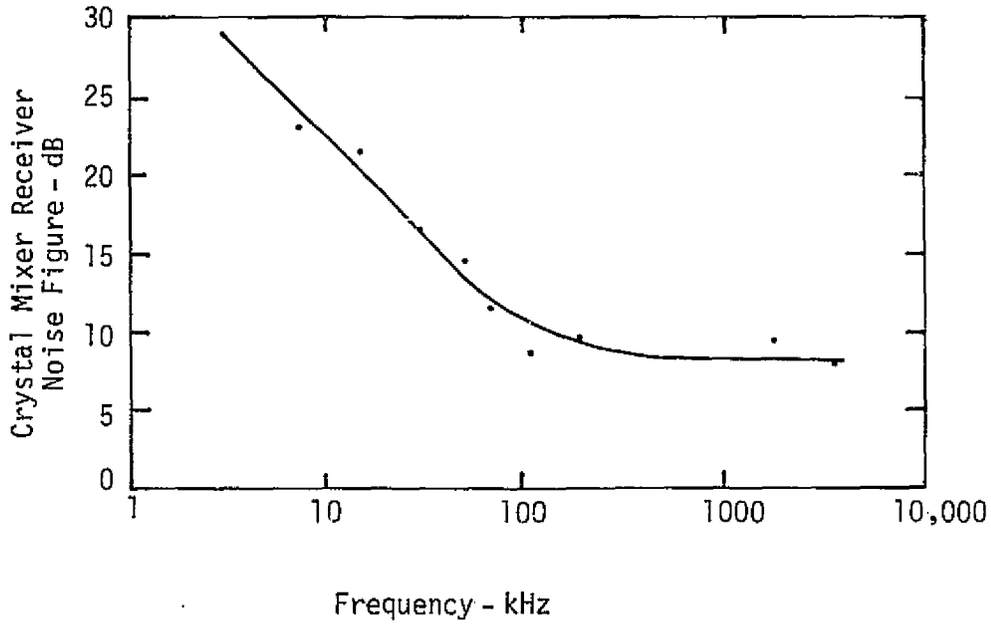

Figure 9. The Crystal Mixer Receiver Noise Figure Performance; Circa 1959 Technology [5]

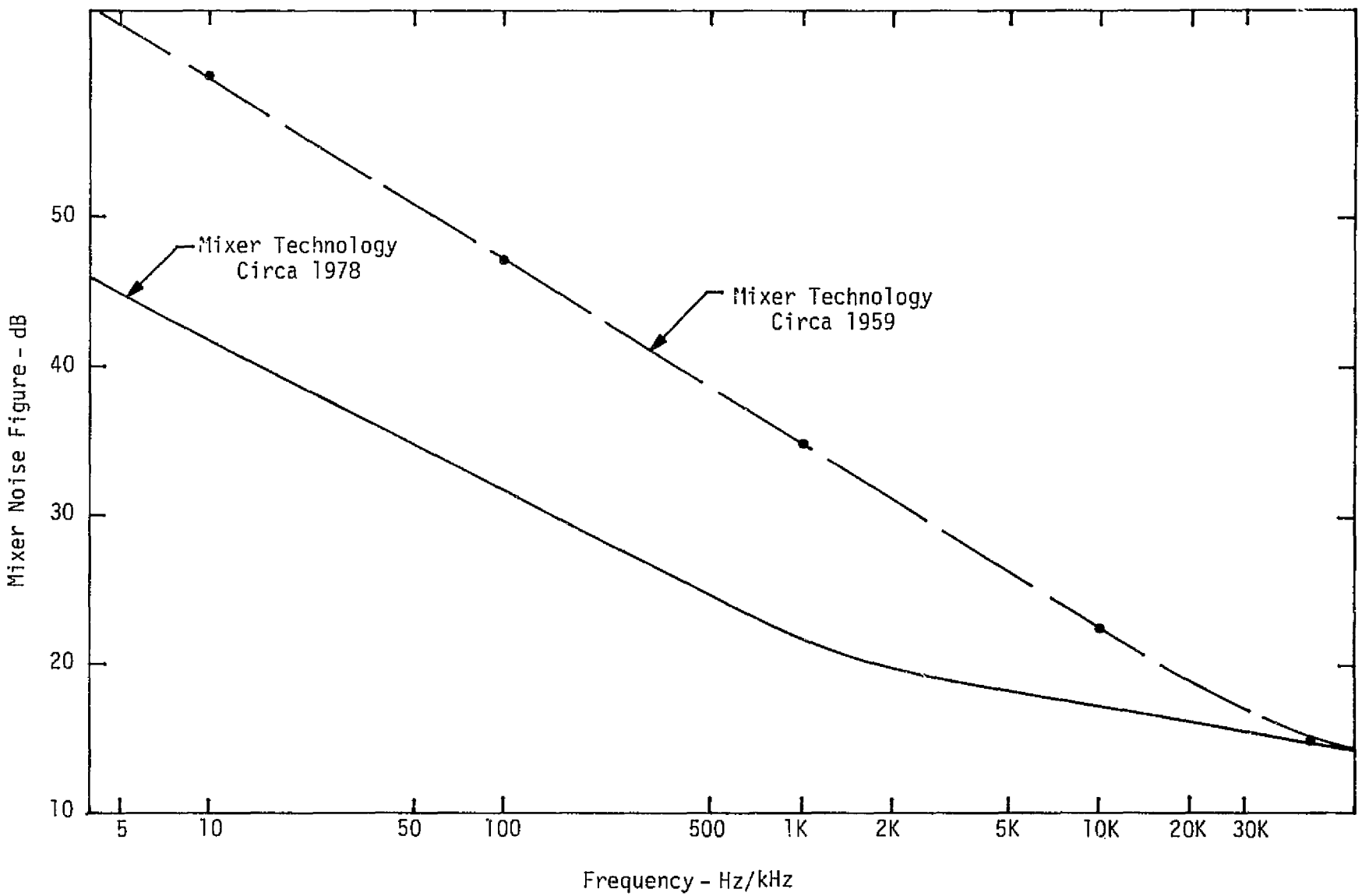

Figure 10. Latest (Circa 1978) Mixer Technology Provides Considerable Improvement in Flicker Noise Performance at Audio and Subaudio Frequencies

and, at 10 kHz, it is about 5 dB. The absolute values of the noise figure across the frequency range of interest are also reduced. As a result of such marked improvement in the microwave crystal mixer technology, the homodyne radar receivers now offer a low-cost alternative to the receivers employing IF amplification. The latter require generation of a local oscillator signal other than the transmitted signal, thus increasing the complexity of the receiver portion of the radar system.

The impact of the crystal mixer flicker noise on the performance of the homodyne radar sensor system can be estimated by calculating the P_r/N_0 values for the target return at various ranges. Figure 11 shows the plots of $P_r/N_0(f)$ versus target return tone frequency (either range or velocity, or both) and the target range. The value of P_r used for these calculations is obtained from the power budget in Table 3, and the values of the noise density $N_0(f)$* are derived from the data in Figure 10.

The data presented in Figure 11 serves as the basis for determining the modulation waveform(s) for the operation of the radar in the various modes (i.e., target detection, acquisition, and tracking). For example, it is evident from the plot for R = 1850 meters (maximum range) that selecting a modulation format which places the target tones at frequencies above 1 kHz provides more favorable $P_r/N_0(f)$ ratios than a modulation format which restricts these tones to less than 1 kHz. However, as the target moves in, the $P_r/N_0(f)$ increases in its absolute value and, consequently, one has more control over the modulation format to be used for a particular radar function. The details of such a modulation technique optimization are discussed in subsequent sections of this report.

2.2.2.3 System Self-Noise

The salient feature of the homodyne radar receivers, namely, the translation of the received signal to "zero Hz" IF frequency by mixing with a portion of the transmitted signal, often raises a question about the effect of the transmitter's FM noise sidebands** on the reception of

*It must be noted that the conventional meaning of symbol N_0 is to define a power density of a flat-spectrum thermal noise. In this report, however, the $N_0(f)$ denotes the spectral power density of the flicker noise at any given frequency "f," i.e., it is frequency-dependent.

**There are also AM sidebands present, but they are several orders of magnitude below the FM sidebands and, thus, they generally are not a threat to system performance.

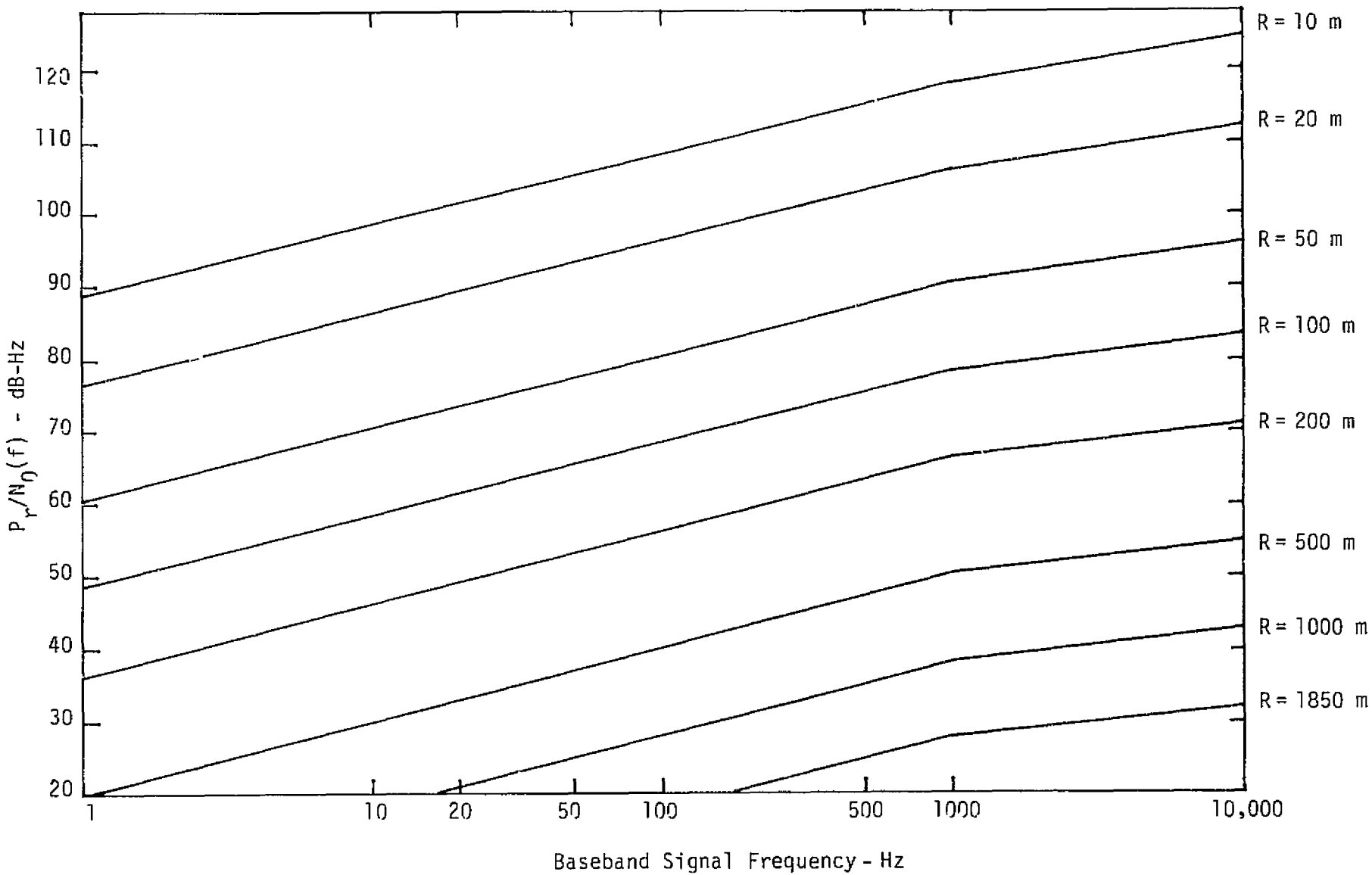

Figure 11. Plots of $P_r/N_0(f)$ for the K-Band Homodyne Radar

the weak signals. At first glance, one would suspect that the FM noise from the transmitter falls directly into the frequency band of the received signals and thus generates a "self-jamming" process.

The detailed analysis of the homodyne mixing, however, indicates that, for the short-range targets, there exists a correlation between the target echo signal and the local oscillator signal (a portion of the transmitter output) which provides for cancellation of the FM noise.

The exact analysis of this correlation effect is carried out in Appendix A of this report. It is shown there that an rms error associated with the measurement of a particular audio tone is bounded by

$$\hat{\sigma}_{f_b} \leq \left(\frac{T_{RT}}{T_{av}}\right) \left[\int_0^{B_{max}} G_{f_N}(f)\ df\right]^{1/2} \text{Hz} \tag{17}$$

where

$\hat{\sigma}_{f_b}$ = rms error of a frequency tone measurement (velocity or range)

T_{RT} = round-trip time to target

T_{av} = averaging time of the frequency counter

$G_{f_N}(f)$ = frequency noise power spectrum (Hz^2/Hz) of the transmitter/local oscillator device

f = noise spectrum frequency

$\hat{f}_b$ = refers to the mean value of the tone frequency measured

It must be pointed out that (17) holds true for $R \leq 2000$ m and $f \leq 1000$ Hz, both of these conditions being satisfied for the radar sensor under consideration.

The measurement of the FM spectra of the actual Gunn oscillator RF sources indicates that, at frequencies less than 1000 Hz away from the carrier, the FM noise has a form

$$G_{f_N}(f) = \frac{K}{f^3} \tag{18}$$

where K is a constant unique to the type of device used and the operating RF frequency. Using the measured data on actual Gunn diode oscillators [4], we estimated, for $f_0 = 24$ GHz, the value of $K = 2450\ Hz^2/Hz$ at $f = 1$ Hz. Solving, for $B = 100$ Hz and using the near-zero f-spectrum approximation shown in Figure 12, one obtains

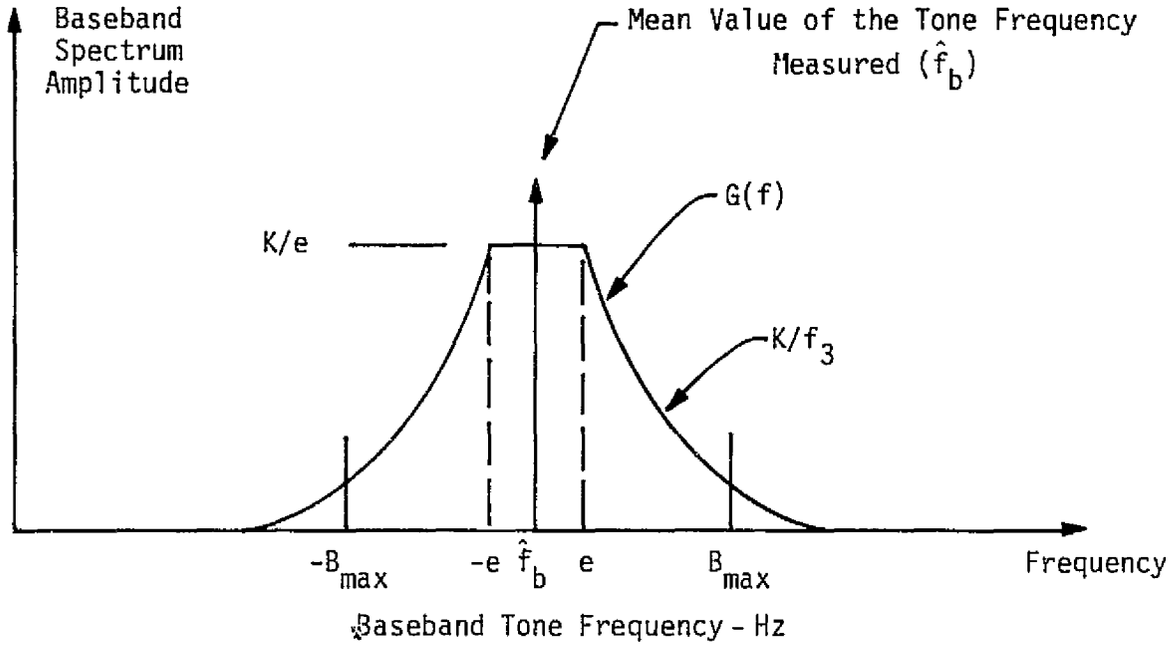

Figure 12. Transmitter FM Noise Spectrum Superimposed on the Baseband Tone Frequency Estimate $\hat{f}_b$ (Spectrum Shape Approximation as in [6])

$$\hat{\sigma}_f = \left(\frac{T_{RT}}{T_{av}}\right) 60.6 \text{ Hz.} \tag{19}$$

Consequently, for R = 1850 m (1 nmi) and T_{av} = 1 sec, we obtain

$$\hat{\sigma}_f = \left(\frac{2 \times 1850}{3 \times 10^8}\right) \times (60.6) \tag{20}$$

$$= 7.47 \times 10^{-4} \text{ Hz}$$

Considering the range and velocity scales involved (inverse scales, in this case), the frequency error is negligible. Thus, it can be concluded that, for the system under consideration, the self-noise is not a limiting factor.

2.3 Measurements Geometry and System Parameters

2.3.1 Geometrical Considerations for Target Acquisition

The geometry of the target/radar relationship existing at the onset of the acquisition sequence is the major determining factor for acquisition timing parameters. To establish the bounds for the target dynamics as determined by the acquisition time limitations, and vice versa, let us consider the following model:

(1) Maximum target velocity is +6.1 m/sec (+20 ft/sec) along the radial (towards the radar) direction and is ±6.1 m/sec in the transverse (with respect to the radar beam) direction.

(2) The radar antenna beamwidth is 12° between the 3 dB points (i.e., similar to the antenna of the K-band breadboard).

This model is depicted in Figure 13.

Using the radar/target geometry shown, we can postulate two velocity-related parameters:

(1) Time to Collision, $T_C = \dfrac{R}{V_{RA}(\max)}$, (21)

(2) Time to Traverse the beam, $T_B = \dfrac{2R \tan 6°}{V_{TR}(\max)}$ (22)

where V_{RA} and V_{TR} represent the radial and the transverse velocities, respectively. Using (21) and (22) and assuming, as stated previously, that $V_{RA}(\max) = V_{TR}(\max) = +6.1$ m/sec, one obtains the corresponding plots

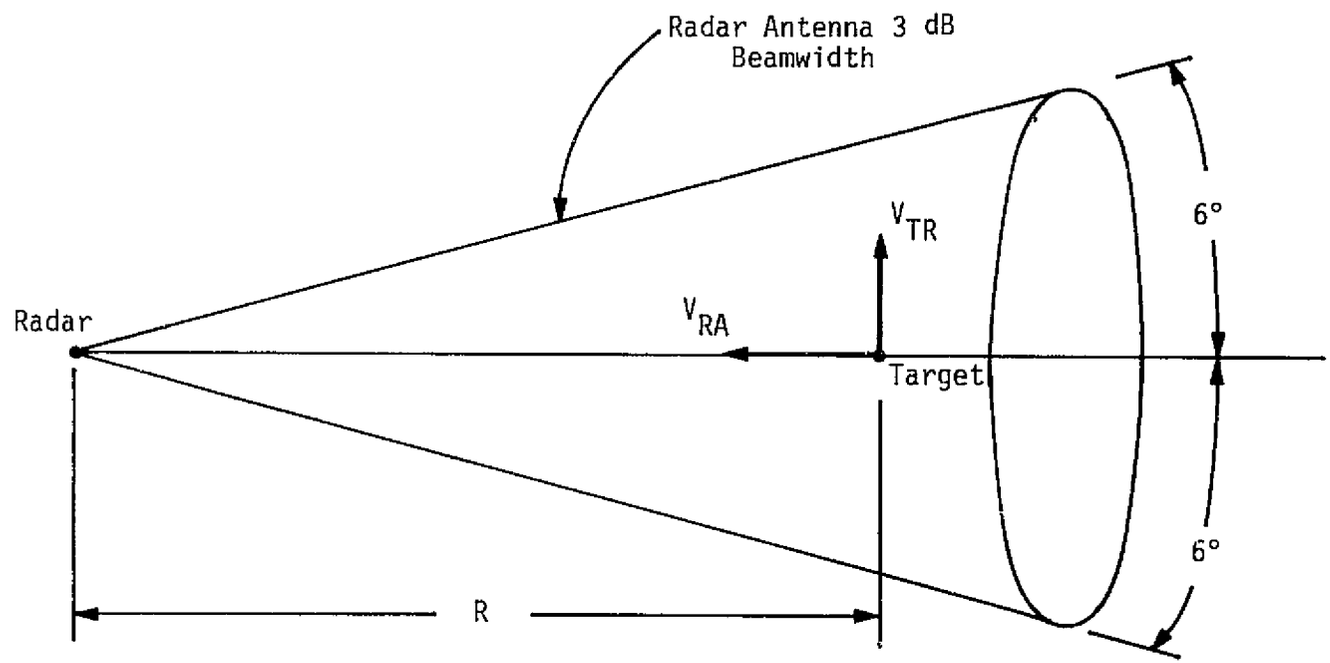

Figure 13. Radar and Target Geometry During Moving Target Acquisition

for T_C and T_B as a function of range. This plot is shown in Figure 14.

From the plot of T_B it is evident that, unless tracked in angle, the target will be within the beam for only about 64 seconds when at the maximum range. At shorter ranges, the time within the beam decreases accordingly, thus driving the requirement towards shorter acquisition times at closer ranges.

On the other hand, if one takes into consideration the fact that the entire acquisition sequence may take about 30 seconds, one comes to the conclusion that, if the target does indeed approach the radar at 6.1 m/sec velocity, there may be no time left to undertake a preventive action against a collision after the target has been acquired.

Thus, it appears reasonable to assume that the maximum velocity component of 6.1 m/sec will not be present at all ranges but, below a certain range, will decrease in proportion to the range. Axiomatix proposes to adopt the following velocity model for the target:

$$V_{RA} \leq 6.1 \text{ m/sec} \qquad \text{for } 200 \text{ m} < R < 1850 \text{ m}$$
$$(656 \text{ ft}) \qquad (6000 \text{ ft})$$
$$V_{RA} \leq K_1 R \times 6.1 \text{ m/sec} \qquad \text{for } 0 < R < 200 \text{ m}$$

and

$$V_{TR} \leq 6.1 \text{ m/sec} \qquad \text{for } 1000 \text{ m} < R < 1850 \text{ m}$$
$$(3281 \text{ ft}) \qquad (6000 \text{ ft})$$
$$V_{TR} \leq K_2 R \times 6.1 \text{ m/sec} \qquad \text{for } 0 < R < 1000 \text{ m}$$

where K_1 and K_2 are constants. The effect of such a proposed velocity restriction is shown by dotted lines in Figure 13. (The constants K_1 and K_2 are 0.035 sec^{-1} and 0.029 sec^{-1}, respectively.

2.3.2 Target Velocity and FM Slope Requirement

To provide for a nonambiguous estimate of the range and velocity information on the target, the relationship between the doppler shift tone f_d and the range tone f_r must always be such that $f_r > f_d(\max)$. This requirement applies, of course, to all ranges up to the maximum detection range.

Because the range frequency f_r is, for any range, determined by the slope S, one can establish the requirement for the minimum value of S to satisfy the $f_r > f_d(\max)$ condition at any given range. For this,

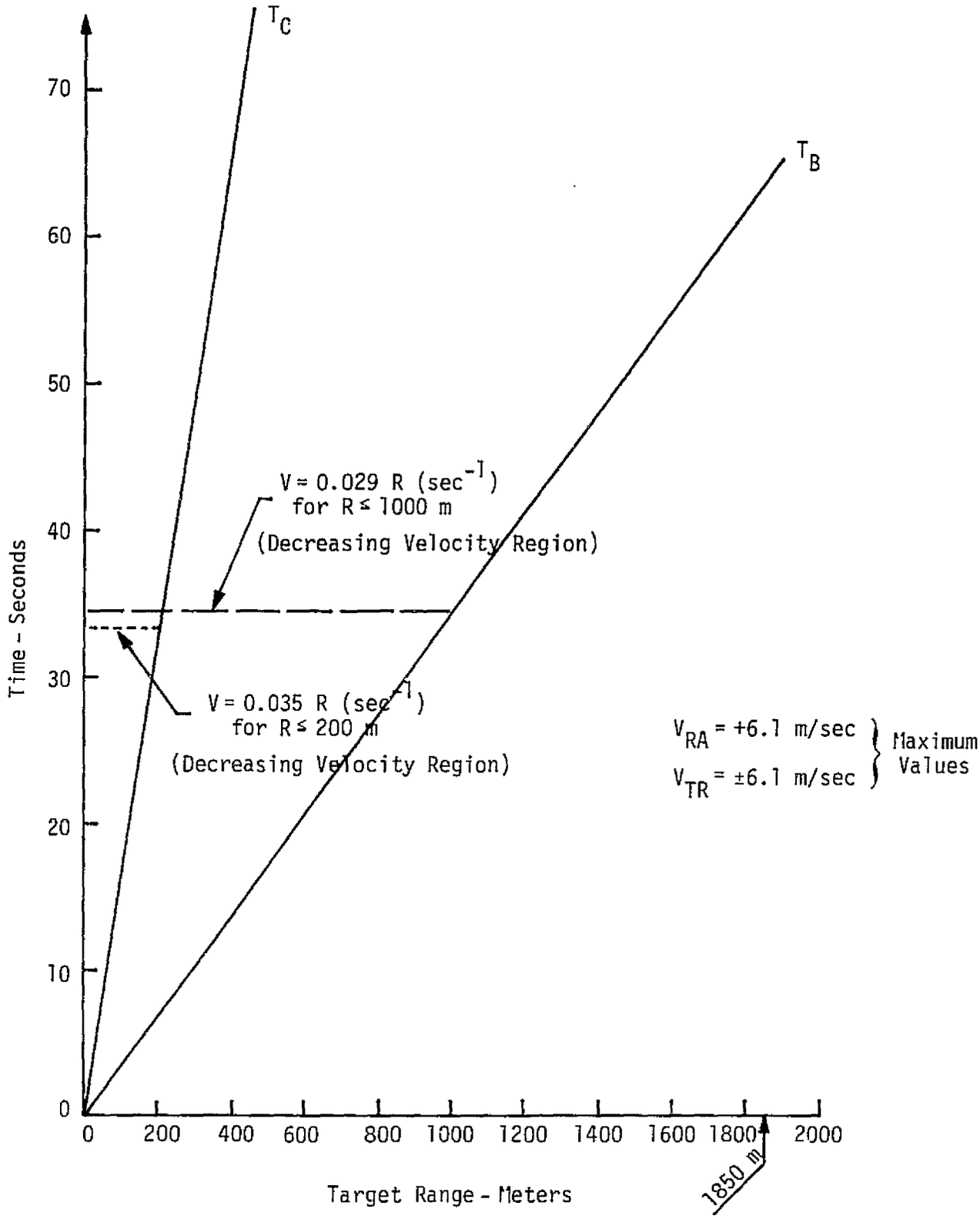

Figure 14. Plot of T_C and T_C versus Target Range For Maximum Values of V_{RA} and V_{TR}

we consider the following two relationships:

$$f_d(\max) = \frac{2V_{RA}(\max)\ f_0}{c} \tag{23}$$

and

$$f_r = S\,\frac{2R}{c} \tag{24}$$

where $V_{RA}(\max)$ = maximum radial target velocity (i.e., +6.1 m/sec)
f_0 = carrier frequencey
R = target range
S = FM slope

Combining (23) and (24) for conditions such that $f_r > f_d$, we obtain

$$S \geq \frac{V_{RA}(\max)}{R}\, f_0 \tag{25}$$

as the requirement for the slope. Figure 15 shows the slope requirements for the case of a 24 GHz radar and $V_{RA}(\max) = +6.1$ meters. The effect of the target velocity profile, as proposed by Axiomatix, is also indicated in this plot as the reduced slope requirement for the target ranges less than 200 m.

2.4 Target Range and Velocity Acquisition

2.4.1 Overview of the Target Acquisition Strategy

Although the operation of the radar sensor system with a priori range information is being considered as one of the operating modes, the baseline design is based on the assumption that, at the onset of system operation, neither the range nor the velocity information is available. Such an assumption provides a realistic and all-inclusive driver to the system design philosophy. Carrying out the baseline design according to this driver results in a ranging/tracking system which can be operated with complete autonomy as well as with the support of external information generating equipment.

Because of the compactness of the system under consideration, the automatic angle (i.e., target direction) search and acquisition is not provided and therefore, in this dimension, the system has to depend on an external sensor. For most cases envisioned, such a sensor may consist of an operator who visually, by means of a boresight, points the

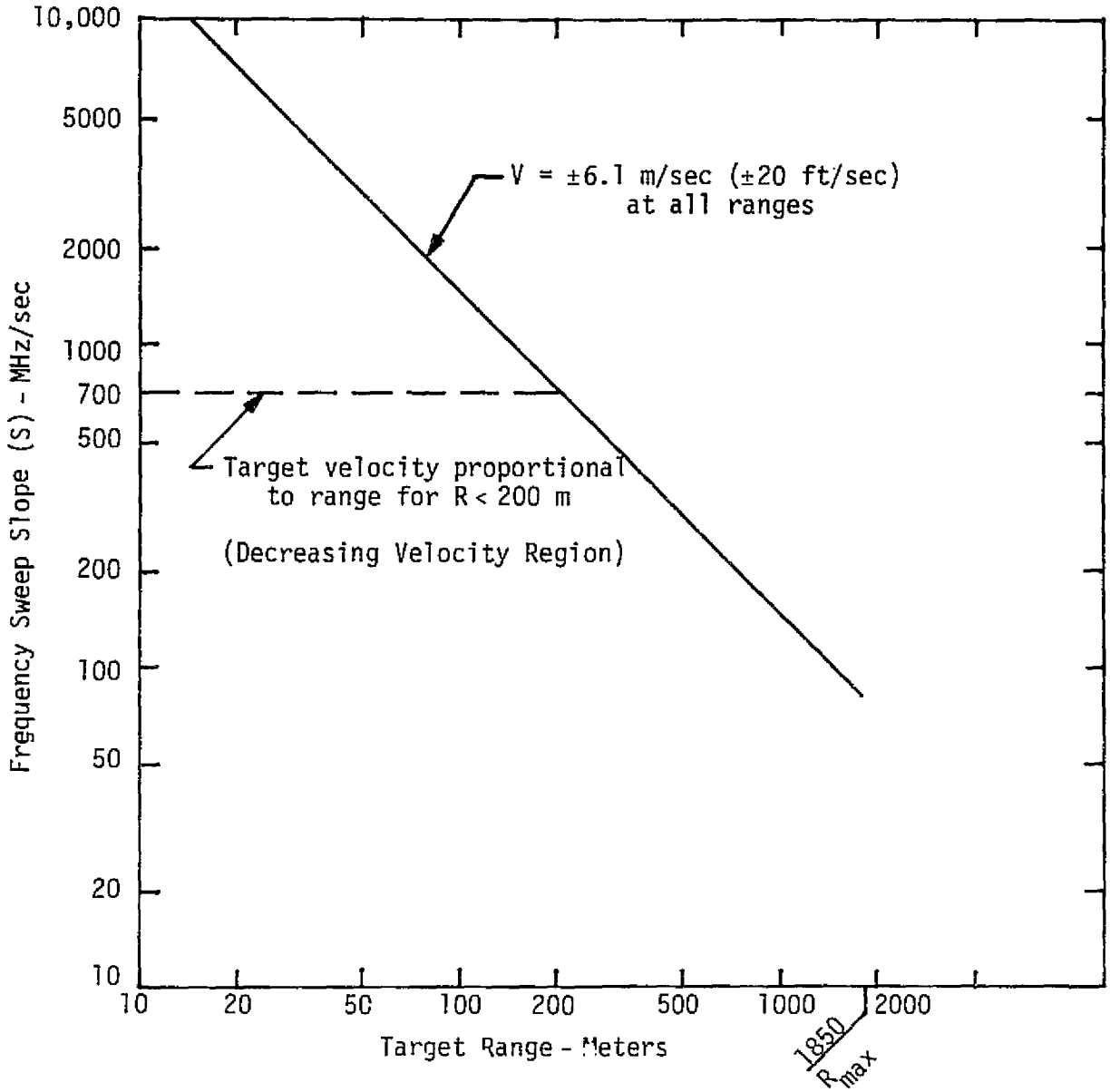

Figure 15. Minimum Slope Required to Prevent Range/Velocity Tone Ambiguity

antenna at the target of interest. Beyond the target direction information, the operator's judgment can be deceiving and thus be only qualitative, such as "target far away" or "target near" or "target pretty close." In darkness, however, when the operator may be sighting only on a beacon light and the target's features are not discernible, the judgment of the distance may be either nearly or totally unavailable. All of the aforementioned arguments point to the fact that the target acquisition strategy must be such that the system, after being pointed in the required direction, automatically searches over the uncertainties of the range and velocity dimensions.

The target range and velocity acquisition algorithm which satisfies this requirement is shown in Figure 16. A corresponding simplified block diagram for implementing such an algorithm is shown in Figure 17. For clarity, only the pertinent receiver and baseband processing subunits are shown there.

As indicated in Figure 16, the proposed algorithm, which provides for the acquisition of the target range and velocity, consists of four segments, or subroutines. These segments and their corresponding range search coverages are as follows:

(1) Short-range search: $R \leq 50$ m (164 ft)

(2) Medium-range search: $50 \text{ m} \leq R \leq 500$ m (164 ft) (1640 ft)

(3) Long-range search: $500 \text{ m} \leq R \leq 1850$ m (1640 ft) (6000 ft)

(4) Velocity-only search: $R =$ designated.

Despite the fact that only the reference to the range is indicated in the listing above, the velocity search and detection are performed simultaneously with the range search. Specifically, because the triangular modulation waveform is used for the search and acquisition sequence, the solution for the velocity information in the case of a moving target is related to the target range as explained earlier in Section 2.1.2.

Although the labeling of the range search segments, such as "short range," "medium range," and long range," is arbitrary and primarily descriptive, the numerical subdivision is not. The purpose behind the indicated subdivision was to eliminate a significant portion of the mixer flicker noise contribution (i.e., the flicker noise below 1 kHz) from the circuitry used for the medium-range and long-range search

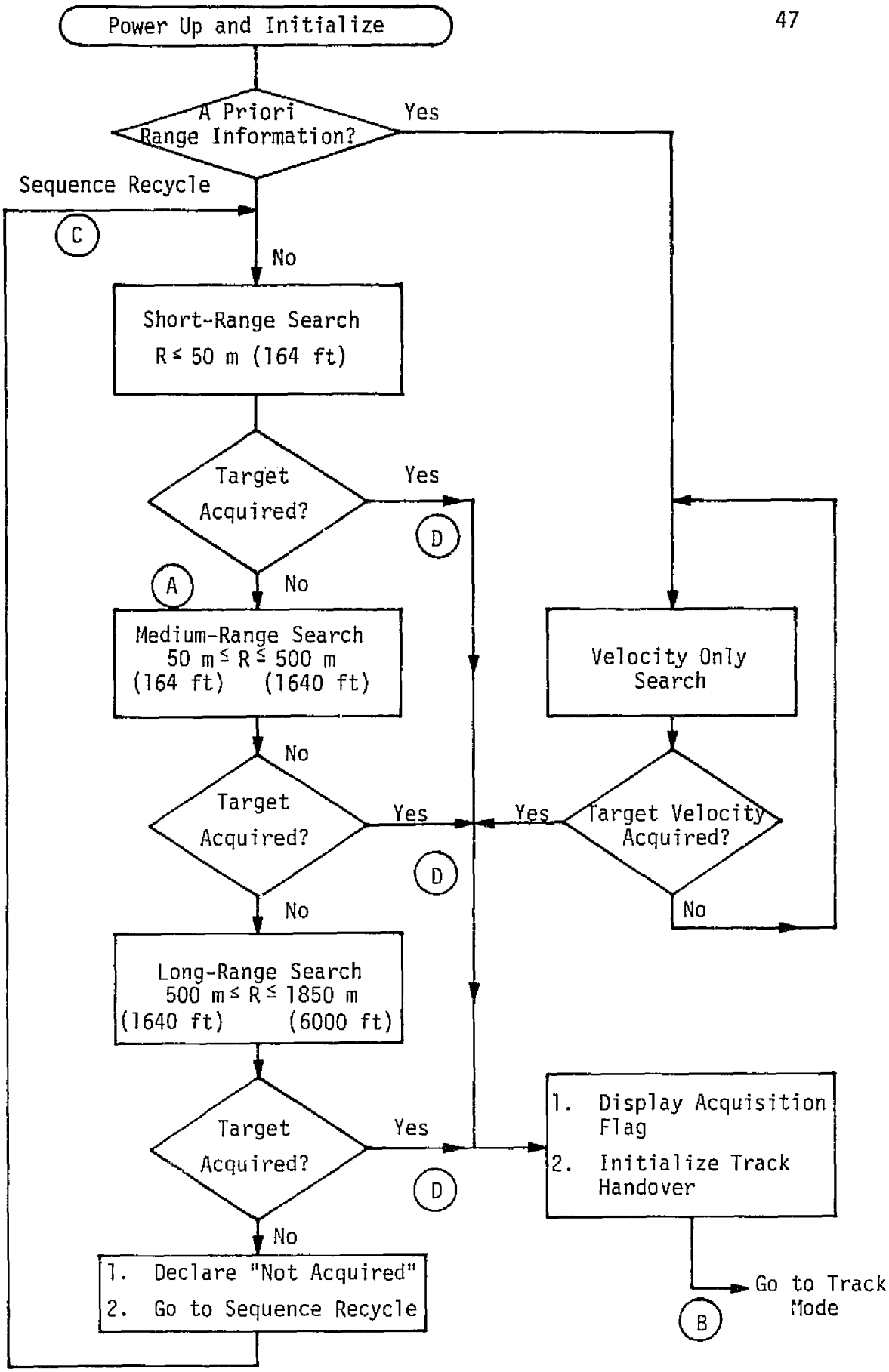

Figure 16. Target Range and Velocity Acquisition Sequence Algorithm

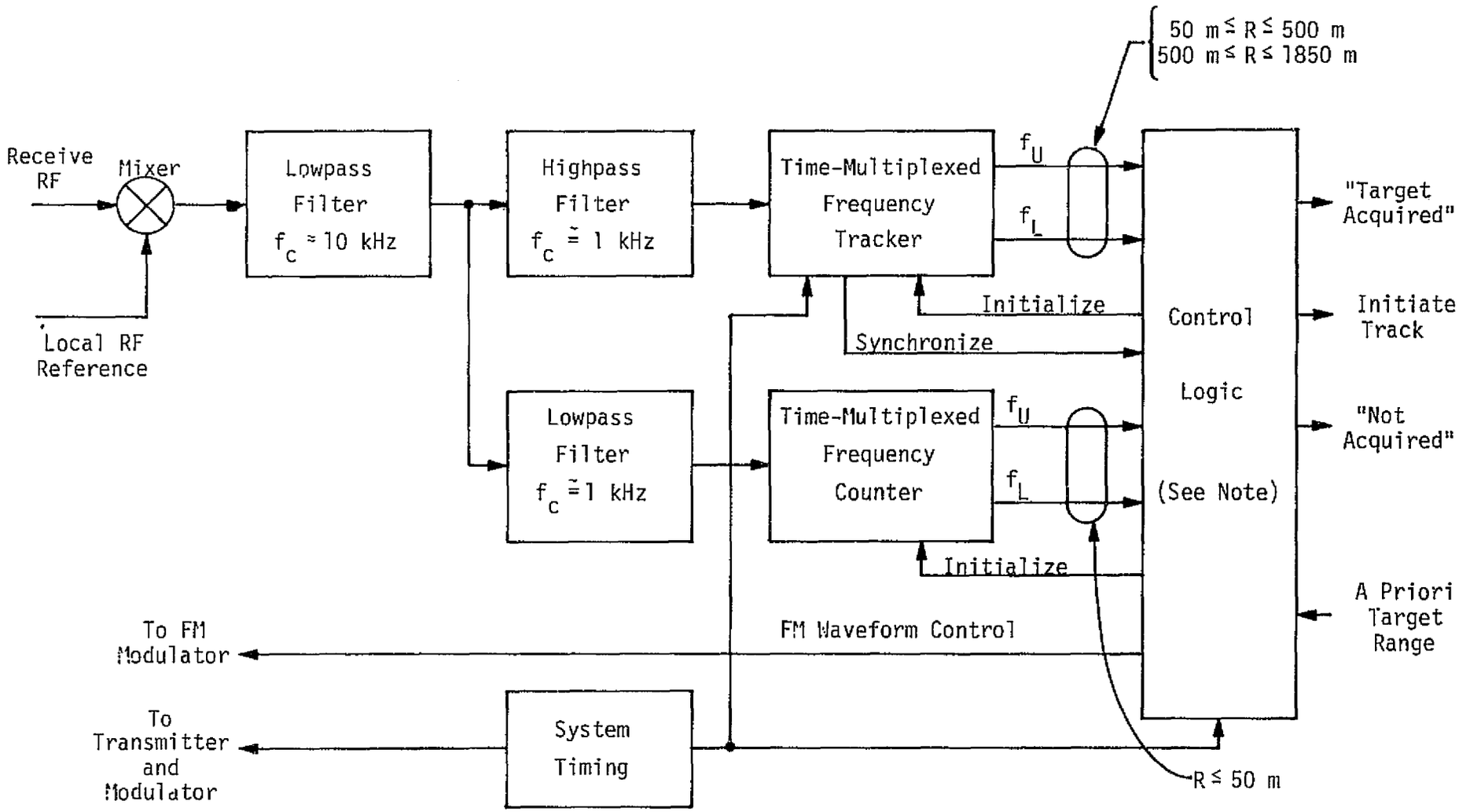

Note: The Control Logic may be a part of a Master System Controller implemented with a microprocessor.

Figure 17. Target Range and Velocity Acquisition Functional Block Diagram (Receiver Portion Only)

acquisition. This suppression is performed by an appropriate selection of the range scales (and of the corresponding FM slopes) as described below.

In the absence of a priori target range information, the sequence of search subroutines shown in Figure 16 corresponds to the range (and velocity) search "outwards," i.e., from the zero range to the maximum range. This appears to be a logical procedure for the case where no a priori range information is available and, consequently, all ranges are equiprobable. Such may be the case, indeed, when the sensor is mounted on an unmanned spacecraft which is controlled remotely. Therefore, after the system power-up and initialization and, in the absence of a priori range information, the baseband data is examined for the presence of the f_U and f_L tones. This examination is performed in the 0 to 1000 Hz region and, as shown in Figure 17, is implemented by a counter. The latter can be used in this case because of the relatively high SNR associated with the close targets. The outcome of this search, which covers ranges of up to 50 meters, is either a "Target Acquired" decision and a command to initiate track, or an instruction to proceed with the search across the next range interval.

The next search interval, i.e., "medium" range, covers the nominal* interval from 50 meters to 500 meters. As described in the subsequent paragraphs, the implementation is not by means of the counter but by means of a pair of frequency trackers which are essentially tuned bandpass filters capable of detecting and indicating the frequencies of the range/velocity lines. The outcomes of this search routine are similar to the one before. In other words, the target is either detected and track is initiated or the search subroutine transfers control to the next phase.

The next and the last phase of the acquisition algorithm is the long-range search covering the range interval from 500 meters to the maximum specified range of 1850 meters (1 nmi). Similar to the medium-range scale, the long-range search utilizes two frequency trackers for detecting the frequency lines of a moving target.

The range scale (and the slope), however, are changed to map the expected target lines into approximately the same frequency region as for the "medium-range" scan. Such scaling provides for maximum commonality

*Actually, the range searches overlap to preclude "blind zones" at the crossovers.

and component savings for the frequency tracker implementation. This sequential time-sharing of the frequency trackers for the short-range and long-range search modes is indicated in the block diagram shown in Figure 17.

The long-range search algorithm, per se, as shown in Figure 16, results in either the declaration of the target acquisition (i.e., an outcome similar to the previous two search routines) or a declaration of an acquisition failure. In the latter case, the algorithm causes the search sequence to recyle, thus repeating the entire sequence.

In the case of a priori range information, the control logic selects the proper range scale and pre-positions the frequency trackers at initial locations required to cover the frequency uncertainty only. This speeds the target acquisition process.

The salient parameters of the entire target acquisition process are summarized in Table 6. The detailed quantitative discussions leading to these parameters are presented in the paragraphs which follow.

2.4.2 Detailed Acquisition Sequence Description

2.4.2.1 Short-Range Acquisition

The algorithm for the short-range acquisition is shown in Figure 18. Figure 19 shows the corresponding range/frequency plot. Note that this plot reflects the assumption (see Section 2.3.3) that the most probable range of velocities of targets closer than 200 meters will be confined within an envelope proportional to R.

The scale selected for this search range is a compromise between the range resolution and the frequency range to be examined. With the scale of 16 Hz/m, the corresponding frequency sweep slope is

$$S = \frac{A}{6.7 \times 10^{-9}} = \frac{16}{6.7 \times 10^{-9}} = 2388 \text{ MHz/sec} \qquad (26)$$

or a design value of 2400 MHz/sec. Reference to Figure 15 indicates that this satisfies the requirement of a nonambiguous range and velocity readout.

With the scale of 16 Hz/m, the 50-meter range corresponds to 800 Hz. Upon this frequency must be superimposed the velocity component* of

$$f_v = \pm \left(\frac{50}{200}\right) (976) = \pm 244 \text{ Hz} \qquad (27)$$

*Assuming the target velocity profile proposed in Section 2.3.1.

Table 6. Summary of Target Acquisition Performance for K-Band Radar Sensor System

Range Designation and Interval	FM Slope	Range Scale	Search BW (see Note 1)	SNR In Search BW	SNR Margin	Estimated Search Time	Probability of Acquisition	Comments
Short R < 50 m (164 ft)	2400 MHz/sec	16 Hz/m	1000 Hz	+30 dB	+24 dB	2 sec	0.99	Range/velocity tones acquired by counting f_U and f_L
Medium 50 m < R < 500 m (164 ft) (1640 ft)	2400 MHz/sec	16 Hz/m	100 Hz (B_L)	+13 dB	+12 dB	6 sec	0.99	Range/velocity acquired by frequency search with two trackers.
Long 500 m < R $\leq$ 1850 m (1640 ft) (6000 ft)	600 MHz/sec	4 Hz/m	50 Hz (B_L)	+11 dB	+ 1 dB	16 sec	0.99	Same method as used for the medium range.
					Total	24 sec		

Note 1

For the case of short-range acquisition, the BW defines the bandwidth of the filter. For the case of medium-range and long-range tracking, BW refers to the one-sided noise bandwidth, B_L, of the frequency tracker.

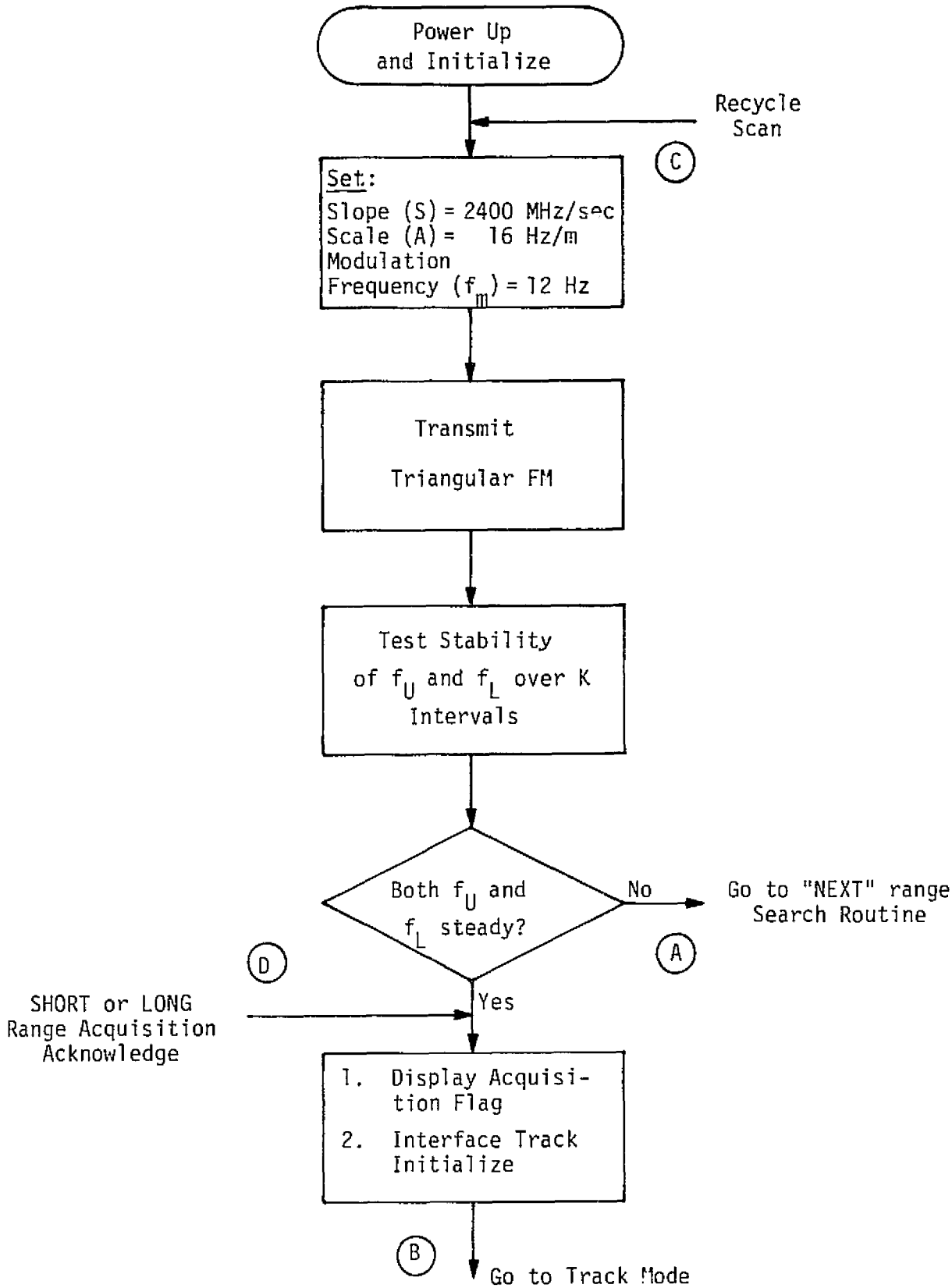

Figure 18. Short-Range/Velocity Acquisition Algorithm

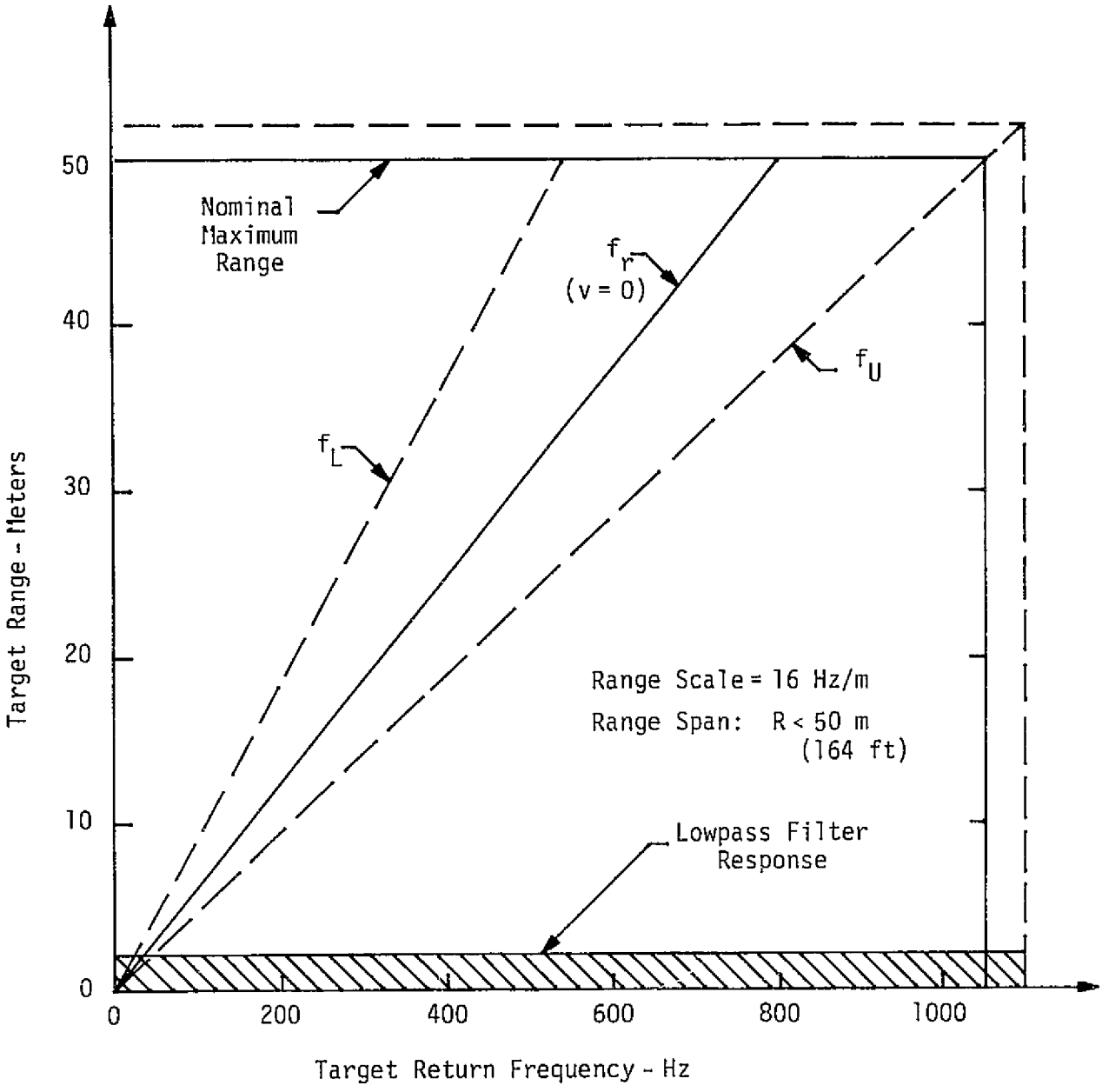

Figure 19. Range/Frequency Plot for Short-Range Target Acquisition

The resultant span of range/velocity line location for a target at 50 meters thus extends from 550 Hz to 1050 Hz. Thus, passing the received signal through a lowpass filter with a cutoff at 1100 Hz will insure that only the targets at ranges less than 50* meters will be examined by the algorithm selected. The block diagram of Figure 17 indicates the use of such a lowpass filter.

Because of the relatively high signal-to-noise ratio associated with the near-zero range targets, a frequency counter is used for determining the values of f_U and f_L. This frequency counter is time multiplexed between the f_U and f_L measurements because these two frequencies appear at the alternate slopes of the modulation waveform (see Figure 5). The stability of the f_U and f_L readings is tested by a number of successive comparisons. With the SNR of about +30 dB in the measurement bandwidth, the frequency estimate is expected to be limited by a quantization error (see Section 2.7) rather than the random (thermal and mixer) noise error.

Also, because of the relatively high SNR for this mode, the time required to declare an acquisition, if the target is present, is expected to be less than 2 seconds.

2.4.2.2 Medium-Range Search Sequence

Figure 20 shows the algorithm for both the medium-range and long-range acquisition sequences. As is evident from the figure, the major portion of the algorithm is the same for both of the searches, with the exception of the scale and slope changes for the long-range sequence.

The range/frequency plot for the short-range search is given in Figure 21. From the frequency scale of this plot, it is evident that the major portion of the frequency uncertainty region lies above 1 Khz, i.e., in the region of the lower mixer noise. The close-range targets do extend the required frequency coverage down to about 500 Hz, but the target return power at these ranges is more than adequate to provide reliable target line detection. It must also be noted that the convergence of the f_U and f_L boundaries towards zero is implied below the range of 200 meters. This is in accordance with the assumptions postulated in Section 2.3.1.

---

*The exact nature of the range limiting is a function of the lowpass filter cutoff frequency and of the rolloff.

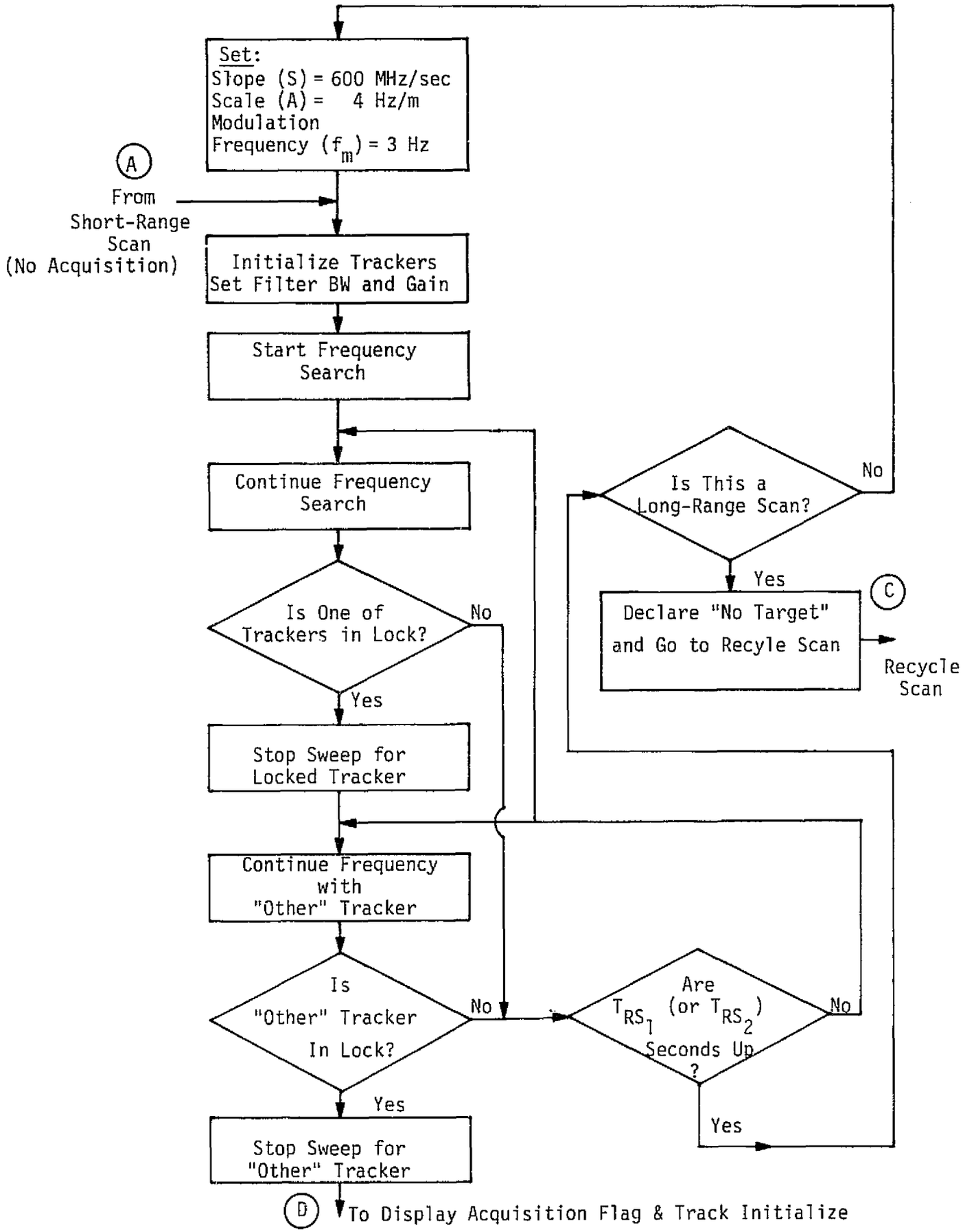

Figure 20. Short- and Long-Range/Velocity Acquisition Algorithm

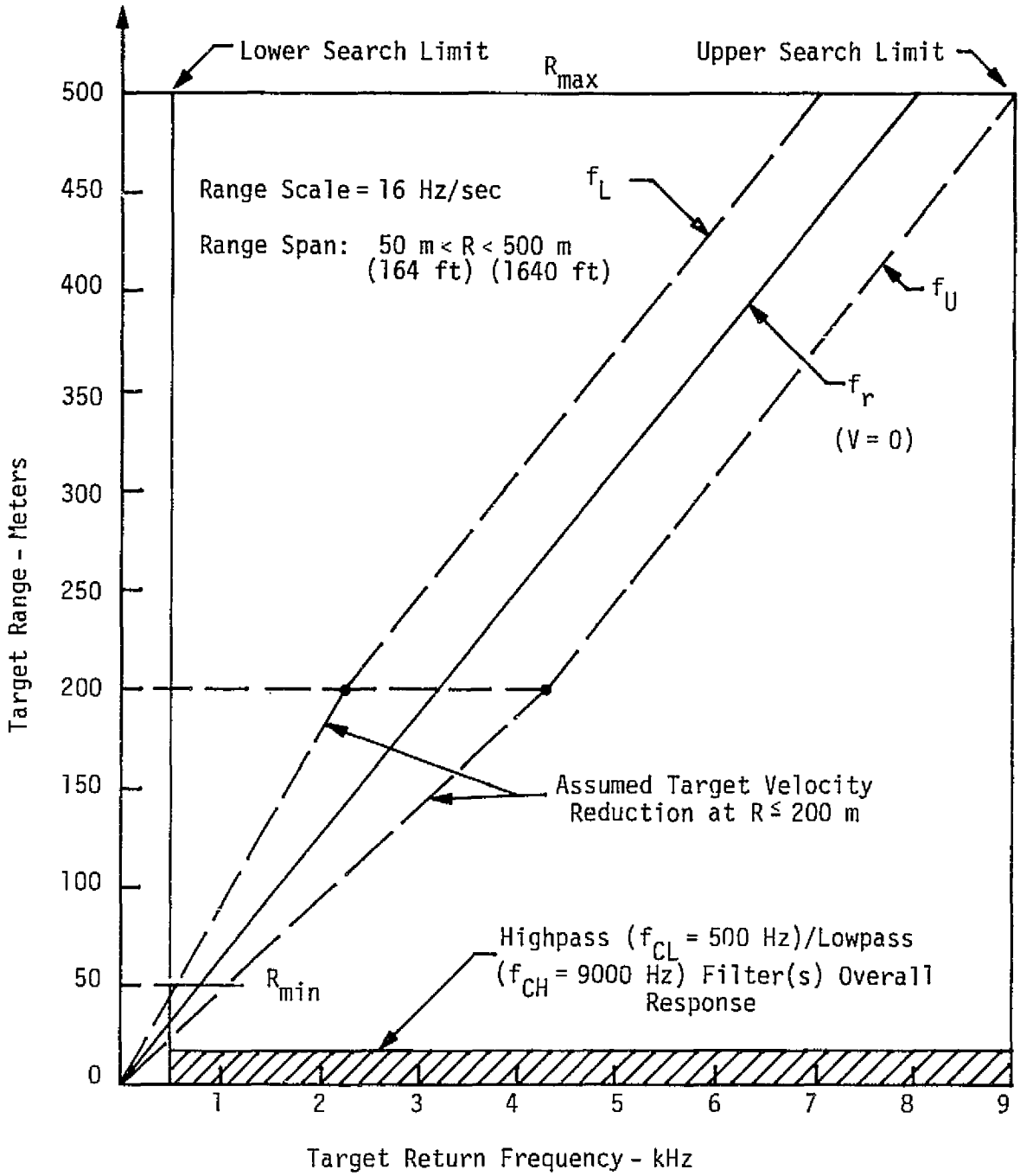

Figure 21. Range Frequency Plot for the Medium-Range Target Acquisition

The upper limit of the frequency range to be searched is at

$$f_{U_{max}} = AR_{max} + f_d(max)$$
$$= (16)(500) + 976$$
$$\cong 9000 \text{ kHz.} \tag{28}$$

Similarly, the lower search limit frequency can be computed:

$$f_{L_{min}} = AR_{min} - \left(\frac{R_{min}}{200}\right) f_d(max)$$
$$= 50 \left(16 - \frac{976}{200}\right)$$
$$\cong 560 \text{ Hz.} \tag{29}$$

For the purpose of covering this range, two frequency trackers will be used. One will start at the upper frequency search limit and will start sweeping downwards, i.e., towards the region of lower frequencies. The second tracker will start at the lower search limit and scan upwards in frequency.

In practice, the frequency tracker implementation may consist of a phase-locked loop (PLL) which is time-multiplexed between the upper and lower scan positions. Figure 22 provides a qualitative demonstration of the two-tracker frequency search implementation. Although the figure depicts a target which is almost in the middle of the frequency search range (thus implying that both trackers will acquire their lines at about the same time), resulting in a minimum search time, in actuality, one must consider the case of the maximum search time.

Examination of the range/frequency plot of Figure 21 indicates that the maximum search time will occur at the close-range end of the scan where the upper tracker is required to move from $f_{U_{max}}$ to a frequency defined as

$$f'_{L_{min}} = 50 \left(16 + \frac{976}{200}\right) \tag{30}$$
$$\cong 1144 \text{ or } 1150 \text{ Hz, nominal}$$

The corresponding frequency range traversed by the upper tracker is

$$\delta F = f_{U_{max}} - f'_{L_{min}}$$
$$= 9000 - 1150 = 7950 \text{ Hz.} \tag{31}$$

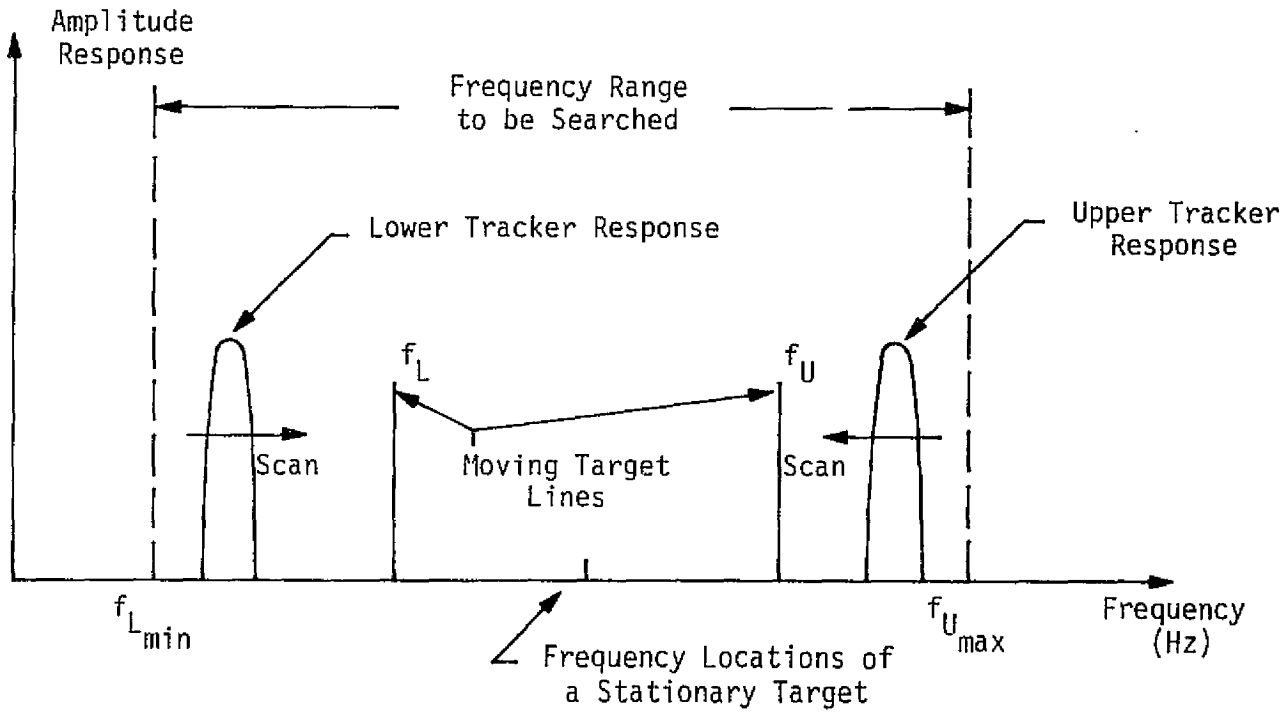

Figure 22. Upper and Lower Trackers Provide for Search and Acquisition of the Moving Target Spectral Lines

Let us compute the time required to search out this frequency range with a phase-locked loop. With the phase-lock loop (PLL), the search time is directly proportional to the δF and inversely proportional to the square of the loop bandwidth. Furthermore, in order to provide a reasonable probability of lock, the SNR in the loop noise bandwidth must be at least +10 dB.

Quantitatively, the required relationship is

$$T_s = \frac{\delta F}{\dot{\Delta} f} \tag{32}$$

where $\dot{\Delta} f$ is the maximum allowable sweep rate to provide a "reliable" acquisition. In terms of one-sided loop noise bandwidth, B_L, the $\dot{\Delta} f$ can be obtained from a modified (and simplified) version of (4-33) in [7] which, for a second-order loop and $\zeta = 0.707$, is

$$\dot{\Delta} f_{max} = 0.566 \left(1 - \frac{1}{\sqrt{SNR_L}}\right) B_L^{\,2} \text{ Hz/sec} \tag{33}$$

where SNR_L is the signal-to-noise ratio in the loop.

To find out what maximum SNR_L is available to us for the short-range sweep, let us consider the lowest P_r/N_0 consistent with our search mode. From Figure 11, one determines at 560 Hz and the range of 500 meters a P_r/N_0 value of 48 dB-Hz. Thus, for $SNR_L = 10$, the B_L can be

$$\begin{aligned} 2B_L(\text{dB}) &= \frac{P_r}{N_0}(\text{dB-Hz}) - SNR_L(\text{dB}) \\ &= 48 - 10 = 38 \text{ dB-Hz , or 6300 Hz} \end{aligned} \tag{34}$$

This value is way too wide for the problem under consideration. A more practical value would be $B_L = 100$ Hz, which is commensurate with the tracker design. With this B_L, the SNR_L is

$$\begin{aligned} SNR_L &= \frac{P_r}{N_0} - 10 \log_{10} 200 \\ &= 48 - 23 = 25 \text{ dB , or 316 value.} \end{aligned} \tag{35}$$

Substituting this into (33) and solving for the value of $\dot{\Delta} f_{max}$, we obtain

$$\dot{\Delta}f_{max} = 0.556 \left(1 - \frac{1}{\sqrt{316}}\right)(100)^2$$

$$\cong 5250 \text{ Hz/sec} \tag{36}$$

With this sweep rate and $B_L = 100$ Hz, the phase error θ_a, which develops in the loop after it acquires the signal but before the frequency sweep is terminated, is calculated to be

$$\theta_a = 1.77 \frac{\dot{\Delta}f_{max}}{B_L^2} \text{ radians}$$

$$= 1.77 \frac{5250}{(100)^2} = 0.925 \text{ radians} \tag{37}$$

This error is considered excessive and one must either reduce the sweep rate or increase the B_L.

If the former approach is taken, it is customary to reduce the $\dot{\Delta}f_{max}$ by a factor of 2 to 4*. Using a reduction of 4 as a very conservative number, the search time becomes

$$T_{ss} = \frac{\delta F}{\dot{\Delta}f} = \frac{7950 \text{ Hz}}{\frac{5250 \text{ Hz/sec}}{4}}$$

$$= 6.06 \text{ seconds} \tag{38}$$

Therefore, one concludes that the time required to detect and acquire the target will be on the order of 6 seconds.

The system margin to consider is that of required SNR_L in the loop. If one considers that (36) holds for SNR $\geq$ 10 dB, we have, according to (35), about a 15 dB margin. Assuming that we wish to keep $SNR_L \geq 13$ dB in a $B_L = 100$ Hz loop, the margin is reduced to 12 dB, which is still a reasonable value.

2.4.2.3 Long-Range Search Sequence

With the exception of a few system parameter changes, the algorithm used for the long-range acquisition is identical to that used for short short-range acquisition. Figure 20 shows both algorithms. As indicated there, the major change is the change of the slope to 4 Hz/m with the concomitant reduction of the slope to 600 MHz/sec. The modulation rate is

*Such reduction assures a 99% probability of lock-on to the line.

also reduced to 3 Hz.

Figure 23 shows the range/frequency plot for the long-range mode. The upper and lower search limits are computed to be 8.4 kHz and 1 kHz, respectively. The maximum search range for either tracker is 5.4 kHz.

Now consider the acquisition time for this mode. From Figure 11, we see that, at 1000 Hz and for R = 1850 m, the P_r/N_0 is 31 dB. For SNR = +10 dB, the maximum B_L is

$$2B_L(\text{dB-Hz}) = \frac{P_r}{N_0} - SNR_L(\text{min})$$

$$= 31 - 10 = 18(\text{dB-Hz})$$

or

$$B_L = 63 \text{ Hz.} \tag{39}$$

The maximum frequency sweep rate commensurate with this B_L and $SNR_L = 10$ is

$$\dot{\Delta} f_{max} = 0.566 \left(1 - \frac{1}{\sqrt{10}}\right)(63)^2$$
$$= 1536 \text{ Hz/sec} \tag{40}$$

The corresponding phase error after lock-up is

$$\theta_a = 1.77 \frac{\dot{\Delta} f_m}{(B_L)^2}$$

$$= 1.77 \frac{(1536)}{(63)^2} = 0.685 \text{ rads} \tag{41}$$

Reduction of this error to at least 0.5 rad will require a Δf reduction as follows

$$\Delta f = \frac{0.500}{0.685} \times 1536 \cong 1120 \text{ Hz/sec} \tag{42}$$

Further reduction of this rate by a factor of 2 will result in a sweep time of

$$T_{SL} = \frac{5400}{560} = 9.65 \text{ seconds.} \tag{43}$$

Consequently, it may be concluded that the long-range search phase will require at least 10 seconds. The SNR_L of +10 dB used in this case, however, leaves no system margin. To provide some margin for the long-range

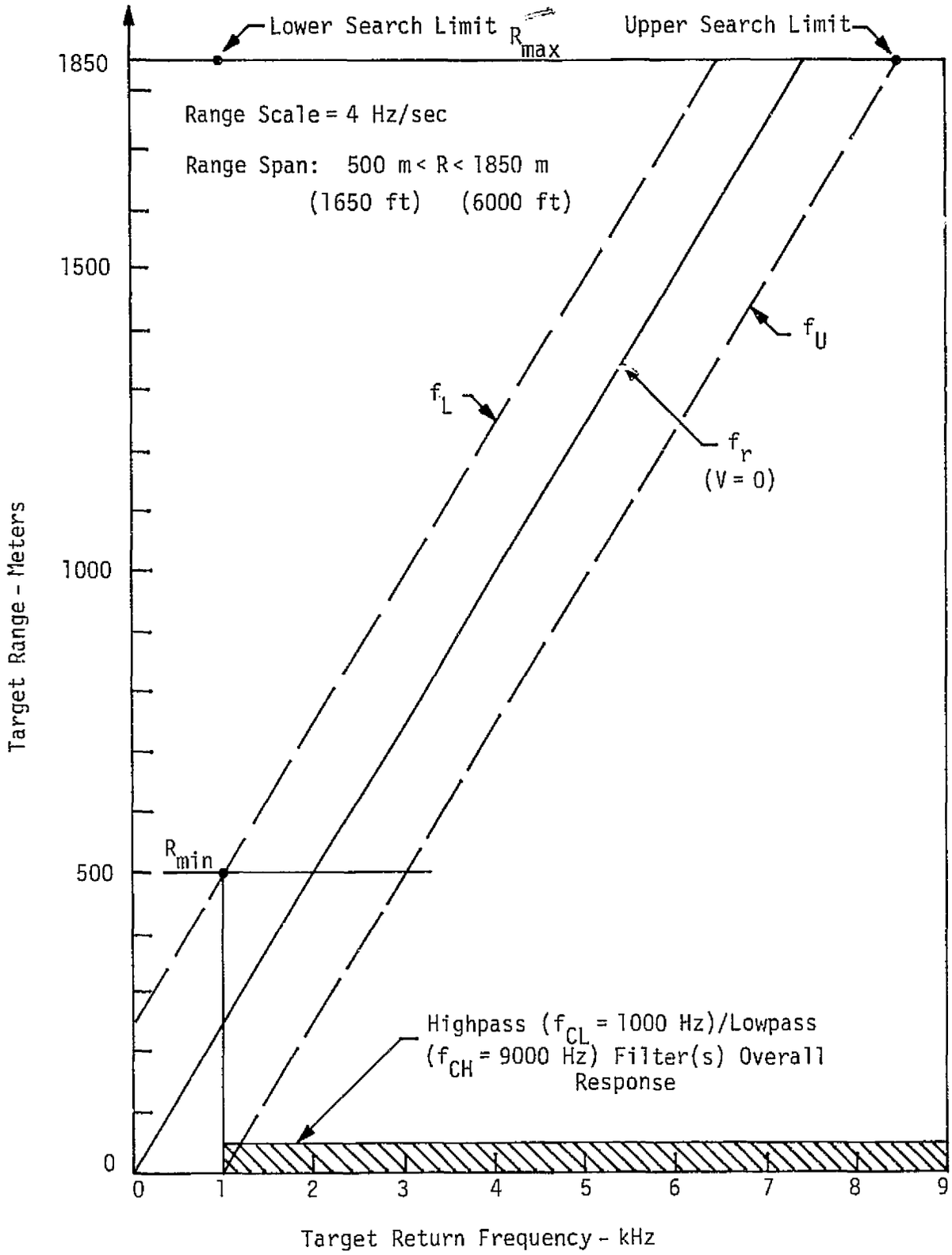

Figure 23. Range/Frequency Plot for the Long-Range Target Acquisition

acquisition phase, one should narrow the loop bandwidth. With $B_L = 50$ Hz (down from 63 Hz), the SNR_L will be +11 dB, thus providing about 1 dB of positive margin. The search time, however, will be increased accordingly to 15.3 seconds. Thus, a 16-second search time for the long-range interval should be considered as a design value.

2.5 Target Tracking

2.5.1 Tracker Design Philosophy

Once the presence of the target range/velocity tones is detected, an accurate estimate of the frequencies of these tone(s) is carried out. Then, after the appropriate scale conversion, both the range and velocity are displayed. For the case of the short-range acquisition, the signal-to-noise ratio (SNR) is sufficiently high so that a continuous tracking of either the range or velocity line does not appear necessary to improve the SNR. Consequently, unless dictated for reasons other than the random noise reduction, target tracking in the short-range mode is not mandatory. Instead, a direct frequency estimate with a frequency counter appears to be the most cost-effective method for providing the range and velocity display at short ranges. Special means to reduce the quantization error and to accommodate the stationary targets may have to be provided, however. The targets at medium and long ranges require frequency tracking to improve the SNR of the signal whose frequency is being measured and displayed as the range and velocity information. Basically, the function of the tracker is to keep the frequency of the tracked tone within some relatively narrow bandwidth, thus optimizing the SNR for the frequency measurement.

We have already discussed the trackers in Section 2.4 in conjunction with the frequency acquisition. In Figure 22 , the trackers were qualitatively represented as tunable bandpass filters whose center frequencies could be tuned to provide for a "capture" of the received target tone(s) within the bandpass of the tracker. Once such "capture" takes place, a target acquisition is declared and, subsequently, the function of the tracker is to keep the bandpass filter essentially "centered" around the line(s) of the received signal. In addition to this band-centering function, the frequency tracker must provide an output which is a close replica of the signal being tracked. This replica is then applied to the

frequency estimator(s) to determine either the range or the velocity or both for the target being tracked. Consequently, an ideal tracker should be a device capable of performing: (1) the initial target acquisition and (2) the post-acquisition tracking of the target's range/velocity tone(s).

Figure 24 shows a generic block diagram of an acquisition/tracking unit capable of performing both the initial frequency search and the subsequent tracking of either a range or a velocity tone.

As shown in the figure, the baseband frequency f_B, which may be either f_r, f_v, f_U, or f_L,* is mixed with the output signal of a voltage-controlled oscillator (VCO). This mixing process generates an intermediate frequency signal, f_I, which is applied to a bandpass filter of bandwidth B_i. During the initial target acquisition phase, the frequency of the VCO is varied according to the waveform generated by the frequency sweep circuit. The VCO frequency is varied (i.e., "swept") in such a manner that the baseband tones appearing at the output of the homodyne RF mixer (not shown in Figure 24) are sequentially applied to the bandpass filter placed at the output of the translation mixer.

When a tone does appear at the input of the bandpass filter, the envelope detector connected to the output of the filter converts the energy of the tone into a dc voltage. This dc voltage is compared against a preset threshold and, when the tone is well within the bandwidth of IF filter, the dc voltage exceeds the threshold. Such crossing of a preset threshold is an indication that a strong tone is present within the bandwidth B and, therefore, a tone acquisition can be declared.

The crossing of the tone acquisition threshold generates a Stop Frequency Search command. The purpose of this command is to terminate the frequency sweeping of the VCO before the tone is "tuned-out" of the bandpass at the f_I. Once the VCO frequency sweep is terminated, the error developed by the frequency discriminator** forces the VCO to adjust its frequency in such a manner that the tone frequency f_B is translated, after mixing, to the center of the S-curve of the discriminator. With a properly designed tracker, the center frequency of the discriminator is also a center frequency of the bandpass filter. Thus, during the

*All of these being the outputs of the homodyne RF mixer.

**The frequency discriminator action can also be implemented by a phase-lock loop (PLL) as described in Section 2.7.

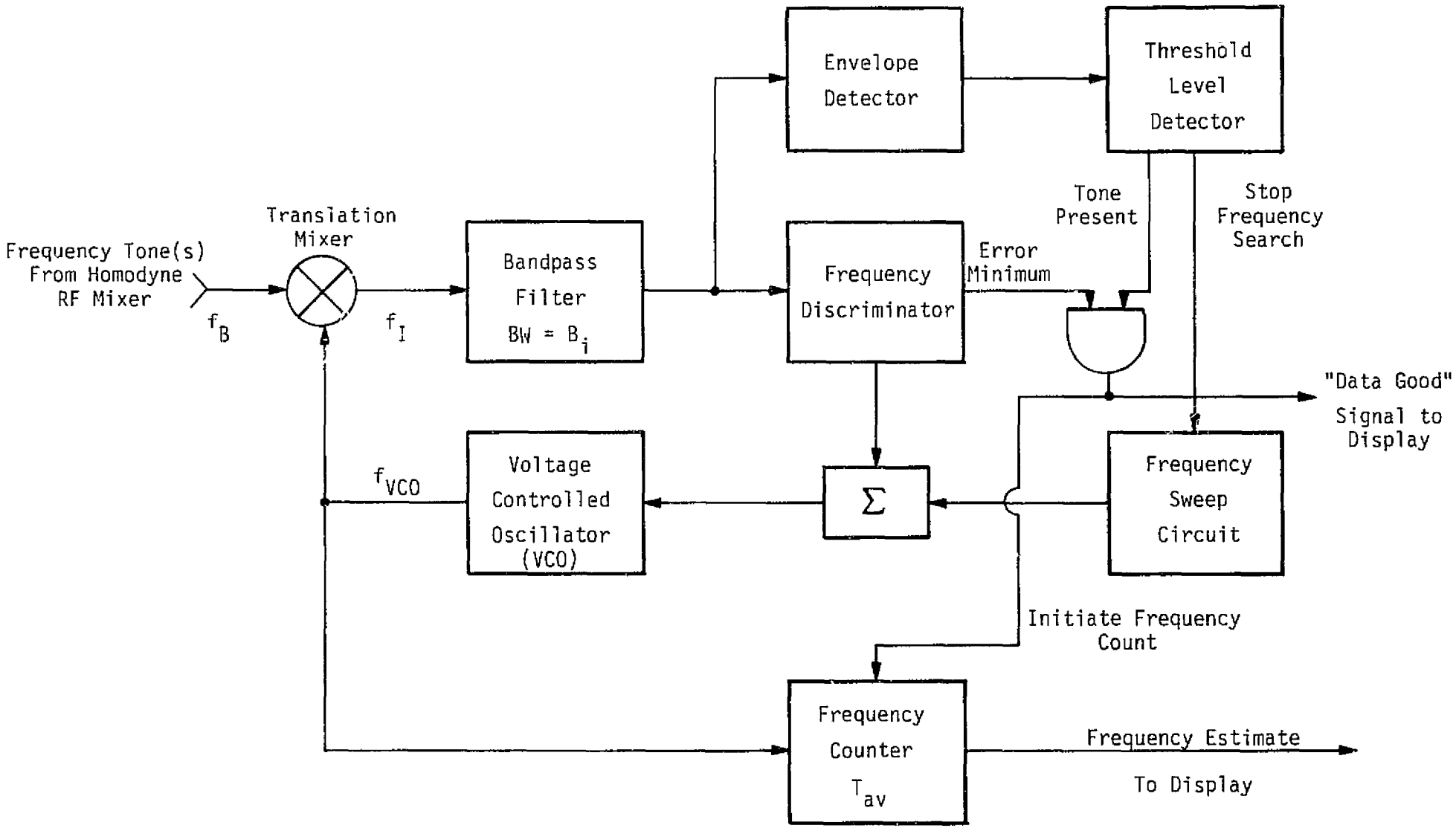

Figure 24. Generic Block Diagram of a Frequency Search and Track Unit

tracking, the SNR is optimized automatically by keeping the IF signal in the peak region of the bandpass amplitude response.

When the centering of the translated f_D is accomplished, the error developed by the frequency discriminator, or an equivalent device, falls below some minimum level, thus indicating an accurate track of the f_D. As a result of low error level, an "Error Minimum" flag* is generated by the discriminator circuit. This flag is logically "and"-ed with the "Tone Present" flag, thus forming the "Data Good" flag. The latter initiates the action of the frequency counter which then counts the VCO frequency for an averaging period of T_{av} seconds. In addition to averaging the VCO, the counter subtracts the f_I frequency from the frequency of the VCO, thus outputting the signal whose estimated frequency is

$$\hat{f}_B = f_{VCO} - f_I .$$

As the tone frequency f_B changes at the output of the RF mixer, the VCO corrects for this change and keeps the f_B translation to the f_I constant. To accomplish this, the VCO adjusts its frequency, thus providing for the tracking action of the received range/velocity tone.

If there are two tones present, such as may be the case for both f_U and f_L, the tracker can track both of them by means of time multiplexing. Such time multiplexing is possible in the case of the f_U and f_L tracking because of the nonsimultaneous generation of their frequencies at the output of the RF mixer. The time multiplexing aspects of a frequency tracker circuit are to be worked out as one of the tasks of the breadboarding phase of the radar sensor.

2.5.2 Tracker Performance Estimate

The tracker considered for the proposed system is a frequency tracker which follows the varying frequency** of the target range and/or velocity tone. The generic implementation of such a tracker was presented in the preceding paragraph. Considered below are the quantitative characteristics of such a tracker from the standpoint of random noise error.

For the case of a target whose aspect angle changes relatively slowly with respect to the radar, the central line of the return spectrum

---

*The "flag" signal is a logic level generated by the logic devices used for the control function of the radar sensor.

**Phase tracking in addition to the frequency tracking is also possible with certain tracker configurations.

has a small bandwidth (on the order of 1 Hz) and, consequently, the frequency error produced by the tracker is primarily a function of the tracker bandwidth and the SNR in this bandwidth. The SNR is, in turn, a function of the system P_r/N_0.

The rms error of a frequency tracker which works with a frequency averaging counter is approximated by the expression [8].

$$\sigma_f = \left[\frac{(0.078)\, B_T \left(1 + \frac{1}{S/N}\right)^2}{T_{av} \left(1 + S/N\right)^{1/2}} \right]^{1/2} \tag{44}$$

where

σ_f = rms frequency error in Hz

B_T = tracker one-sided noise bandwidth

T_{av} = averaging time of the counter

S/N = signal-to-noise ratio in the two-sided bandwidth of the tracker.

Figure 25 shows the plot of σ_f versus P_r/N_0 for several values of tracker bandwidth. The averaging time is 0.5 sec for all of the plots shown in that figure.

The range of values of P_r/N_0 shown in Figure 25 is typical for a target at the far end of the system range, i.e., at 1200 m to 1850 m (see Figure 11).

Furthermore, the averaging period of 0.5 seconds is characteristic of the proposed system owing to the requirement for updating both the range and velocity readings at 1-second intervals. Specifically, if the range and velocity are obtained by measuring (i.e., tracking) f_U and f_L, only 0.5 seconds are available for estimating the value of each of these frequency components. Consequently, at the end of a 1-second interval, there are two frequency tracker outputs available, each with its own σ_f. The resultant error for the composite (derived) frequency estimate of either the f_r or f_v tone is

$$\sigma_{f_r} = \sigma_{f_v} = \frac{\sqrt{\sigma_{f_U}^{\,2} + \sigma_{f_L}^{\,2}}}{2} \tag{45}$$

For the case where the system operation is in the relatively "flat" portion of the flicker noise and when the separation between f_U and f_L is

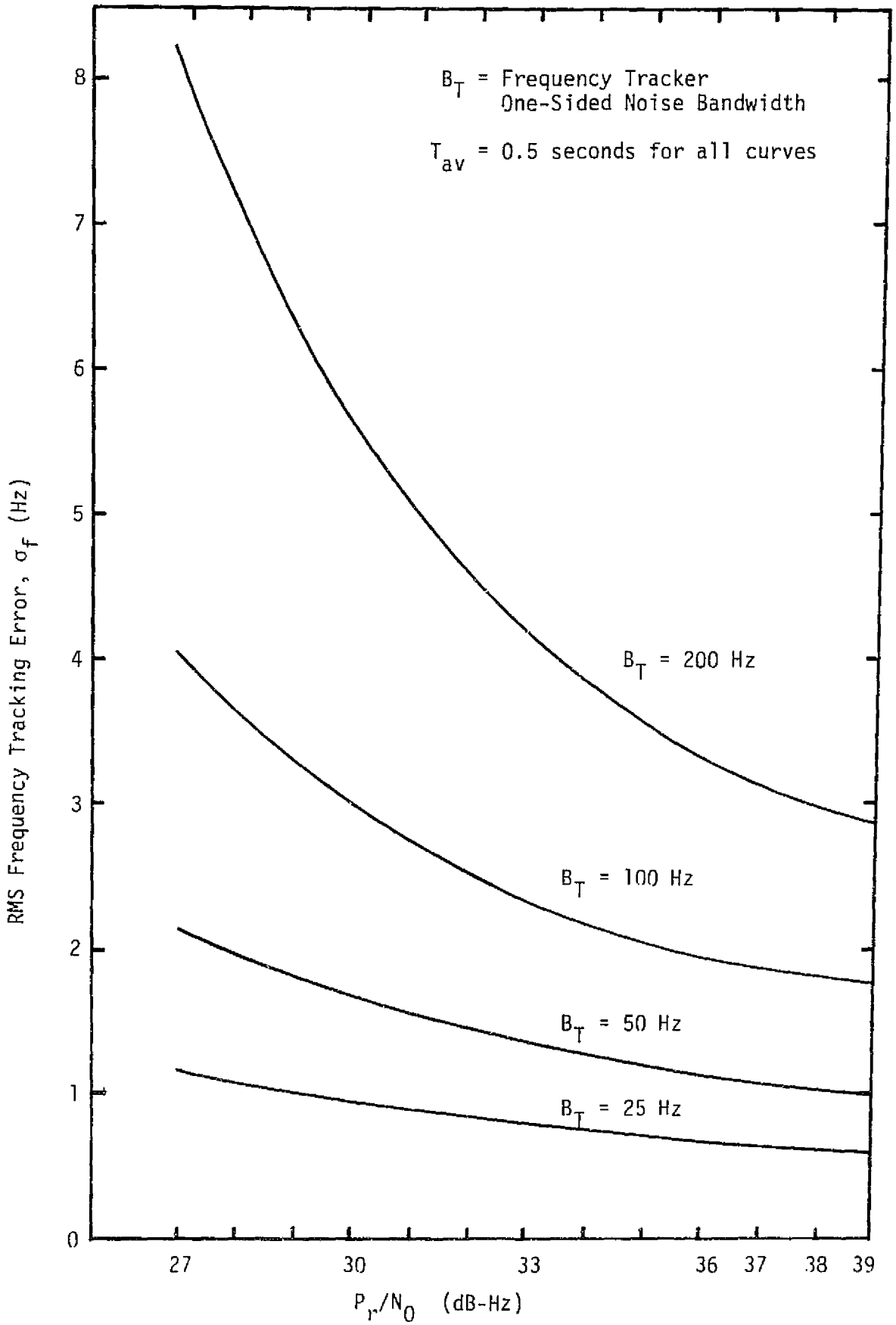

Figure 25. RMS Frequency Tracking Error σ_f versus P_r/N_0 and Tracker Bandwidth (T_{av} = 0.5 seconds)

small, the above expression can be approximated by $\sigma_{f_r} = \sigma_{f_v} = \sigma_f/\sqrt{2}$, where σ_f is computed by taking the average value of the $P_r/N_0(t)$ between f_U and f_L with reference to the data in Figure 11.

2.6 System Error Budget Estimate

For estimating the total error budget for the radar ranging and velocity measuring system, the following generic types of errors must be considered:

(1) Errors caused by system parameter values variation.

(2) Errors caused by the inherent properties of the modulation technique selected for the range/velocity measurement.

(3) Errors caused by the random noise fluctuations at the input stages of the receiver.

The first type of error is generally referred to as the "bias" error because the rates of fluctuations for the bias error range from minutes to hours (i.e., like the thermal drift of an oscillator); these errors can be corrected, at least in principle, by self-calibration. The errors caused by the modulation techniques are known as "quantization" errors; the methods for their correction or reduction consist of adding certain refinements to either the modulation method itself or to the method of modulation recovery. Finally, the random noise fluctuation is one of the most fundamental and, consequently, the methods for its control involve such fundamental parameters as those included in the power budget, system noise and averaging time of the parameter measurement.

In addition to the aforementioned sources of the system-originated errors, there are errors due to the target. These are called the target effects errors. However, because, at this point in time, the physical characteristics of the sensor's targets have not been established, the error estimates presented below do not include the target effects.

2.6.1 Ranging Errors

2.6.1.1 Random Noise Error

The worst-case random noise error is at the maximum range of the radar operation. This error can be estimated using the data presented in Figures 11 and 25.

From Figure 11, we determine that, for $R = 1850$ m (6000 ft), the $P_r/N_0(f) \cong 32$ dB at 7400 Hz.*

---

*This is the range tone corresponding to a target at 1850 m with the range scale of 4 Hz/m: $f_r = 4 \times 1850 = 7400$ Hz.

Assuming the tracker bandwidth of 50 Hz, we then determine from Figure 25 that the corresponding $\sigma_f = 1.4$ Hz for the 0.5 second interval. For two consecutive estimates, the rms range error is $\sigma_{fr} = 1.4/\sqrt{2} \approx 1.0$ Hz. Converting to range error

$$\sigma_r = \sigma_{fr} \times \frac{1}{A_R} = 1 \text{ Hz} \times \frac{1}{4 \text{ Hz/m}} = 0.25 \text{ m} > 0.20 \text{ m } (0.66 \text{ ft}) \qquad (46)$$

Thus, we see that, with a 50 Hz tracker bandwidth, the system accuracy is not met at the maximum range.

One method to reduce this error would be to narrow the tracker bandwidth. This, however, will make the tracker behavior "sluggish" with respect to target dynamics. An alternate approach would be to let $1\sigma = 0.33$ m (1.1 ft) at $R = 1850$ m. With a 50 Hz tracker bandwidth, this would allow a 3 dB margin in system operation. Thus, at a shorter range, i.e., ~ 1500 m, where the signal increases by at least 3 dB, one can reinstate the original $1\sigma = 0.20$ m for $R \leq 1500$ m (4920 ft). We will use this argument in suggesting specification modification for the breadboard model.

2.6.1.2 Range Quantization Error

The quantization error stems from the fact that, with a periodic modulation waveform such as that shown in Figure 5, the averaging counter can read only those values of the range frequency which are multiples of the modulation frequency f_m. To determine the magnitude of the quantization error, consider the expression for the range frequency. For this, we repeat (1a):

$$f_r = \frac{4Rf_m \Delta F}{c} \qquad (47)$$

But, because of the aforementioned restriction on the values of the range frequencies, $f_r = nf_m$. Substituting the latter relationship into (47) and rearranging terms, one obtains

$$R = n \frac{c}{4\Delta F} \qquad (48)$$

But we can also state that the counter can output an adjacent frequency line which will represent a different range:

$$R' = (n \pm 1) \frac{c}{4\Delta F} \qquad (49)$$

The maximum range quantization error is thus obtained by subtracting (48) from (49):

$$\Delta R_q = \left|(n\pm1) - n\right| \frac{c}{4\Delta F} = \frac{c}{4\Delta F} \tag{50}$$

Equation (50) represents the maximum quantization error. The average error will thus be one-half of that, i.e.,

$$\overline{\Delta R_q} = \frac{c}{8\Delta F} \tag{51}$$

With our baseline assumption of $\Delta F = 100$ MHz, the $\overline{\Delta R_q}$ becomes

$$\overline{\Delta R_q} = \frac{3 \times 10^8}{8 \times 100 \times 10^6} = 0.38 \text{ m } (1.25 \text{ ft}) \tag{52}$$

This error exceeds the specification value of 0.2 m. Furthermore, it is independent of range and thus does not diminish at closer ranges. The quantization error, however, applies only to the direct counter readings of the range frequency. If the range tone is first frequency-tracked, as described in the preceding paragraphs, then applied to an averaging counter, the quantization can be reduced [2] by a factor of at least 5 [8]. This means a $\overline{\Delta R_q}$ of 0.08 m (0.26 ft), which is well below the specified value of $1\sigma = 0.2$ m (0.66 ft).

The potential reduction of the quantization error provided by the frequency tracker/counter combination suggests that, at short ranges, such frequency tracking may have to be used to meet the range accuracy specifications. Such use differs from the use of a tracker for the purpose of the signal-to-noise ratio improvement as in the case for the long-range targets.

2.6.1.3 Modulation Format Error

The modulation format error consists of the variation in either the frequency deviation ΔF or the modulation period T_m, or both. The effect of either one of these parameters, or of the combination thereof, changing with time and/or temperature results in a change in the frequency sweep slope. Because, with an FM CW radar, the sweep slope determines the range reading, the slope error results in a range error. The relationship

between the slope error and the range error is

$$\Delta R = \left(\frac{\Delta S}{S}\right) R \tag{53}$$

where

ΔR = range measurement error

S = FM-CW modulation waveform slope, in MHz/sec

R = target range

ΔS = slope error, in MHz/sec

It is important to emphasize here that the slope error considered in this case is not a nonlinearity error, such as a deviation from a straight line, but the error in the slope as defined by end points of ΔF and the T_m parameters. As pointed out in Appendix D, the shape of the modulation waveform does not affect the average range reading as long as the end points defining S are constant. Thus, it is the effect of the end points errors on the ΔS that we are defining here.

Figure 26 shows graphically how the timing error δT and the frequency deviation error δf alter the slope of the nominal waveform ① defined by $\Delta F/(T_m/2)$ or $\Delta F/t_m$. As shown in the case of waveform ②, the error is in timing only. In the case of waveform ③, both timing and frequency deviation errors are present.

To define quantitatively the effect of δf and δT, consider the worst-case slope error occurring when

$$S' = S + \Delta S = \frac{\Delta F + \delta F}{t_m - \delta t} \tag{54}$$

The right-hand side of (54) can be expanded as follows:

$$\frac{\Delta F + \delta f}{t_m - \delta t} = \left(\frac{\Delta F}{t_m} + \frac{\delta F}{t_m}\right) \frac{1}{\left(1 - \frac{\Delta T}{T}\right)} = \left(\frac{\Delta F}{t_m} + \frac{\delta F}{t_m}\right) \left[\sum_{k=0}^{\infty} \left(\frac{\delta t}{t_m}\right)^k\right]$$

$$= \left(\frac{\Delta F}{t_m} + \frac{\delta F}{t_m}\right) \left[1 + \frac{\delta t}{t_m} + \left(\frac{\delta t}{t_m}\right)^2 + \ldots\right] \tag{55}$$

Neglecting the higher-order terms, one can reduce the above equation to the following four terms:

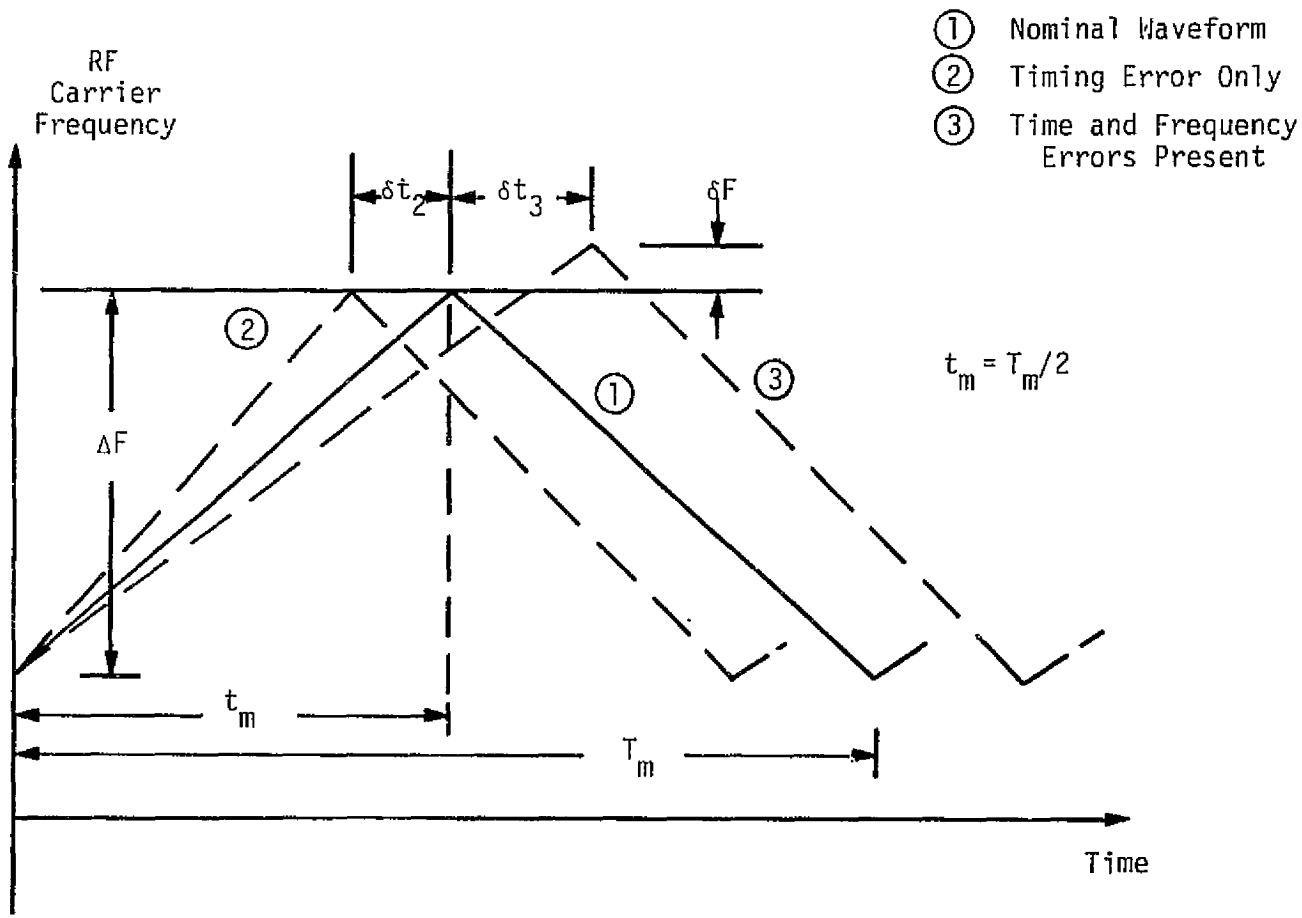

Figure 26. Timing and Carrier Frequency Deviation are the Potential Causes of the Modulation Format (Slope) Error

$$S + \Delta S = \underbrace{\frac{\Delta F}{t_m}}_{S} + \underbrace{\frac{\delta F}{t_m} + \frac{\Delta F\ \delta t}{t_m^{\ 2}} + \frac{\delta F\ \delta t}{t_m^{\ 2}}}_{\Delta S} \tag{56}$$

Dividing both sides by S, one obtains

$$\frac{\Delta S}{S} = \frac{\delta F}{F} + \frac{\delta t}{t_m} + \frac{\delta F\ \delta t}{\Delta F\ t_m} \tag{57}$$

The last term in (57) can be neglected because, for a reasonably accurate system, this term will be negligible compared to the other two terms on the right-hand side of the equation. Therefore, we finally obtain the desired result, i.e.,

$$\frac{\Delta S}{S} = \frac{\delta F}{F} + \frac{\delta t}{t_m} \tag{58}$$

The significance of (58) is that it tells us that the fractional slope error is simply a sum of the fractional errors in the ΔF and t_m parameters.

As described in Section 2.7.1 dealing with the implementation of the frequency modulation, the accuracy of both ΔF and t_m will be determined by a 16-bit binary digital counter. The accuracy of such control is $1/2^{16}$. Therefore, the effect of the slope error on the range accuracy at the maximum range of 1850 m (6000 ft) can be calculated:

$$\Delta R = \left(\frac{1}{2^{16}} + \frac{1}{2^{16}}\right) 1850 \text{ m} = \left(\frac{2}{65{,}536}\right) 1850$$

$$= 0.056 \text{ m or } 5.6 \text{ cm } (0.185 \text{ ft})$$

This bias error is relatively small compared to the 1σ value of 20 cm (0.67 ft) specified for the ranging error. Furthermore, any significant changes in δF and δt will be sensed and corrected for by the system control microprocessor.

2.6.2 Velocity Errors

2.6.2.1 Random Noise Velocity Error

The estimate of the velocity error due to random noise proceeds along the same lines as that of the range error. The only difference is

the conversion factor from σ_f to σ_v. Specifically, if we use the same number as in the previous example of range accuracy estimate, we obtain $\sigma_{fv} \approx 1.0$ Hz. Converting this to the velocity error, we obtain

$$\sigma_v = \sigma_{fv} \times \frac{1}{A_v} = 1.0 \times \frac{1}{160 \text{ Hz/m/sec}} \tag{59}$$

$$= 0.00625 \text{ m/sec } (0.021 \text{ ft/sec})$$

This estimated value is better than the $1\sigma = 0.01$ m/sec (0.033 ft/sec) specification value.* Converting the difference between the estimated σ_v and the specification value, one observes, using the curve for $B_T = 50$ Hz in Figure 26, that there is about +5 dB margin available in system performance at the far range.

2.6.2.2 Velocity Quantization Error

Similar to the generation of the range quantization error, the periodic nature of the linear FM-CW waveform gives rise to the velocity quantization error. Therefore, the reasoning used for obtaining the velocity quantization error is analogous to the one used for the derivation of the range quantization error. Let us recall the familiar expressions for doppler frequency due to target motion:

$$f_d = \frac{2 f_0 v}{c} \tag{60}$$

where v is the target velocity (m/sec), f_0 is the carrier frequency (Hz) and c is 3×10^8 (m/sec). Solving for an estimate of v, i.e., $\hat{v}$, we obtain

$$\hat{v} = \frac{c}{2 f_0} \widehat{f_d} \tag{61}$$

The general expression for the quantization error thus follows:

$$\Delta\hat{v} = \frac{c}{2 f_0} \widehat{\Delta f_d} \tag{62}$$

where $\widehat{\Delta f_d}$ is the error caused by the line structure of the $\widehat{f_d}$ return. Because the line structure is related to f_m and, on the average, the quantization is to the nearest line, we have

---

*A tracker bandwidth of 50 Hz is assumed, as in the case of the range noise.

$$\widehat{\Delta_{fb}} = \frac{1}{2T_m} \tag{63}$$

Substitution of (63) into (62) results in

$$\widehat{\Delta v} = \frac{c}{4 f_0 T_m} \tag{64}$$

But

$$S = \frac{F}{T_m/2} = \frac{2\Delta F}{T_m}$$

and

$$\frac{1}{T_m} = \frac{S}{2\Delta F} \tag{65}$$

Again, substituting (65) into (64), we obtain the required expression:

$$\widehat{\Delta v} = \frac{S}{f_0} \left(\frac{c}{8\Delta F}\right) \tag{66}$$

This equation is similar to (51) for the range quantization error. The important difference, however, is the direct proportionality of the velocity error on the frequency sweep slope S.

Using (66), let us evaluate the magnitude of the velocity quantization error for FM slopes of S = 600 MHz/sec and 2400 MHz/sec. These slopes correspond to long-range and medium/short-range acqusition modes respectively. For both of these slopes, f_0 = 24 GHz and ΔF = 100 MHz.

Case 1: S = 600 MHz/sec

$$\Delta v_1 = \frac{S}{f_0} \left(\frac{c}{8\Delta F}\right) = \frac{600 \times 10^6}{24 \times 10^9} \frac{(3 \times 10^8)}{(8 \times 100 \times 10^6)} \tag{67}$$

$$= 0.0094 \text{ m/sec } (0.031 \text{ ft/sec})$$

Case 2: S = 2400 MHz/sec

$$\Delta v_2 = 4\,\Delta v_1 = (4)(0.0094) = 0.0375 \text{ m/sec } (0.123 \text{ ft/sec}) \tag{68}$$

The results above are rather interesting because they show that, for the long-range mode, the quantization error is less than the specified velocity error and yet, for the medium- and short-range modes, the quantization error exceeds the specified accuracy.

This result requires that methods for reducing quantization error

at the medium ranges and particularly at the short ranges be employed. Frequency tracking in combination with frequency counting will reduce the quantization error by a factor of at least 5. Thus, at short and medium ranges, the tracking is expected to reduce the quantization error to less than 0.0075 m/sec (0.0246 ft/sec) which is within the specification.

An alternate technique would be to modify the modulation waveform to include intervals of unmodulated CW transmission. During these intervals, the velocity estimation can be performed without any quantization errors. Implementation considerations for the utilization of this approach are presented in Section 2.7.

2.6.2.3 Transmitter Frequency Shift Effects

Consider now the effect of the transmitter frequency variation on the accuracy of the velocity measurement. Such frequency variations may be caused primarily by temperature changes in the sensor environment.

Let us start with the conventional expression for the doppler frequency due to target motion with velocity v:

$$f_d = f_0 \left(\frac{2v}{c}\right) \tag{69}$$

where f_0 is the initial, unchanged value of the transmitter frequency.

When the transmitter frequency changes by an amount equal to Δf, a different doppler frequency appears at the output of the receiver mixer:

$$f_d' = \left(f_0 + \Delta f\right)\left(\frac{2v}{c}\right) = f_0 \left(\frac{2v}{c}\right)\left[1 + \frac{\Delta f}{f_0}\right] \tag{70}$$

From (70), it is evident that the change in the doppler frequency is proportional to the normalized frequency drift of the transmitter frequency. Rewriting (70) in a form which shows the apparent velocity change, we obtain

$$f_d' = f_0 \left(\frac{2}{c}\right)\left[v + v\left(\frac{\Delta f}{f_T}\right)\right] = f_0 \left(\frac{2}{c}\right)\left[v + \Delta v\right] \tag{71}$$

Equation (71) indicates that the apparent velocity change (i.e., the error) is proportional not only to the normalized transmitter frequency drift but also to the velocity itself. Using this relationship, we can solve for the allowable normalized frequency drift at the maximum

velocity of 6.1 m/sec (20 ft/sec).

$$\Delta v = 0.03 \text{ m/sec} = 6.1 \text{ m/sec} \left(\frac{\Delta f}{f_0}\right)$$

or

$$\frac{\Delta f}{f_0} = \frac{0.03}{6.1} = 0.005 \text{ or } 0.5\% \tag{72}$$

For a carrier frequency of 24,000 MHz (24 GHz), this corresponds to a maximum Δf of about 120 MHz. A frequency drift of an unstabilized varactor-tuned, wideband Gunn diode VCO may be 1 MHz/°C. This means that the device temperature can vary over the temperature range of 120°C (say, from -40°C to +80°C) without causing the velocity uncertainty to get out of specified tolerance range.

Temperature compensation of the oscillator, if required by more severe environmental conditions, can reduce the drift by a factor of 5 to 10, thus permitting operation over the extended range.

For the breadboard model of the radar, the environmental temperature variation is not expected to be a problem. Also, self-calibration techniques utilizing a stable crystal oscillator will be considered during the breadboard phase to insure that the future space-qualified model of the sensor possesses adequate stability for operation in a space-type environment.

2.6.3 Range and Velocity Error Summary

Tables 7 and 8 present the summary of the ranging and velocity errors, respectively.

Table 7. Range Measurement Errors

Error Source	1σ Error		
	Fixed Random	Fluctuating (Noise)	Comments
Random Error	--	0.25 m (0.82 ft) (R = 1850 m)	This error is for the maximum range of 1850 m. At a range of 1240 m (4067 ft), this error is 0.18 m (0.59 ft)
Quantization ΔF = 100 MHz	0.08 m (1.25 ft)	--	Frequency tracking is utilized for minimizing the quantization error.
Modulation Format Error (Slope)	0.056 m (0.185 ft)	--	Modulation slope is calculated from monitored values of ΔF and t_m.

$$\text{Total RMS } (\sigma_R) = \sqrt{(0.25)^2 + (0.08)^2 + (0.056)^2} = 0.268 \text{ m } (0.88 \text{ ft}) \text{ at } 1850 \text{ m } (6000 \text{ ft})$$

Table 8. Velocity Measurement Errors

Error Source	1σ Error		
	Fixed Random	Fluctuating (Noise)	Comments
Transmitter Frequency (0° to 70°S)	0.00029 V (For V = ±6.1 m/sec ΔV = 0.00177 m/sec)	---	Temperature coefficient of 0.1 MHz/°C nominal temperature range (0 to 70°C) assumed for breadboard. Low temperature compensation coefficient achieved by temperature compensation and self-calibration
Quantization S = 600 MHz/sec ΔF = 100 MHz	0.0019 m/sec (0.00623 ft/sec) 0 (due to CW)	---	1. Triangular waveform modulation and tracking used for range interval of 200 m to 1850 m. 2. For 0 < R < 200 m, triangular waveform alternates with CW at 50% duty cycle.
Random Error (Flicker Noise)	---	0.00625 m/sec (R = 1850 m)	At maximum range with tracker bandwith (one-sided, noise bandwidth) of 50 Hz.
Data Processing	Negligible	Negligible	Double-precision (16-bit) processing keeps this error at a negligible level.

$$\text{Total RMS } (\sigma_V) = \sqrt{(0.00625)^2 + (0.0019)^2 + (0.0029V)^2}$$

$$\text{For } \left\{ \begin{array}{l} V = \pm 6.1 \text{ m/sec (max)} \\ R = 1850 \text{ m (max)} \end{array} \right\} \sigma_V = 0.007 \text{ m/sec } (0.022 \text{ ft/sec})$$

2.7 Implementation Details

The designs and implementation trade-offs to synthesize several of the critical radar functions presented in the report are discussed in this section. In general, the designs reflect the motivation to achieve a small, lightweight radar that is relatively inexpensive yet meets NASA's performance goals. The most critical of the radar functions and, consequently, the ones discussed here are frequency modulation synthesis, FM sweep waveform generation, audio amplification (zero IF), and frequency/phase tracking.

2.7.1 Frequency Modulation Synthesis

The originally proposed method for linearly sweeping the Gunn oscillator, as shown in Figure 27, has been studied in detail. As a review, the method of sweeping the Gunn oscillator is to change the divider index in the phase-locked Gunn oscillator loop in small steps. Thus, from Figure 28, it can be seen that, if the divider index is changed from N to N+1, the frequency output of the divider will change from $Nf_0/N = f_0$ to $Nf_0/(N+1)$. Since the output of the divider must be equal to f_0, the Gunn VCO must change frequency by $N/(N+1)f_0$ for the loop to stay in lock. By adjusting the response time of the loop, e.g., narrowing the loop bandwidth, the VCO frequency can be made to change "smoothly," thus approximating a linear ramp. This principle is illustrated in Figure 29. The corresponding time history of the divider index is shown in Figure 30.

The size of the divider index step change must be chosen carefully. Too large a change will cause the loop to lose lock. Reference to Figure 4 of Appendix C shows that, for a step change in counter index, the frequency changes approximately linearly for a normalized time given by

$$\omega_n t \leq 0.5 \tag{73}$$

where ω_n is the loop undamped natural resonant frequency. Reference to Figure 3 of Appendix C shows that the normalized loop error at this value of time is

$$\frac{\omega_n}{\delta\omega}\theta = 0.25 \tag{74}$$

where $\delta\omega$ is the magnitude of the frequency step and θ is the loop error.

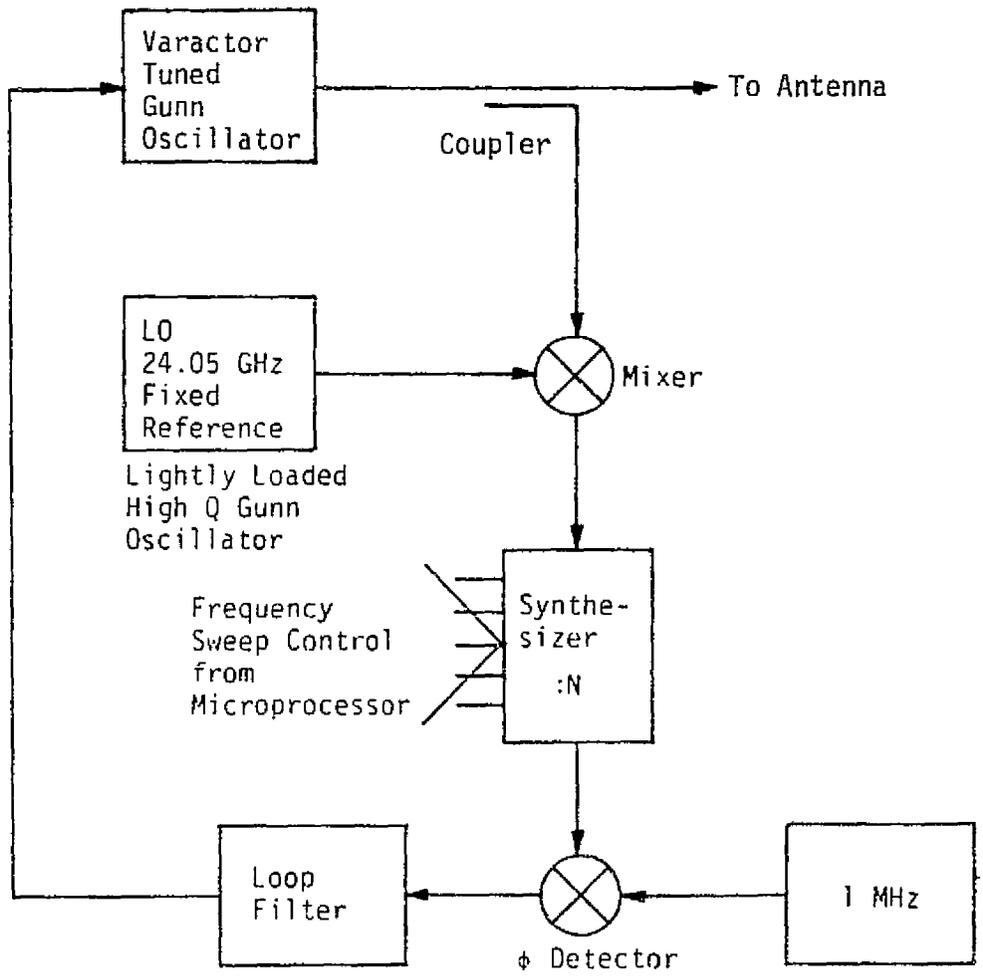

Figure 27. Originally Proposed Implementation of FM-Ramp CW Modulation

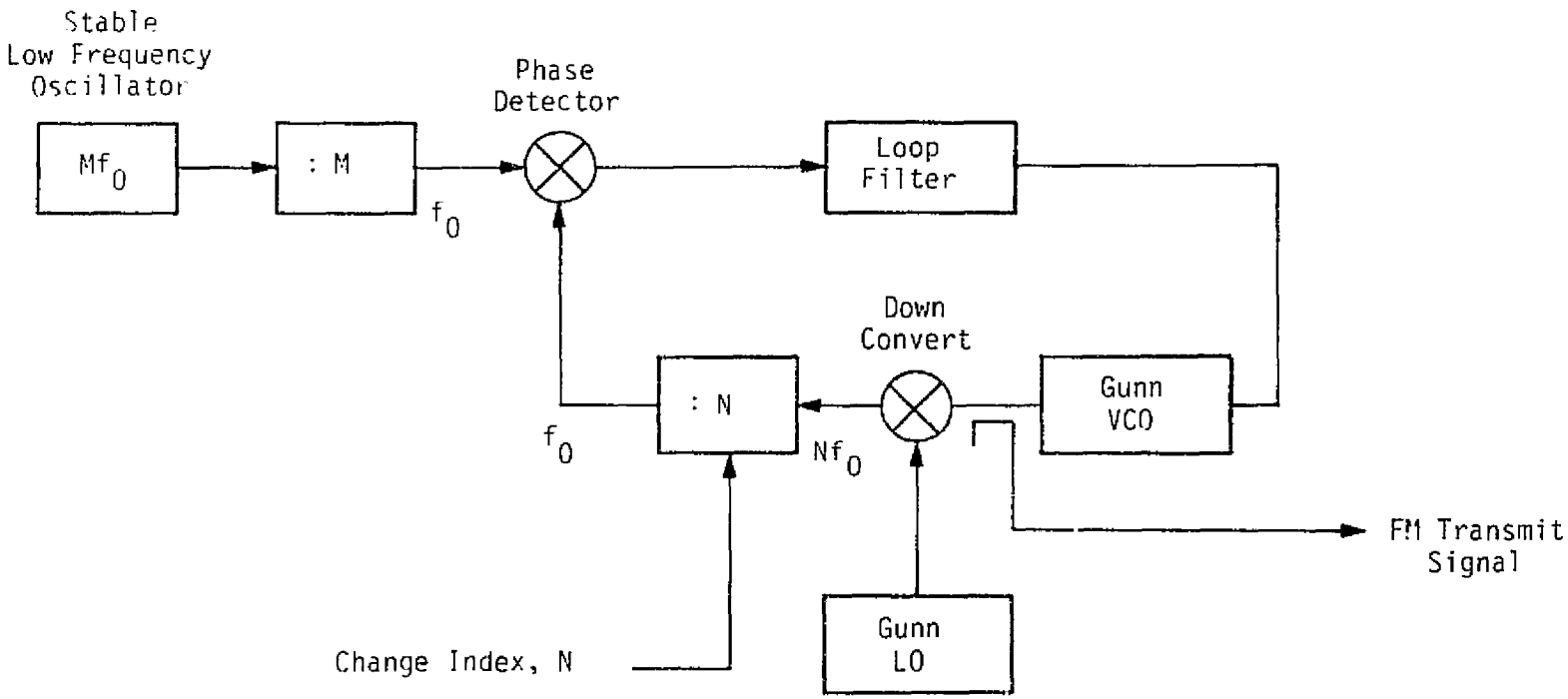

Figure 28. Model of Frequency Stepper

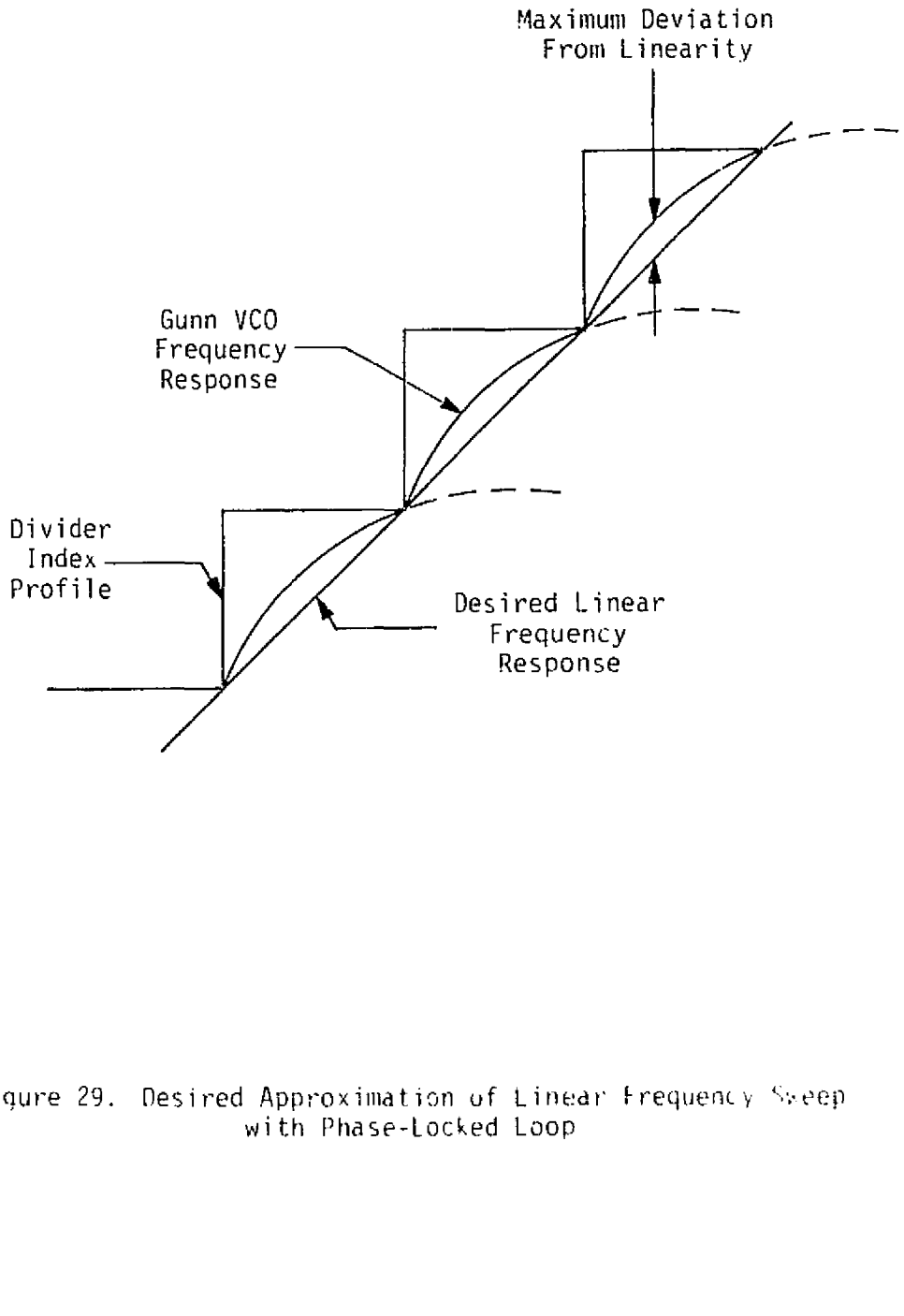

Figure 29. Desired Approximation of Linear Frequency Sweep with Phase-Locked Loop

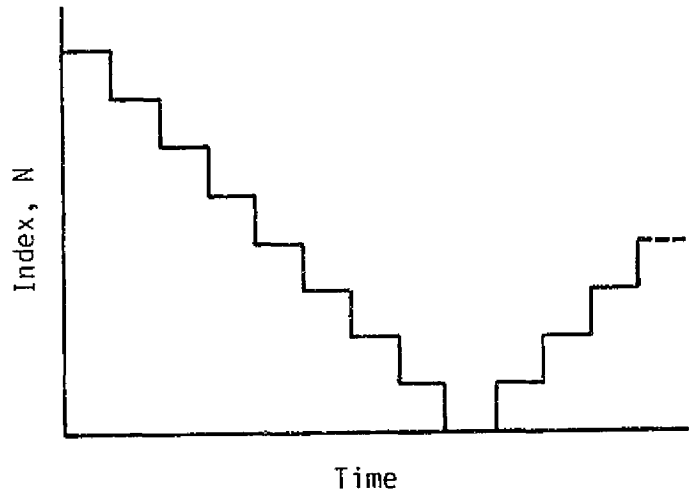

Figure 30. Time History of Divider Index for "Sawtooth" Sweep

The time t is related to the number of steps by

$$t = \frac{T}{N} \tag{75}$$

where T is the time duration of the linear ramp and N is the number of steps or counter index changes. Similarly,

$$\delta\omega = \frac{\Delta\omega}{N} \tag{76}$$

where $\Delta\omega$ is the total frequency excursion for the linear ramp (or sawtooth). If $\theta = 1$ radian is allowed (loop will remain locked because of no noise), and (73), (75), and (76) are substituted into (74), the number of steps, N, is found to be given by

$$N = \sqrt{\frac{\Delta\omega T}{2}} \tag{77}$$

For the case of $T = 1/6$ second and $\Delta f = 100$ MHz, N is found to be approximately 7000 steps. Thus, considering the highest practical input frequency to a divider network to be 500 MHz, the stable oscillator reference frequency is found to be $f = (500\ \text{MHz})/7000 = 71$ kHz. Since the divide index must change 7000 times in 1/6 of a second, the detailed design of this technique must be investigated further.

The preceding discussion of Gunn oscillator frequency sweep generation was based on a requirement for a linear sweep. However, it has been shown in Appendix D that, with certain restrictions, the sweep shape does not affect the accuracy of the range measurement. The restrictions are that the sweep function must be monotonically increasing and that, at time T, the frequency must be equal to Δf Hz, where $\Delta f/T$ is the slope used for the accuracy calculations. This fact has led to the frequency sweep implementation shown in Figure 31.

This technique differs from the previous one inasmuch as this technique is an open-loop sweep of the varactor-tuned Gunn oscillator. The previously discussed technique is a closed-loop technique. The principle of operation of this technique is as follows. A linear ramp voltage is applied to the tuning terminals of the Gunn oscillator, causing the frequency to sweep more or less linearly. The linearity depends

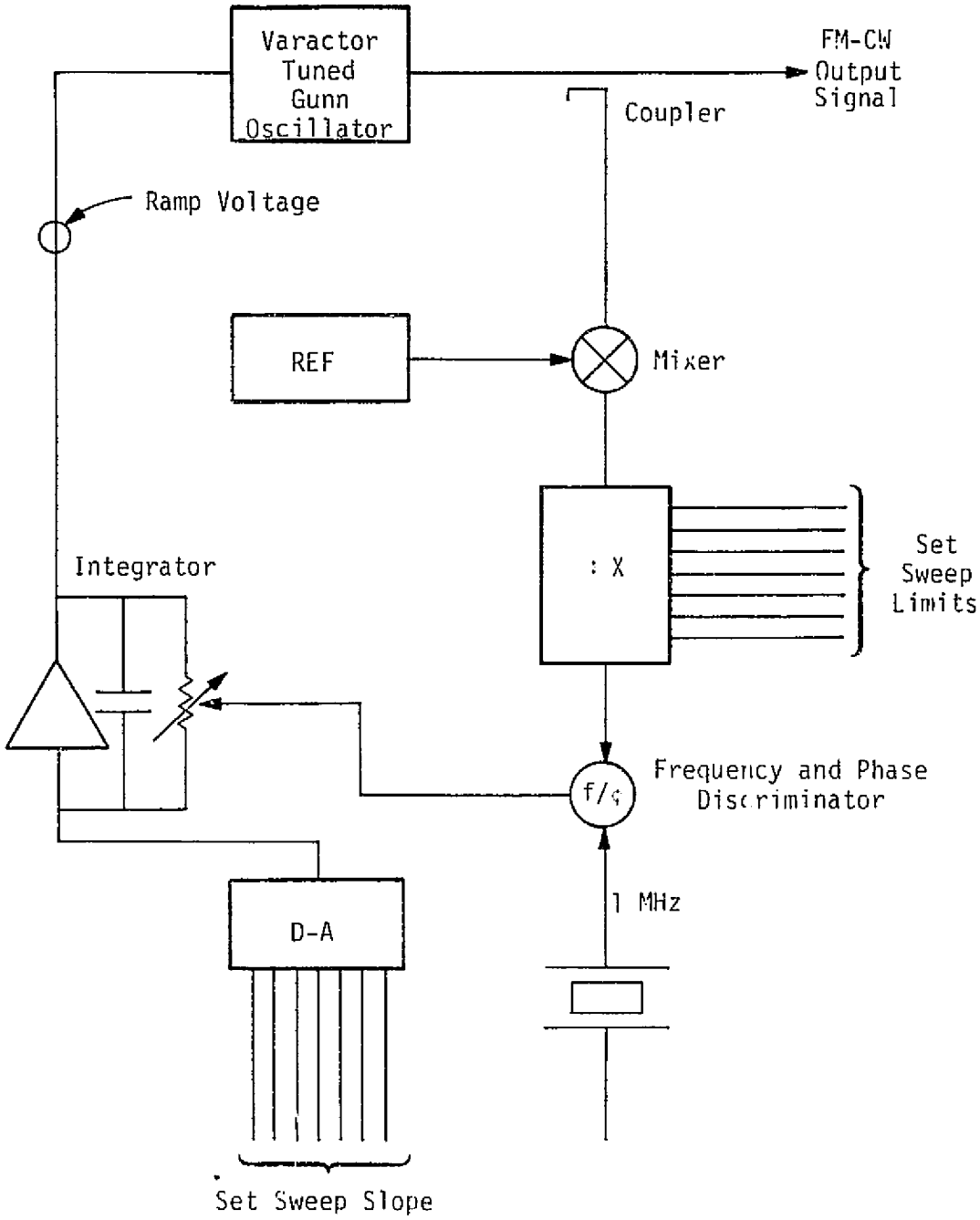

Figure 31. Alternate Sweep Generation Technique

on the frequency versus voltage tuning curve for the Gunn oscillator. The output of the Gunn is mixed with an LO Gunn so that a maximum frequency of approximately 500 MHz is applied to the counter input. The output of the divider is fed to a phase-locked frequency tracker or discriminator. A 1 MHz stable reference is also fed into the discriminator. This discriminator has the characteristics shown in Figure 32. When the input frequency to the tracker from the divider output reaches ΔF, the output voltage saturates. At this point, a logic-generated pulse is applied to the circuit that is generating the sweep voltage. This pulse dumps the integrator, causing the sweep to stop and, at the same time, applies a voltage of the opposite polarity to the input of the integrator. This causes the sweep to start in the opposite direction, but with the same slope. The slope is determined by the magnitude of the voltage applied to the integrator. This is easily adjusted by means of the digital-to-analog converter (DAC). The sweep limits are adjusted by picking the appropriate divider index.

The two frequency sweep techniques discussed above are designed to precisely control the sweep modulation slope by precisely setting ΔF and ΔT. An alternate approach is to allow the slope to be less precise and accurately measure the actual slope by independently measuring ΔF and ΔT. A functional block diagram of this approach is shown in Figure 33. A waveform generator is used to generate the triangular waveform that tunes the varactor-tuned Gunn oscillator. The result is that the total frequency deviation of the sweep is nominally the design value and the time intervals of the up and down sweep are nominally the design values. However, the counter is used to accurately measure each time interval during the sweep so that ΔT is precisely known. At the peak of the sweep, the counter stops measuring the time interval and measures the peak frequency. Thus, ΔF is precisely known and, consequently, the slope $S = \Delta F/\Delta T$, is precisely known. This information is utilized by the microprocessor to convert the beat note to range data. Details of the waveform generator are discussed in Subsection 2.7.2.

A counter with a binary resolution of 18 bits is required to represent the maximum sweep interval of approximately 167,000 μsec and ΔF of 100 MHz. However, since only 16 bits are utilized by the microprocessor, a 2.55 μsec time resolution and a 1500 Hz frequency resolution result.

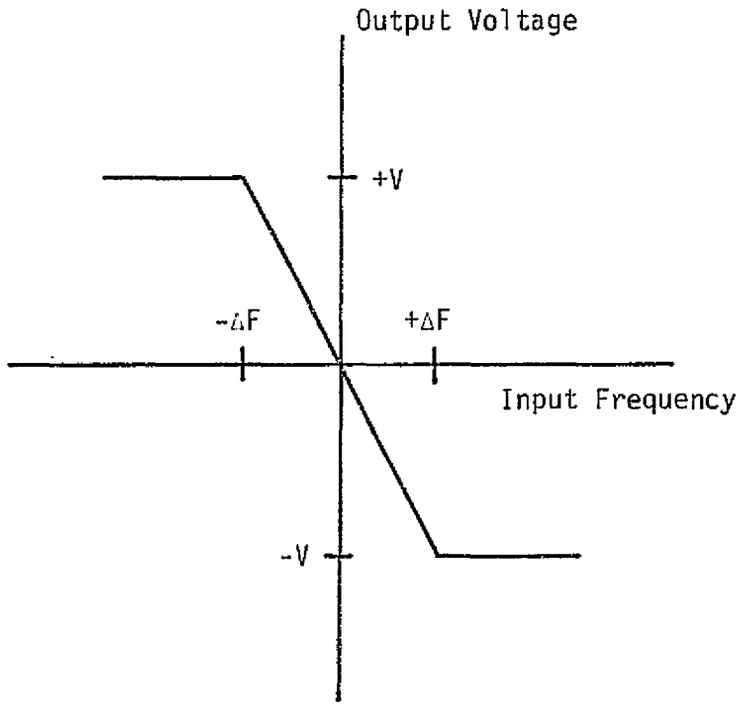

Figure 32. Frequency Tracker Characteristics for Sweeping Gunn Oscillator

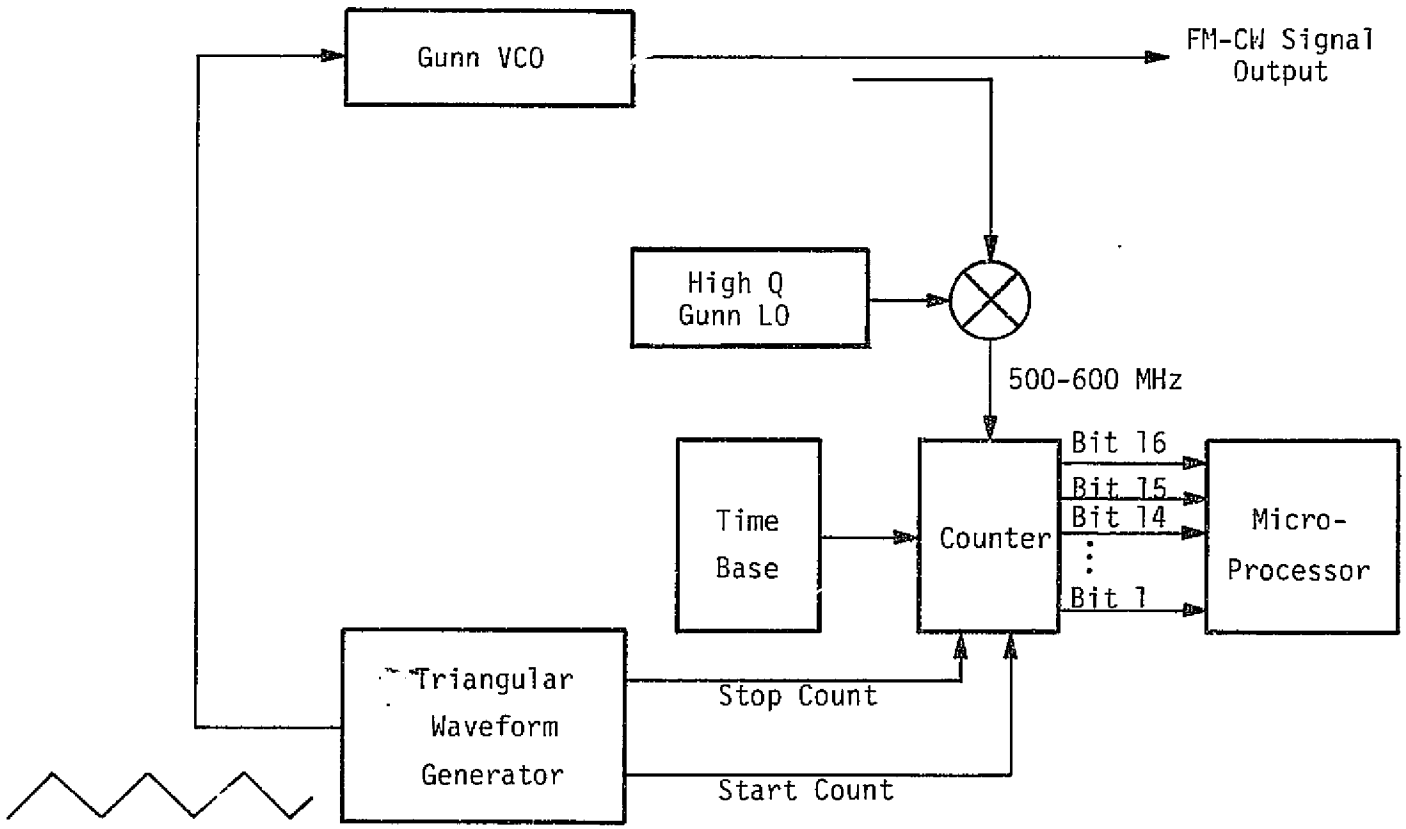

Figure 33. Sweep Modulation with Precision Measurement of Actual Slope

The range resolution or range quantization error resulting from the 16-bit quantization is shown in Subsection 2.6.1.3 to be 5.6 cm (0.185 ft). This is a reasonable value for quantization error.

2.7.2 FM Sweep Waveform Generator

The purpose of the sweep generator is to provide a waveform required for the frequency deviation of the Gunn oscillator transmitter. Figure 34 shows the detailed diagram of such a precision sweep generator. As shown in the figure, a voltage reference diode develops a precision reference voltage V_R. This voltage is also divided to a second, lower voltage. The original V_R and its reduced fraction kV are applied to separate voltage followers whose outputs are therefore two precision reference voltages V_{R1} and V_{R2}, respectively, with the relationship being $V_{R1} > V_{R2}$. V_{R1} and V_{R2} are then applied to a selector switch. For the high sweep rate, this switch selects V_{R1} and, for the low sweep rate, the switch selects V_{R2}. The reference V_{R1} is also applied to the upper limit detector comparator. Furthermore, the polarity-inverted value of V_{R1} is applied to the lower limit detector comparator. The voltage selected by the sweep rate select switch is applied to an integrator where it is converted into a precision ramp. Note that either a positive or negative version of the precision reference selected is available for the generation of either the positive or negative section of the sweep waveform, respectively.

When the ramp generated by the sweep integrator reaches its limit (either high or low), a corresponding comparator provides a pulse which inhibits further sweep in the same direction. Also, a command is sent to the microprocessor indicating the end of the sweep in that particular direction. The microprocessor then makes a decision (based on the mode of operation) to either: (1) open the alternate transmission gate and initiate the sweep in the opposite direction or (2) let the integrator output voltage "coast" at the constant value, thus enabling the transmitter to generate a CW waveform.

2.7.3 Baseband Amplifier/Filter and AGC Unit

Figure 35 provides a functional schematic of an amplifier/filter and AGC unit. The purpose of this amplifier unit is threefold:

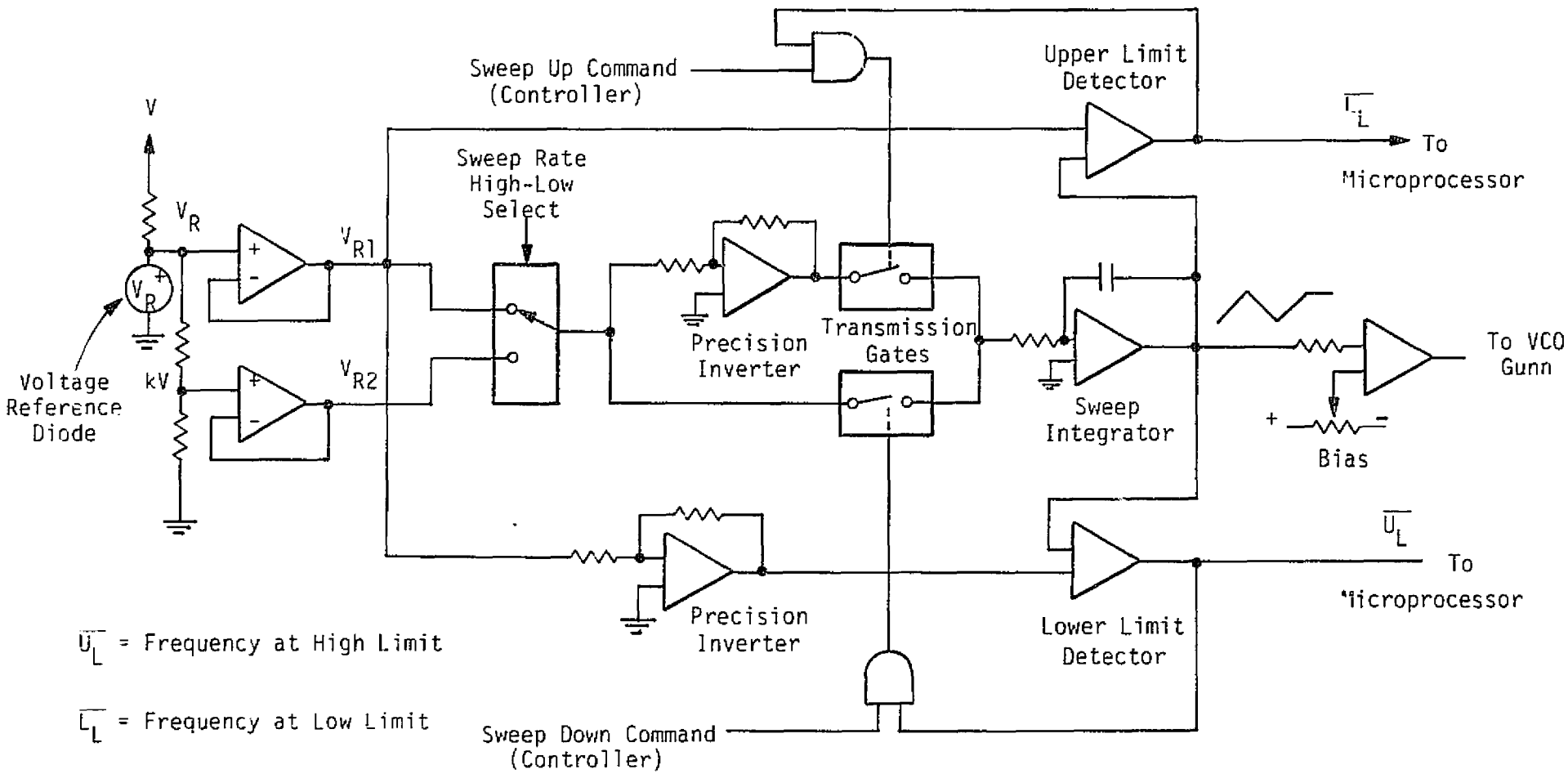

Figure 34. Sweep Generator Detail

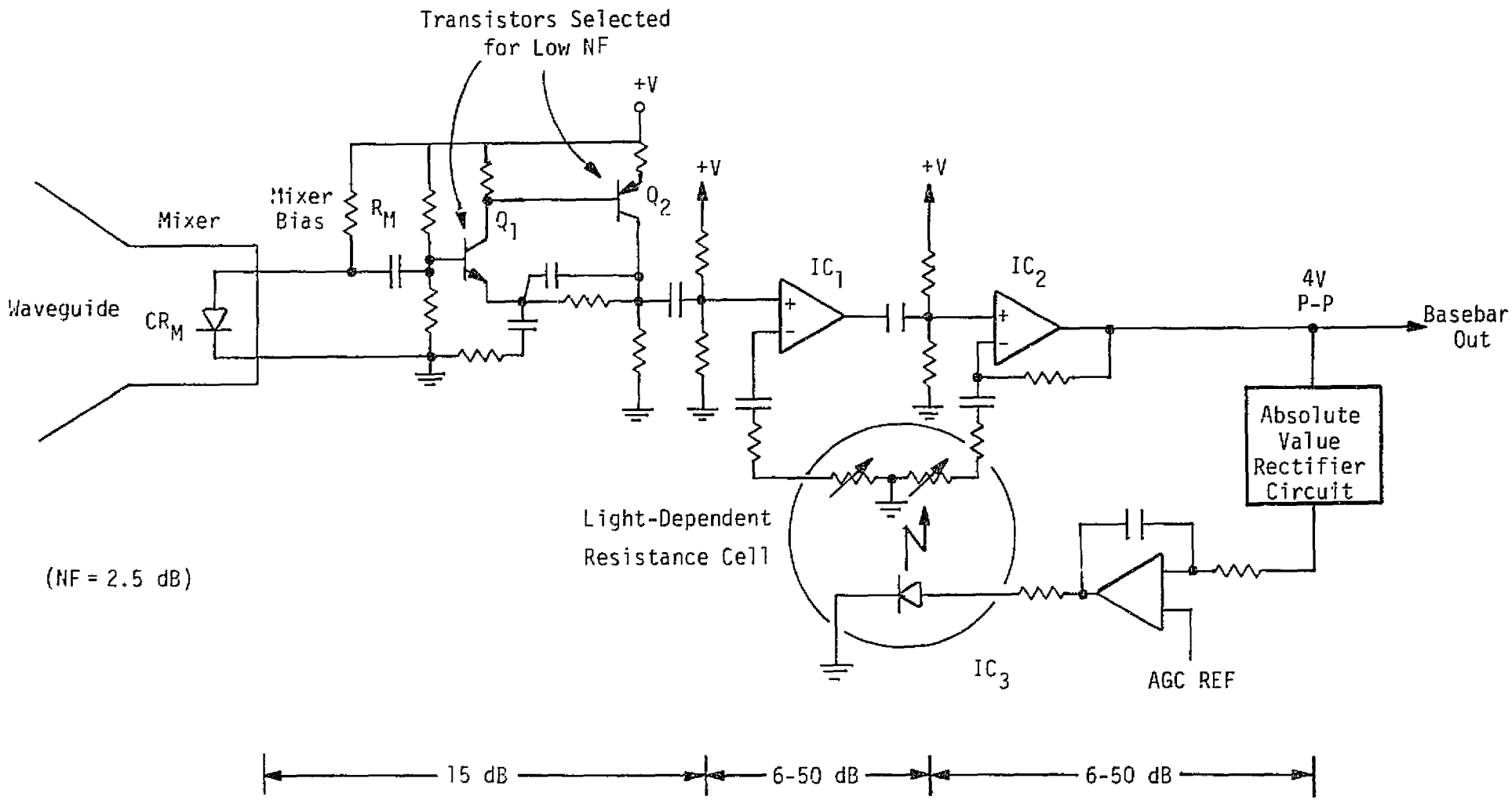

Figure 35. Baseband Amplifier/Filter and AGC

(1) to bring the level of the detected baseband range/velocity tones to a level suitable for signal processing,

(2) to provide lowpass and highpass filtering of the received range/velocity tones, and

(3) to provide automatic gain control (AGC) function for the purpose of minimizing the variation of the absolute level of the signals applied to the baseband signal processor.

As shown in the figure, the first stages of amplification are provided by a discrete component circuitry. Specifically, transistors Q_1 and Q_2 are selected for best low noise performance. The result of such selection is the amplifier overall noise figure of 2.0 to 2.5 dB. The discrete-component amplifier stage also provides the lowpass and highpass filtering which is implemented as an active filter. Resistor R_M provides for setting the bias current through the homodyne RF mixer diode CR_M. The discrete-component amplifier section provides about 15 dB of gain.

Following the discrete-component amplifier are the gain-controlled amplifier stages. These stages are comprised of IC_1 and IC_2. The maximum and minimum gain provided by these stages is 100 dB and 12 dB, respectively. The voltage for controlling the gain of this amplifier is developed by an absolute value rectifier circuit.

The voltage developed by the rectifier circuit is filtered and applied to a light-dependent resistance cell. This cell provides for linear control of the amplifier gain. The AGC reference voltage determines the level at which the gain control function is actuated.

2.7.4 Frequency/Phase Tracker

The basic measurement process involved in the radar is the determination of the frequency of a beat note(s). Since, for much of the operating range of the radar, the beat note is a noisy signal, it is necessary to filter it prior to frequency measurement. The method chosen as a baseline design is a phase-lock tracker. A block diagram of the tracker is shown in Figure 36. The noise filtering is accomplished by virtue of the fact that the frequency measurement is made of the loop VCO. Since the loop has a relatively narrow noise bandwidth, typically 50 Hz (one-sided), the frequency and phase fluctuations of the VCO are minimized.

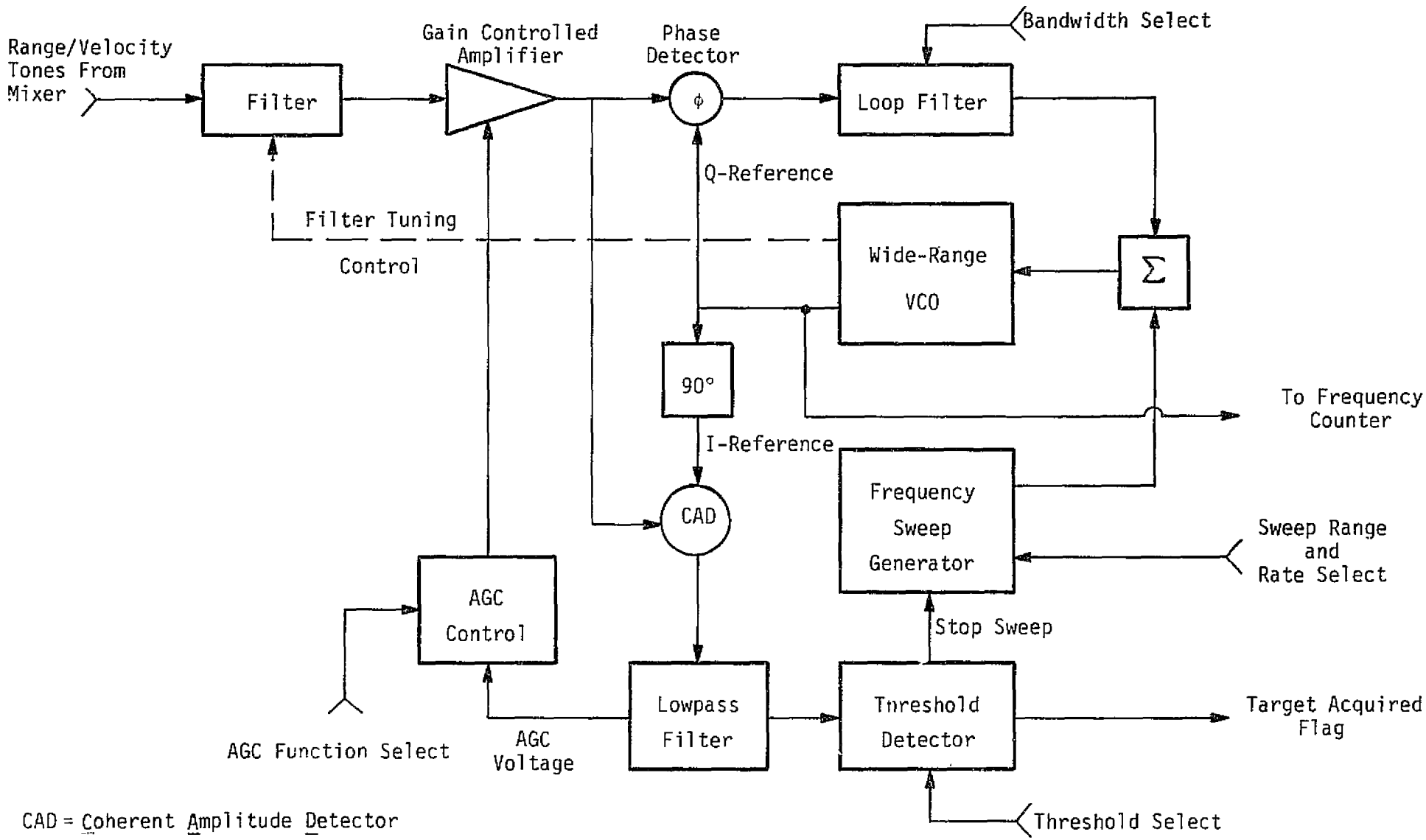

Figure 36. Phase-Locked Loop (PLL) Implementation of the Frequency Tracker

From Figure 36, it is seen that the phase-lock tracker is a classical I and Q tracker in which the I channel is used to generate lock indication and coherent AGC control voltage. The tracker acquires by means of an acquisition sweep voltage that tunes the VCO across the frequency uncertainty. When the I channel develops the "in-lock" signal, the signal developed by the coherent amplitude detector (CAD) is used to stop the sweep.

A similar phase-lock tracker is presently being used in the Kustom police radars. This design will be examined in detail in Phase II to determine its suitability for NASA space proximity missions.

2.8 Special Problems

2.8.1 Near-Zero Velocity Measurement

The analysis of the radar's velocity performance presented in Section 2.6 demonstrates that the NASA velocity accuracy measurement goal can be met. However, this analysis did not consider the limitations of the specific frequency counter implementation used to measure the doppler frequency. If one considers the desired measurement update interval of 1 second, it can be seen that there is an inherent 2 Hz counter ambiguity. This is because effectively 0.5 second of the interval would be devoted to counter velocity measurement and 0.5 second would be devoted to counter range measurement. If the full 1 second were devoted to velocity measurement, the counter ambiguity would be 1 Hz. One way to devote the full 1 second to velocity measurement would be to make the range measurement while utilizing the triangular waveform modulation, then switch to a CW mode in which only velocity would be measured. Range would still be automatically updated by virtue of integrating the velocity measurement. Even the 1 Hz counter resolution error, however, is on the same order as the 1σ error of 1.6 Hz. (The 1.6 Hz value corresponds to 0.01 m/sec 1σ velocity measurement accuracy.) Thus, where near-zero velocity measurement is desired, such as in spacecraft station-keeping operations, the measurement or integration interval should be increased to 10 seconds. This makes the counter resolution or round-off error an order of magnitude less than the errors analyzed in Section 2.6. Thus, Axiomatix recommends a "station-keeping" radar mode during which a CW is transmitted for the major portion of a 10 second

interval and the velocity measurements are updated every 10 seconds. The range measurement for this mode would take only about 1 second, and its update rate would also be over in 10 seconds.

2.8.2 Near-Zero Range Measurement

The problem of near-zero range measurement is similar to the near-zero velocity measurement problem, i.e., counter measurement of very low frequencies. In Section 2.4, it is shown that, for a modulation range scale of 16 Hz/m, the resultant beat note is 3.2 Hz at the range of 0.2 m (0.7 ft). Thus, for a measurement count interval of 0.5 second, the 2 Hz round-off error is of the same order as the frequency to be measured. This problem can be solved by utilizing a 10-second measurement interval, i.e., a "docking" radar mode. Also, since at close ranges, the signal-to-noise ratio is very high, it is possible to multiply the range tone frequency before counting it. Thus, multiplication by a factor of 10 would decrease the round-off error to an order of magnitude less than the frequency to be measured. The velocity in this case (i.e., high SNR) can be obtained by differentiating the range information.

3.0 CONCLUSIONS AND RECOMMENDATIONS

A baseline system design for a ranging/tracking radar for space proximity operations has been developed. The analysis of this CW radar has demonstrated that NASA's performance goals for range rate measurement of $\sigma = 0.01$ m/sec (0.03 ft/sec) can be met. Analysis of the ranging performance has indicated that the range accuracy goal of $\sigma = 0.2$ m (0.66 ft) will be met at ranges up to 2100 m (4000 ft) and the range accuracy will be $\sigma = 0.268$ m (0.88 ft) at the maximum range of 1850 m (1 nmi).

The system design developed is a practical design which can be implemented in Phase II with existing commercial components; yet it reflects state-of-the-art component utilization such as the use of microprocessors. Furthermore, the range rate measurement potential for the latest technology was experimentally verified during the Phase I contract. Using a Kustom police radar modified to measure low velocities, Axiomatix measured velocities as low as 0.018 m/sec (0.06 ft/sec). This radar was by no means optimized for this task. Further details of the test are reported in Appendix F.

The system design developed in Phase I will be breadboarded and tested in Phase II. However, Axiomatix strongly recommends that NASA authorize the detailed analysis of the effects on the system design of target scintillation, extended targets, and multipath. Due to the limitations of Phase I funding, these effects were not analyzed in detail. The experimental tests performed by Axiomatix, however, indicated that target effects and multipath will affect radar performance.

An area closely related to the target effects is consideration of using radar reflectors on some, or possibly all, of the targets with which the sensor will operate. In case of adverse findings from further target effect studies, utilization of a passive, cooperative reflector mounted on a complex target may be the most promising approach towards meeting the measurement accuracies specified by NASA. Consequently, further studies directed towards defining, specifying, and utilizing passive, cooperative reflectors in conjunction with realistic targets are also strongly recommended.

REFERENCES

1. Exhibit A: Statement of Work for a Ranging/Tracking System for Proximity Operations. NASA Lyndon B. Johnson Space Center Document No. RFP9-BC73-38-8-48P, May 1978.

2. M. I. Skolnik. Introduction to Radar Systems. New York: McGraw-Hill Book Company, 1962.

3. A. J. Hymans and J. Lait. "Analysis of a Frequency-Modulated Continuous Wave Ranging System," Proceedings of the IEEE, Paper No. 3264E, July 1960, pp. 365-372.

4. Microwave Associates. "Gunn Diode Circuit Handbook," Document #HB-9000, February 1971.

5. C. B. Andrews and H. A. Bazydlo. "Crystal Noise Effects on Zero IF Receiver," Proceedings of the IRE, Vol. 47, February 1959, pp. 2018-2019.

6. A. Blanchard. Phase-Locked Loops: Application to Coherent Receiver Design. New York: John Wiley & Sons, 1976.

7. F. M. Gardner. Phaselock Techniques. New York: John Wiley & Sons, 1966.

8. D^2C. "Final Report for a Study for Optimizing the Rendezvous Radar Function for the Space Shuttle," under Contract NAS 9-14615, December 1975.

APPENDIX A

THE EFFECT OF PHASE NOISE ON CW RADAR PERFORMANCE

PRECEDING PAGE BLANK NOT FILMED

APPENDIX A

THE EFFECT OF PHASE NOISE ON CW RADAR PERFORMANCE

by

Charles L. Weber

1.0 SUMMARY

The performance of the proposed CW radar in the presence of additive white Gaussian noise has been developed and is reported in [1]. In this appendix, the performance of the proposed CW radar is determined in the presence of phase noise on the local oscillator. The effect of phase noise on performance is essentially identical for both the range and range rate estimators. This is because both involve a frequency estimate.

The results take into account the correlation that exists in the frequency noise process over the round trip time to the target. The results are shown to be independent of received signal power, power in the local reference, and gain of the receiver mixers.

2.0 ANALYTICAL DESCRIPTION OF PROPOSED CW RADAR SYSTEM IN THE PRESENCE OF PHASE NOISE

A block diagram of the proposed CW radar system is shown in Figure 1. The transmitter is tunable at K-band, where the input is proportional to the instantaneous frequency $f_i(t)$. The range and range rate estimations are performed in a TDM (time-division-multiplexed) manner. Depending on how the final implementation is chosen, the doppler bias error in the range error can be removed by use of the range rate estimate or by proper choice of the instantaneous frequency modulation $f_i(t)$. For details, see [1].

One candidate instantaneous frequency modulation is shown in Figure 2a. The system parameters shown in this figure are:

ΔF = total deviation of the instantaneous frequency (Hz)

T_m = total measurement time for one range measurement (sec)

T_0 = measurement time for the range rate measurement (sec)

k = slope of the linear FM instantaneous frequency variation (Hz/sec).

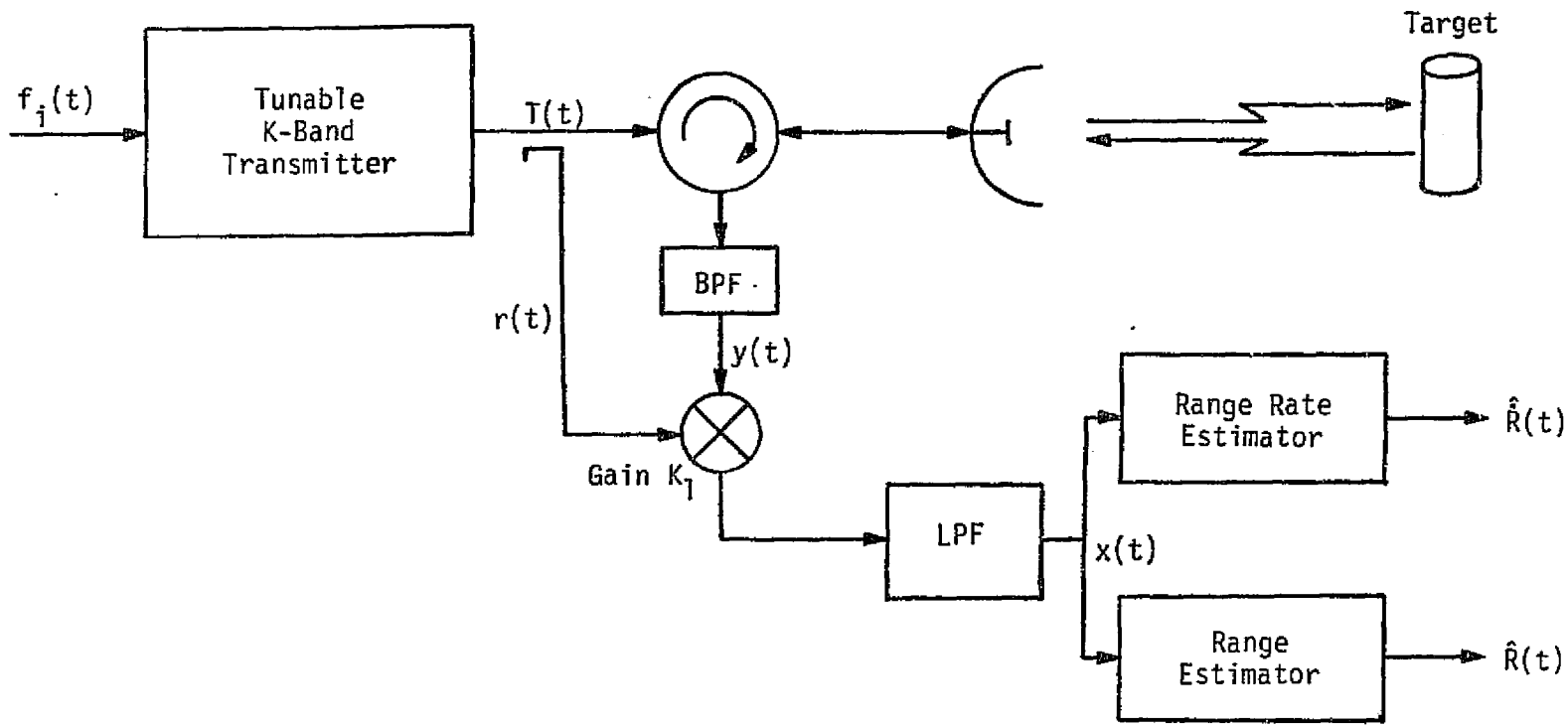

Figure 1. Simplified Block Diagram of Proposed CW Radar System

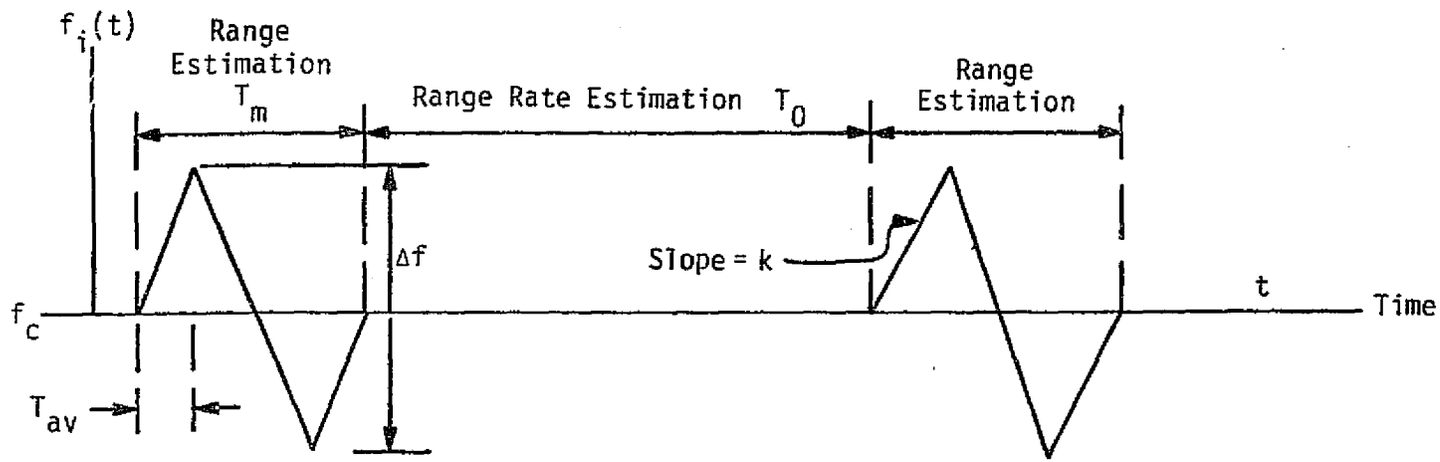

Figure 2a. Transmitted Version of the Instantaneous Carrier Frequency

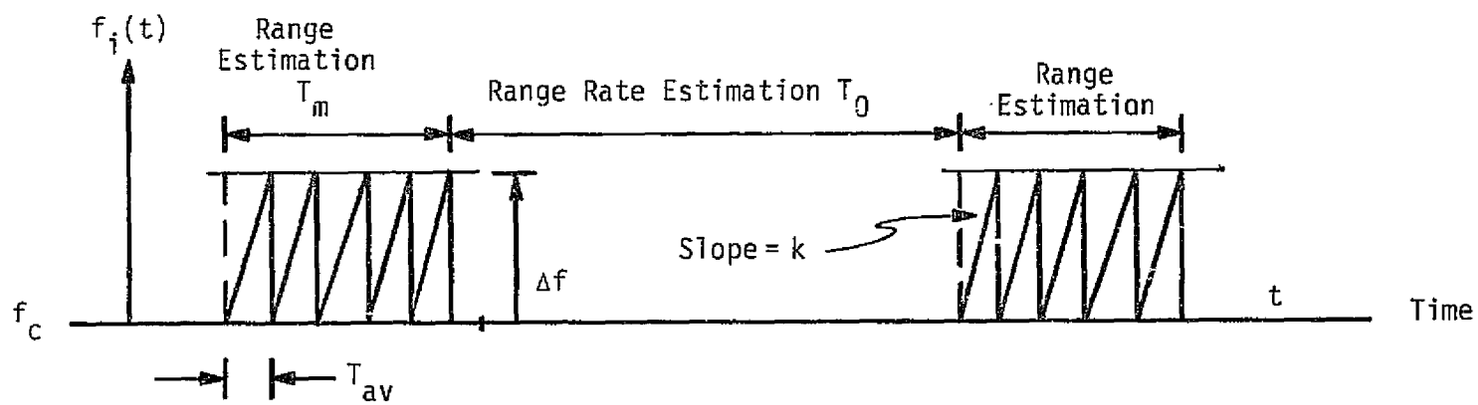

Figure 2b. Alternate Version of the Instantaneous Carrier Frequency

An alternate version of the instantaneous carrier frequency is shown in Figure 2b. There are advantages and disadvantages to both choices of instantaneous carrier frequency modulation. Among them, as shall be shown, is that, in Figure 2a, the choice of $f_i(t)$ will allow range measurement without knowledge of the range rate, whereas in Figure 2b, the $f_i(t)$ requires knowledge of range rate in order to provide an estimate of range. The second alternative, however, is simpler to implement and the sign of the doppler correction is not a problem, as will be shown. This could possibly be a problem in the first alternative.

From Figure 2, it is seen that a CW linear FM waveform is used during range estimation and a pure CW is used for range rate estimation.

For a target at range R, the round-trip time to the target, T_{RT}, is given by

$$T_{RT} \triangleq \frac{2R}{c} , \tag{1}$$

where R is the range to the target and c is the speed of light. From Figure 2a,

$$\frac{\Delta F}{2} = k T_v = k T_m/4 . \tag{2}$$

For range measurement, the basic approach is to estimate the change in instantaneous frequency (termed the beat frequency) over the round-trip time to the target. Designating the beat frequency as f_b, we have that

$$f_b = k T_{RT} = 2\Delta F T_{RT}/T_m . \tag{3}$$

In what follows, only the effects of phase noise are considered, and the signal-to-noise ratio (SNR) is assumed to be sufficiently large that the effects of additive white Gaussian noise (AWGN) can be neglected.

During range estimation, the transmitted signal is given by (see Figure 1):

$$T(t) = \sqrt{2 P_T} \cos \left[\omega_0 t + \int_{t_0}^{t} 2\pi f_i(\tau)\, d\tau + \theta_T + \theta_{PN}(t) \right] , \tag{4}$$

where P_T = transmitted average power

$\omega_0 = 2\pi f_0$ = carrier frequency (rad/sec)

$f_i(\tau)$ = instantaneous frequency deviation from the carrier

t_0 = arbitrary starting time for the transmitted waveform

θ_T = random reference phase of the transmitted signal, uniformly distributed over $(0,2\pi)$

$\theta_{PN}(t)$ = phase noise process, generated by the K-band oscillator in the transmitter.

Modeling of the phase noise process $\theta_{PN}(t)$ will be considered subsequently.

The received signal at time t, after passage through the bandpass filter (BPS) shown in Figure 1, is given by

$$y(t) = \sqrt{2P_R}\cos\left[\omega_0 t + \omega_d t + \int_{t_0}^{t-T_{RT}} 2\pi f_i(\tau)\,d\tau + \theta_R + \theta_{PN}(t-T_{RT})\right], \qquad (5)$$

where the AWGN has been neglected, and

P_R = average received power of the desired signal

$\omega_d = 2\pi f_d$ = doppler frequency shift (rad/sec)

θ_R = random reference phase of the received signal, uniformly distributed over $(0,2\pi)$

$\theta_{PN}(t-T_{RT})$ = phase noise process delayed by the round-trip time delay T_{RT}.

As can be observed from Figure 1, the mixer carries out the operation

$$x(t) = y(t)\,r(t)\Big|_{BB}, \qquad (6)$$

where the notation implies that only the difference frequency contribution is maintained. The reference signal r(t) is an attenuated version of the transmitted signals, so that

$$r(t) = \sqrt{2P_{LO}}\cos\left[\omega_0 t + \int_{t_0}^{t} 2\pi f_i(\tau)\,d\tau + \theta_T + \theta_{PN}(t)\right]. \qquad (7)$$

The output of the LPF following the mixer is therefore given by

$$x(t) = \sqrt{P_R P_{LO}}\, K_1 \cos\left[2\pi \int_{t-T_{RT}}^{t} f_i(\tau)\, d\tau - \omega_d t + \theta_0 + \theta_{PN}(t) - \theta_{PN}(t-T_{RT})\right], \tag{8}$$

where P_{LO} is the average power in the reference waveform, and θ_0 is also a uniformly distributed random phase over $(0,2\pi)$.

The round-trip time delay T_{RT} is assumed to be much smaller than the observation or averaging time T_{av}, i.e.,

$$T_{RT} << T_{av}, \tag{9}$$

so that any end effects at the beginning and end of the observation interval can be neglected.

For linear FM, the slope of the FM can be modeled as the function $k(\tau)$. The instantaneous frequency is then given by

$$f_i(\tau) = \int^{\tau} k(\alpha)\, d\alpha\ . \tag{10}$$

If the rate of change of FM is constant (as shown in Figure 3, for example), then the FM varies linearly, which is also shown in Figure 3. The extent to which linearity is a requirement in this CW radar is discussed in Appendix D. Henceforth in this development, it is assumed $k(\tau)$ is piecewise constant and $f_i(\tau)$ is linear (sawtooth) as ideally shown in Figure 3.

The accumulated beat phase in (8) can be written as

$$\begin{aligned} 2\pi \int_{t-T_{RT}}^{t} f_i(\tau)\, d\tau &= 2\pi \int_{t-T_{RT}}^{t} d\tau \int_{t-T_{RT}}^{\tau} k(\alpha)\, d\alpha \\ &= 2\pi \int_{t-T_{RT}}^{t} \tau(\pm k)\, d\tau \\ &= \pm 2\pi k \left[T_{RT} t - T_{RT}^2/2\right] \\ &= \pm 2\pi f_b t + \theta_1\ , \end{aligned} \tag{11}$$

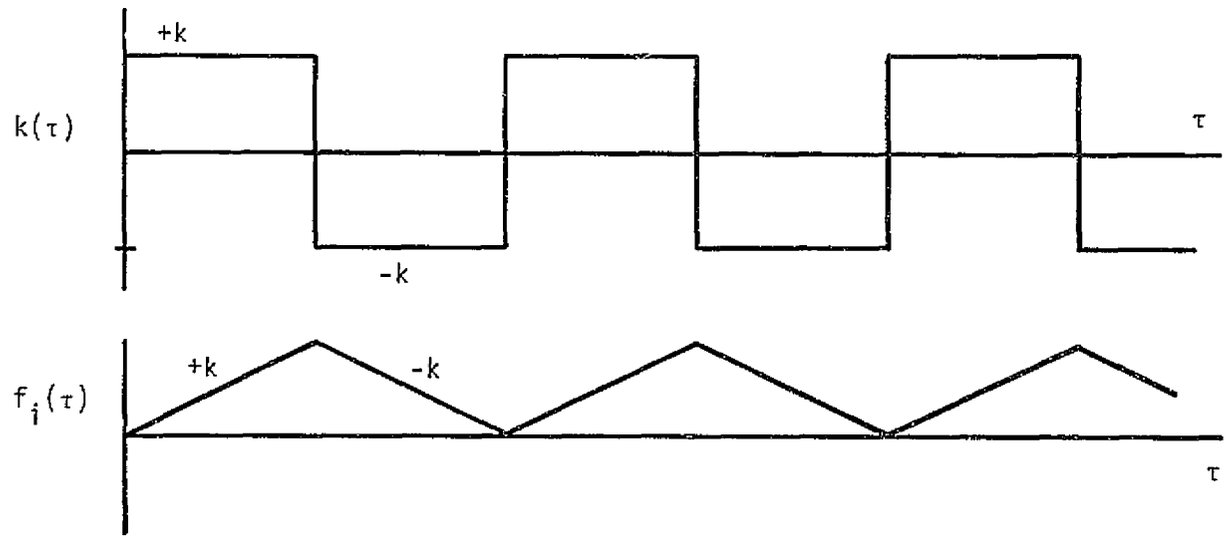

Figure 3. Instantaneous Frequency $f_i(\tau)$ and Its Slope $k(\tau)$

where the beat frequency is given by

$$f_b = |k| T_{RT} \tag{12}$$

and the additional phase θ_1 can be absorbed into θ_0.

The signal at the input to the range estimator in Figure 1 is then described by

$$x(t) = \sqrt{P_R P_{LO}}\, K_1 \cos\left[2\pi f_b t \pm 2\pi f_d t + \theta_0 + \theta_{PN}(t) - \theta_{PN}(t-T_{RT})\right] . \tag{13}$$

3.0 PERFORMANCE OF RANGE AND RANGE RATE ESTIMATION IN THE PRESENCE OF PHASE NOISE

From (13), it is seen that the estimation of range has been reduced to the estimation of the beat frequency, $f_b = k T_{RT}$. In terms of the range itself,

$$\hat{R} = \left(\frac{c}{2}\right) \hat{T}_{RT} = \left(\frac{c}{2k}\right) \hat{f}_b , \tag{14}$$

so that the standard deviation of range can be expressed in terms of that of f_b, namely,

$$\sigma_R = \left(\frac{c}{2k}\right) \sigma_{f_b} . \tag{15}$$

Whether Alternative 1 or Alternative 2 is used as the instantaneous frequency modulation, it will be assumed that the effects of the doppler frequency are either eliminated or subtracted out. With the doppler frequency removed, the input to the frequency estimation device for range estimation is given by

$$x(t) = \sqrt{P_R P_{LO}}\, K_1 \cos\left[2\pi f_b t + \theta_0 + \theta_{PN}(t) - \theta_{PN}(t-T_{RT})\right] . \tag{16}$$

On the other hand, when range rate is being estimated, there is no beat frequency and the input to the frequency estimator is equal to

$$x(t) = \sqrt{P_R P_{LO}}\, K_1 \cos\left[2\pi f_d t + \theta_0 + \theta_{PN}(t) - \theta_{PN}(t-T_{RT})\right] . \tag{17}$$

For range rate,

$$\hat{\dot{R}} = \left(\frac{c}{2f_c}\right)\hat{f}_d \tag{18}$$

and

$$\sigma_{\dot{R}} = \left(\frac{c}{2f_c}\right)\sigma_{f_d} . \tag{19}$$

In what follows, range and range rate estimation can be simultaneously analyzed by determining the variance of the frequency estimator. Then, via (15) or (19), the standard deviation of range and range rate can be determined, respectively.

4.0 PERFORMANCE OF FREQUENCY ESTIMATION IN THE PRESENCE OF PHASE NOISE

There are various methods of implementing an effective frequency estimator, including a hard-limiter plus frequency counters, and a bank of narrowband filters plus an interpolation algorithm [2]. The first of these appears quite attractive and, as a result, the performance of frequency estimation in the presence of phase noise will be determined for a frequency counter.

After a hard-limiter, all of the information in x(t) in (16) is contained in its phase argument:

$$\Delta(t) = 2\pi f_b t + \theta_0 + 2\pi \int_{t-T_{RT}}^{t} f_N(\tau)\, d\tau \quad \text{(radians)} , \tag{20}$$

where $f_N(t)$ is the instantaneous frequency noise process associated with the phase noise process $\theta_{PN}(t)$. Therefore,

$$\theta_{PN}(t) - \theta_{PN}(t-T_{RT}) = 2\pi \int_{t-T_{RT}}^{t} f_N(\tau)\, d\tau . \tag{21}$$

The frequency counter essentially counts zero crossings for a period of T_{av} seconds, T_{av} being the averaging time. This can be modeled analytically by saying that the frequency counter examines

$$c(t) \triangleq \frac{\Delta(t)}{2\pi} = \int_{t-T_{RT}}^{t} f_b(\tau)\, d\tau + \int_{t-T_{RT}}^{t} f_N(\tau)\, d\tau = f_b t + \int_{t-T_{RT}}^{t} f_N(\tau)\, d\tau \,. \tag{22}$$

By observing (counting) c(t) for T_{av} seconds and averaging (dividing by T_{av}), the frequency counter estimate can be analytically described as

$$\hat{f}_b = \frac{c(T_{av})}{T_{av}} = f_b + \frac{1}{T_{av}} \int_{T_{av}-T_{RT}}^{T_{av}} f_N(\tau)\, d\tau \,, \tag{23}$$

where T_{av} is the counting (or averaging) time.

It is noted that the quality of this estimate is distorted by the phase noise process, and that the estimate is <u>independent</u> of the received signal power P_R, the power in the local oscillator P_{LO}, and the gain K_1 of the mixer in Figure 1. The phase noise process is assumed by definition to have zero mean. Therefore,

$$E[f_N(\tau)] = 0 \,, \quad \text{for all } \tau \,, \tag{24}$$

and as a result

$$E[\hat{f}_b] = f_b \,. \tag{25}$$

Hence, the frequency counter provides an <u>unbiased</u> estimate of the unknown frequency f_b. The variance of the estimate is therefore given by

$$\sigma_{\hat{f}_b}^2 = E\left\{\left[\frac{1}{T_{av}} \int_{T_{av}-T_{RT}}^{T_{av}} f_N(\tau)\, d\tau\right]^2\right\}$$

$$= \left(\frac{T_{RT}}{T_{av}}\right)^2 E\left\{\left[\frac{1}{T_{RT}} \int_0^{T_{RT}} f_N(\tau)\, d\tau\right]^2\right\} , \tag{26}$$

where the translation in integration time is done for convenience and is justified since the phase noise process is assumed to be stationary. Using the stationary assumption further, (26) can be expressed as

$$\sigma_{\hat{f}_b}^2 = \left(\frac{T_{RT}}{T_{av}}\right)^2 \frac{1}{T_{RT}^2} \iint_0^{T_{RT}} E\left[f_N(t_1)\, f_N(t_2)\right] dt_1\, dt_2 \,, \tag{27}$$

where

$$E\left[f_N(t_1)\, f_N(t_2)\right] \triangleq R_{f_N}(t_1 - t_2) \tag{28}$$

is the autocorrelation function of the frequency noise process $f_N(t)$. By substituting (28) into (27) and letting $\tau = t_1 - t_2$, the variance in (27) simplifies to [3]:

$$\sigma_{\hat{f}_b}^2 = \left(\frac{T_{RT}}{T_{av}}\right)^2 \frac{2}{T_{RT}} \int_0^{T_{RT}} \left(1 - \frac{\tau}{T_{RT}}\right) R_{f_N}(\tau)\, d\tau \,. \tag{29}$$

What is typically available on "Spec" sheets is power spectral density (PSD) information instead of autocorrelation function information [4]. In terms of the two-sided PSD $S_{f_N}(f)$ of $f_{PN}(t)$, where

$$S_{f_N}(f) = \mathscr{F}\left\{R_{f_N}(\tau)\right\} \tag{30}$$

is the Fourier transform of the autocorrelation function, (29) is equal to

$$\sigma_{\hat{f}_b}^2 = \left(\frac{T_{RT}}{T_{av}}\right)^2 2 \int_0^{\infty} \left[\frac{\sin\,(\pi f T_{RT})}{\pi f T_{RT}}\right]^2 S_{f_N}(f)\, df \,. \tag{31}$$

The "Spec" sheets for frequency noise processes typically provide single-sided power spectral densities [4]. Therefore, we define the <u>single-sided</u> PSD of $f_N(t)$ as

$$G_{f_N}(f) \triangleq 2\, S_{f_N}(f) \,. \tag{32}$$

The standard deviation of the frequency estimate due to the frequency noise process of $f_{PN}(t)$ is therefore given by

$$\sigma_{\hat{f}_{PN}} = \left(\frac{T_{RT}}{T_{av}}\right) \left[\int_0^{\infty} \left[\frac{\sin\,(\pi T_{RT} f)}{\pi T_{RT} f}\right]^2 G_{f_N}(f)\, df\right]^{1/2} \text{Hz} \,. \tag{33}$$

It is noted that the effect of phase noise in frequency estimation decreases as the inverse of the averaging time T_{av}. The effect on performance of the correlation that exists in the phase noise process over the round-trip transmission time T_{RT} shows up in (33) via the weighting function $[\sin(\pi T_{RT} f)/(\pi T_{RT} f)]^2$.

If the maximum frequency of interest in the frequency noise process is B_{max}, then in this application the range is sufficiently short that

$$B_{max} << \frac{1}{T_{RT}} . \tag{34}$$

For example, if R = 2000 meters, then T_{RT} = 13.33 μsec, and T_{RT}^{-1} = 75 kHz. Hence, (34) would be satisfied for B_{max} equal to a few kHz. When (34) is satisfied, the performance in (33) can be tightly upper bounded by

$$\sigma_{\hat{f}_{PN}} \leq \left(\frac{T_{RT}}{T_{av}}\right)\left[\int_0^{B_{max}} G_{f_N}(f)\, df\right]^{1/2} \text{Hz} . \tag{35}$$

Using the results in either (33) or (35), the standard deviation of the effects of phase noise on frequency estimation can be determined. The simplest certainly would be to substitute the "Spec" sheet frequency noise PSD for a particular oscillator directly into (35) and integrate.

REFERENCES

1. "Ranging/Tracking System for Proximity Operations," Axiomatix Technical Proposal RFP 9-BC73-38-8-48P, May 24, 1978.

2. C. L. Weber. "Theory and Design of Coherent Digital Systems Which Track Doppler Frequency," Proc. IEEE, Vol. 58, No. 6, June 1970, pp. 865-875.

3. A. Papoulis. Probability, Random Variables, and Stochastic Processes. New York: McGraw-Hill, 1965.

4. R. Gagliardi. Introduction to Communication Engineering. Wiley, 1978.

APPENDIX B

BEAT NOTE ANALYSIS IN AN FM-CW RADAR

PRECEDING PAGE BLANK NOT FILMED

APPENDIX B

BEAT NOTE ANALYSIS IN AN FM-CW RADAR

by

Teferi Nessibou

1.0 INTRODUCTION

This appendix presents a derivation of the discrete power spectrum of the beat note in an FM-CW radar when the modulating waveform is a symmetrical sawtooth.

2.0 MATHEMATICAL DEVELOPMENT

2.1 System Model

Figure 1 shows the receiving end of the FM-CW radar where the reflected signal v_R is mixed with the transmitted signal v_T to generate the beat note v_B.

2.2 Symmetrical Sawtooth FM

Figure 2 gives the frequencies for a stationary target. From this figure, $f_B = 4T\,\Delta f\, f_m$.

Over the interval $[0,\tau_m]$, f_T can be described by

$$f_T = f_0 + \frac{4\Delta f}{\tau_m}\left(t - \frac{\tau_m}{4}\right); \qquad 0 \le t \le \frac{\tau_m}{2}, \tag{1}$$

$$f_T = f_0 - \frac{4\Delta f}{\tau_m}\left(t - \frac{3\tau_m}{4}\right); \qquad \frac{\tau_m}{2} \le t \le \tau_m, \tag{2}$$

$$\phi_T = \int_t 2\pi f_T \, dt. \tag{3}$$

$$\phi_T = \int 2\pi \left[f_0 + \frac{4\Delta f}{\tau_m}\left(t - \frac{\tau_m}{4}\right)\right] dt + \int 2\pi \left[f_0 - \frac{4\Delta f}{\tau_m}\left(t - \frac{3\tau_m}{4}\right)\right] dt; \qquad 0 \le t \le \tau_m. \tag{4}$$

The transmitted signal is given by

$$v_T = V_T \sin \phi_T \tag{5}$$

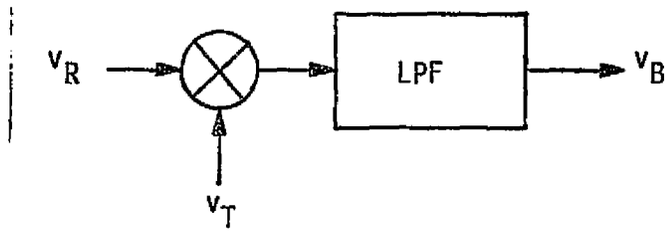

$$v_T = V_T \sin \phi_T$$
$$v_R = V_R \sin \phi_R$$
$$v_B = V_B \cos (\phi_R - \phi_T)$$

Figure 1. Receiver Simplified Block Diagram

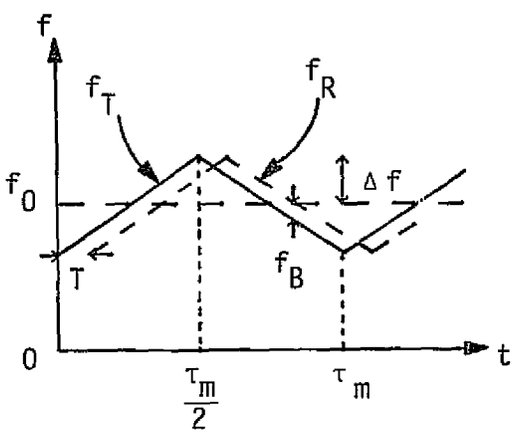

$f_0 = \frac{\omega_0}{2\pi}$ = Mean Frequency

Δf = Maximum Deviation

$\tau_m = \frac{2\pi}{\omega_m} = \frac{1}{f_m}$ = Modulation Period

$T = \frac{2D}{C}$ = Round Trip Delay

D = Distance Between Target and Transmitter

$f_B = \frac{\omega_B}{2\pi}$ = Beat Frequency

f_T = Transmitted Frequency (for a homodyne system, $f_T = f_{LO}$)

Figure 2. Frequencies for a Stationary Target

and can be expressed as

$$v_T = V_T \sin\left[2\pi f_0 t - 8\pi \Delta f t + 4\Delta f\, 2\pi f_m \frac{t^2}{2} + \phi_1\right];$$

$$0 \le t \le \frac{\tau_m}{2}, \tag{6}$$

and

$$v_T = V_T \sin\left[2\pi f_0 t + 6\pi \Delta f t - 4\Delta f\, 2\pi f_m \frac{t^2}{2} + \phi_2\right];$$

$$\frac{\tau_m}{2} \le t \le \tau_m. \tag{7}$$

The corresponding received signal is of the form

$$v_R = V_R \sin \phi_R \tag{8}$$

and can be written as

$$v_R = V_R \sin\left[2\pi f_0 (t - T) - 8\pi \Delta f (t - T) + 4\Delta f\, 2\pi f_m \frac{(t-T)^2}{2} + \phi_3\right];$$

$$0 \le t \le \frac{\tau_m}{2}, \tag{9}$$

and

$$v_R = V_R \sin\left[2\pi f_0 (t - T) + 6\pi \Delta f (t - T) - 4\Delta f\, 2\pi f_m \frac{(t-T)^2}{2} + \phi_4\right];$$

$$\frac{\tau_m}{2} \le t \le \tau_m. \tag{10}$$

The output of the mixer (neglecting double frequency terms) is the beat note of interest of the form

$$v_B = K v_T v_R; \tag{11}$$

$$v_B = \frac{K V_T V_R}{2} \cos(\phi_R - \phi_T); \tag{12}$$

therefore,

$$v_B = V_B \cos\left[-2\pi f_B t + \left(2\pi \frac{f_B}{2} + 8\pi \Delta f - 2\pi f_0\right) T + \phi\right] ;$$

$$0 \le t \le \frac{\tau_m}{2} , \tag{13}$$

and

$$v_B = V_B \cos\left[2\pi f_B t - \left(2\pi \frac{f_B}{2} + 6\pi \Delta f + 2\pi f_0\right) T + \phi\right] ;$$

$$\frac{\tau_m}{2} \le t \le \tau_m , \tag{14}$$

where

$$V_B = \frac{K V_T V_R}{2} , \tag{15}$$

and ϕ is a constant phase shift due to reflection, the transmitting and receiving antennas, and the mixer.

Let

$$\theta_1 = \left(\frac{\omega_B}{2} + 8\pi \Delta f - \omega_0\right) T + \phi \tag{16}$$

$$\theta_1 = \left[2\pi\left(\frac{\omega_B}{\omega_m}\right) + (2\omega_m T \Delta f - \omega_0) T + \phi\right] \tag{17}$$

and

$$\theta_2 = \left(-\frac{\omega_B}{2} - 6\pi \Delta f - \omega_0\right) T + \phi \tag{18}$$

$$\theta_2 = \left[-\frac{3\pi}{2}\left(\frac{\omega_B}{\omega_m}\right) - (\omega_0 + 2\omega_m T \Delta f) T + \phi\right] . \tag{19}$$

Over the interval $[0,\tau_m]$, v_B can be expressed as

$$v_B = V_B \left[\cos\left(-\omega_B t + \theta_1\right) + \cos \omega_B t + \theta_2\right] . \tag{20}$$

Equation (20) can also be written as

$$v_B = 2V_B \cos\left[\frac{(\theta_1 + \theta_2)}{2}\right] \cos\left[\omega_B t + \frac{(\theta_1 - \theta_2)}{2}\right] . \tag{21}$$

It can be easily checked that v_B is periodic with period τ_m.

2.3 Frequency Domain Representation of v_B

The beat note v_B is now expanded in a Fourier series as follows:

$$v_B(t) = \sum_{n=-\infty}^{\infty} V_n \exp(jn\omega_m t) , \tag{22}$$

where

$$V_n = \frac{1}{\tau_m} \int_0^{\tau_m} v_B(t) \exp(-jn\omega_m t)\, dt . \tag{23}$$

Substituting for v_B in its exponential form, we get

$$V_n = \frac{1}{\tau_m} \left\{ \int_0^{\tau_m/2} \frac{V_B}{2} [\exp(-j\omega_B t + j\theta_1) + \exp(j\omega_B t - j\theta_1)] \exp(-jn\omega_m t)\, dt \right.$$

$$\left. + \int_{\tau_m/2}^{\tau_m} \frac{V_B}{2} [\exp(j\omega_B t + j\theta_2) + \exp(-j\omega_B t - j\theta_2)] \exp(-jn\omega_m t)\, dt \right\} , \tag{24}$$

which can be rewritten as

$$V_n = \frac{V_B}{2} \left\{ \int_0^{\tau_m/2} \frac{1}{\tau_m} [\exp(-j(\omega_B + n\omega_m)t) \exp(j\theta_1) + \exp(j(\omega_B - n\omega_m)t) \exp(-j\theta_1)]\, dt \right.$$

$$\left. + \int_{\tau_m/2}^{\tau_m} \frac{1}{\tau_m} [\exp(j(\omega_B - n\omega_m)t) \exp(j\theta_2) + \exp(-j(\omega_B + n\omega_m)t) \exp(-j\theta_2)]\, dt \right\} \tag{25}$$

Evaluating the integrals yields the following expression:

$$V_n = V_B \cos\theta_1 \left\{ \frac{1}{j2\pi\left(\frac{\omega_B}{\omega_m}+n\right)} \left[1 - \exp\left(-j\pi\left(\frac{\omega_B}{\omega_m}+n\right)\right)\right] + \frac{1}{j2\pi\left(\frac{\omega_B}{\omega_m}-n\right)} \left[\exp\left(j\pi\left(\frac{\omega_B}{\omega_m}-n\right)\right) - 1\right]\right\}$$

$$+ V_B \cos\theta_2 \left\{ \frac{1}{j2\pi\left(\frac{\omega_B}{\omega_m}-n\right)} \left[\exp\left(j2\pi\left(\frac{\omega_B}{\omega_m}-n\right)\right) - \exp\left(j\pi\left(\frac{\omega_B}{\omega_m}-n\right)\right)\right] + \frac{1}{j2\pi\left(\frac{\omega_B}{\omega_m}-n\right)} \left[\exp\left(-j\pi\left(\frac{\omega_B}{\omega_m}+n\right)\right) - \exp\left(-j2\pi\left(\frac{\omega_B}{\omega_m}+n\right)\right)\right]\right\} \tag{26}$$

with $\omega_B/\omega_m \neq \pm n$.

Equation (26) can be broken down into its real and imaginary parts:

$$\mathrm{Re}\{V_n\} = \frac{V_B}{2} \frac{1}{\pi\left[n^2-\left(\frac{\omega_B}{\omega_m}\right)^2\right]} \left\{ (\cos\theta_1 - \cos\theta_2)\left[n\cos\left(\pi\frac{\omega_B}{\omega_m}\right)\sin\pi n - \left(\frac{\omega_B}{\omega_m}\right)\sin\left(\pi\frac{\omega_B}{\omega_m}\right)\cos\pi n\right] + \cos\theta_2\left[n\cos\left(2\pi\frac{\omega_B}{\omega_m}\right)\sin 2\pi n - \left(\frac{\omega_B}{\omega_m}\right)\sin\left(2\pi\frac{\omega_B}{\omega_m}\right)\cos 2\pi n\right]\right\}; \tag{27}$$

$$\mathrm{Im}\{V_n\} = \frac{V_B}{2} \frac{1}{\pi\left[n^2-\left(\frac{\omega_B}{\omega_m}\right)^2\right]} \left\{ (\cos\theta_1 - \cos\theta_2)\left[n\cos\left(\pi\frac{\omega_B}{\omega_m}\right)\cos\pi n + \left(\frac{\omega_B}{\omega_m}\right)\sin\left(\pi\frac{\omega_B}{\omega_m}\right)\sin\pi n\right] + \cos\theta_2\left[n\cos\left(2\pi\frac{\omega_B}{\omega_m}\right)\cos 2\pi n + \left(\frac{\omega_B}{\omega_m}\right)\sin\left(2\pi\frac{\omega_B}{\omega_m}\right)\sin 2\pi n\right] - n\cos\theta_1\right\}. \tag{28}$$

Since n is an integer and ω_B/ω_m is an integer greater than 1, $R_e\{V_n\} = 0$. The $Im\{V_n\}$ can be further reduced by considering the two cases below.

Case 1: ω_B/ω_m even:

$$Im\{V_n\} = \frac{V_B}{2} \frac{n^2}{\left[n^2 - \left(\frac{\omega_B}{\omega_m}\right)^2\right]} \left[\cos\theta_1 \left(\frac{\cos \pi n}{\pi n} - \frac{1}{\pi n}\right) + \cos\theta_2 \left(2\,\frac{\cos 2\pi n}{2\pi n} - \frac{\cos \pi n}{\pi n}\right)\right]. \tag{29}$$

$$Im\{V_n\} = \frac{V_B}{2} \frac{n^2}{\left[n^2 - \left(\frac{\omega_B}{\omega_m}\right)^2\right]} \left\{-\cos\theta_1 \operatorname{sinc}^2(n/2) + \cos\theta_2 \left[\operatorname{sinc}^2(n/2) - 2\operatorname{sinc}^2 n\right]\right\}. \tag{30}$$

Case 2: ω_B/ω_m odd:

$$Im\{V_n\} = \frac{V_B}{2} \frac{n^2}{\left[n^2 - \left(\frac{\omega_B}{\omega_m}\right)^2\right]} \left[-\cos\theta_1 \left(\frac{\cos \pi n}{\pi n} + \frac{1}{\pi n}\right) + \cos\theta_2 \left(2\,\frac{\cos 2\pi n}{2\pi n} + \frac{\cos \pi n}{\pi n}\right)\right]. \tag{31}$$

$$Im\{V_n\} = \frac{V_B}{2} \frac{n^2}{\left[n^2 - \left(\frac{\omega_B}{\omega_m}\right)^2\right]} \left\{\cos\theta_1 \left[\operatorname{sinc}^2(n/2) - \frac{2}{\pi n}\right] + \cos\theta_2 \left[\frac{2}{\pi n} - 2\operatorname{sinc}^2 n - \operatorname{sinc}^2(n/2)\right]\right\}, \tag{32}$$

where $\operatorname{sinc} n = (\sin \pi n)/\pi n$.

In Case 1, when n is even, $Im\{V_n\} = 0$ (by inspection). When n is odd, the expression reduces to

$$\mathrm{Im}\{V_n\} = \frac{V_B}{2} \frac{n^2}{n^2 - \left(\frac{\omega_B}{\omega_m}\right)^2} (\cos\theta_2 - \cos\theta_1)\ \mathrm{sinc}^2(n/2)\ . \tag{33}$$

In Case 2, when n is even, we have

$$\mathrm{Im}\{V_n\} = \frac{V_B}{2} \frac{n^2}{n^2 - \left(\frac{\omega_B}{\omega_m}\right)^2} \left(\frac{2}{\pi n}\right) (\cos\theta_2 - \cos\theta_1)\ ; \tag{34}$$

when n is odd, we have

$$\mathrm{Im}\{V_n\} = \frac{V_B}{2} \frac{n^2}{n^2 - \left(\frac{\omega_B}{\omega_m}\right)^2} (\cos\theta_2 - \cos\theta_1) \left[\frac{2}{\pi n} - \mathrm{sinc}^2(n/2)\right] . \tag{35}$$

In either case, the magnitude spectrum of v_B is obtained from

$$|V_n| = \frac{1}{2}\sqrt{(\mathrm{Im}\{V_n\})^2}\ . \tag{36}$$

In summary, when ω_B/ω_m is even and $\omega_B/\omega_m \neq \pm n$, then

$$|V_n| = \frac{1}{2}\left[\frac{V_B}{2} \frac{n^2}{\left|n^2 - \left(\frac{\omega_B}{\omega_m}\right)^2\right|} |\cos\theta_2 - \cos\theta_1|\ \mathrm{sinc}^2(n/2)\right] , \quad \text{with } n \text{ odd}\ ; \tag{37}$$

when ω_B/ω_m is odd and $\omega_B/\omega_m \neq \pm n$, then

$$|V_n| = \frac{1}{2}\left[\frac{V_B}{2} \frac{n^2}{\left|n^2 - \left(\frac{\omega_B}{\omega_m}\right)^2\right|} \left(\frac{2}{\pi n}\right) |\cos\theta_2 - \cos\theta_1|\right] , \quad \text{for } n \text{ even}, \tag{38}$$

and

$$|V_n| = \frac{1}{2}\left[\frac{V_B}{2}\,\frac{n^2}{\left|n^2-\left(\frac{\omega_B}{\omega_m}\right)^2\right|}\,|\cos\theta_2-\cos\theta_1|\,\left|\frac{2}{\pi n}-\mathrm{sinc}^2\,(n/2)\right|\right], \quad n \text{ odd}. \tag{39}$$

When $\omega_B/\omega_m = \pm n$, V_n is evaluated directly from (25) to yield

$$V_n = \frac{V_B}{4}\left[\exp\,(\pm j\theta_1) + \frac{\exp\,(\pm j\theta_1)}{j2\pi n}\left(1-\exp\,(-j2\pi n)\right) + \exp\,(\pm j\theta_2)\right.$$

$$\left. + \frac{\exp\,(\pm j\theta_2)}{j2\pi n}\left(\exp\,(-j2\pi n)-\exp\,(-j4\pi n)\right)\right], \tag{40}$$

which reduces to

$$V_n = \frac{V_B}{2}\left[(\cos\theta_2+\cos\theta_1) \pm j(\sin\theta_2-\sin\theta_1)\right]; \tag{41}$$

in either case,

$$|V_n| = \frac{V_B}{2}\left|\cos\left(\frac{\theta_1+\theta_2}{2}\right)\right|. \tag{42}$$

2.4 Examples of Calculations for $\omega_B/\omega_m = 2$ and $\omega_B/\omega_m = 5$

In this section, the spectrum of the beat note is calculated and presented graphically for different values of θ_1 and θ_2 when ω_B/ω_m is equal to 2 and 5.

For simplicity, ϕ is set to 0 in the equations for θ_1 and θ_2.

Case 1: $\omega_B/\omega_m = 2$

$$\theta_1 = 4\pi + 2\omega_m T\Delta fT - \omega_0 T. \tag{43}$$

$$\theta_2 = -3\pi - 2\omega_m T\Delta fT - \omega_0 T. \tag{44}$$

Four distinct subcases emerge:

a. $\theta_1 = 2\pi$, $\theta_2 = \pi$

$$|V_n| = V_B \frac{n^2}{|n^2 - 4|} \operatorname{sinc}^2(n/2) ; \qquad n \text{ odd}$$

$$|V_n| = 0 ; \qquad \text{otherwise} \tag{45}$$

b. $\theta_1 = \pi/2$, $\theta_2 = \pi/2$

$$|V_n| \equiv 0 . \tag{46}$$

c. $\theta_1 = 7\pi/4$, $\theta_2 = 3\pi/4$

$$|V_n| = \frac{V_B}{2} \frac{n^2}{|n^2 - 4|} \sqrt{2} \operatorname{sinc}^2(n/2) ; \qquad n \text{ odd} \tag{47}$$

$$|V_n| = (0.707)\frac{V_B}{4} ; \qquad n = 2 \tag{48}$$

$$|V_n| = 0 ; \qquad \text{otherwise} . \tag{49}$$

Let V_p be such that

$$|V_p|^2 = \frac{|V_2|^2}{|V_B|^2} = 0.0625 . \tag{50}$$

Equation (50) represents the total power normalized by $|V_B|^2$; we assume that $V_B = 1$. The function

$$S = \frac{|V_n|^2}{|V_p|^2} \tag{51}$$

is shown in Figure 3.

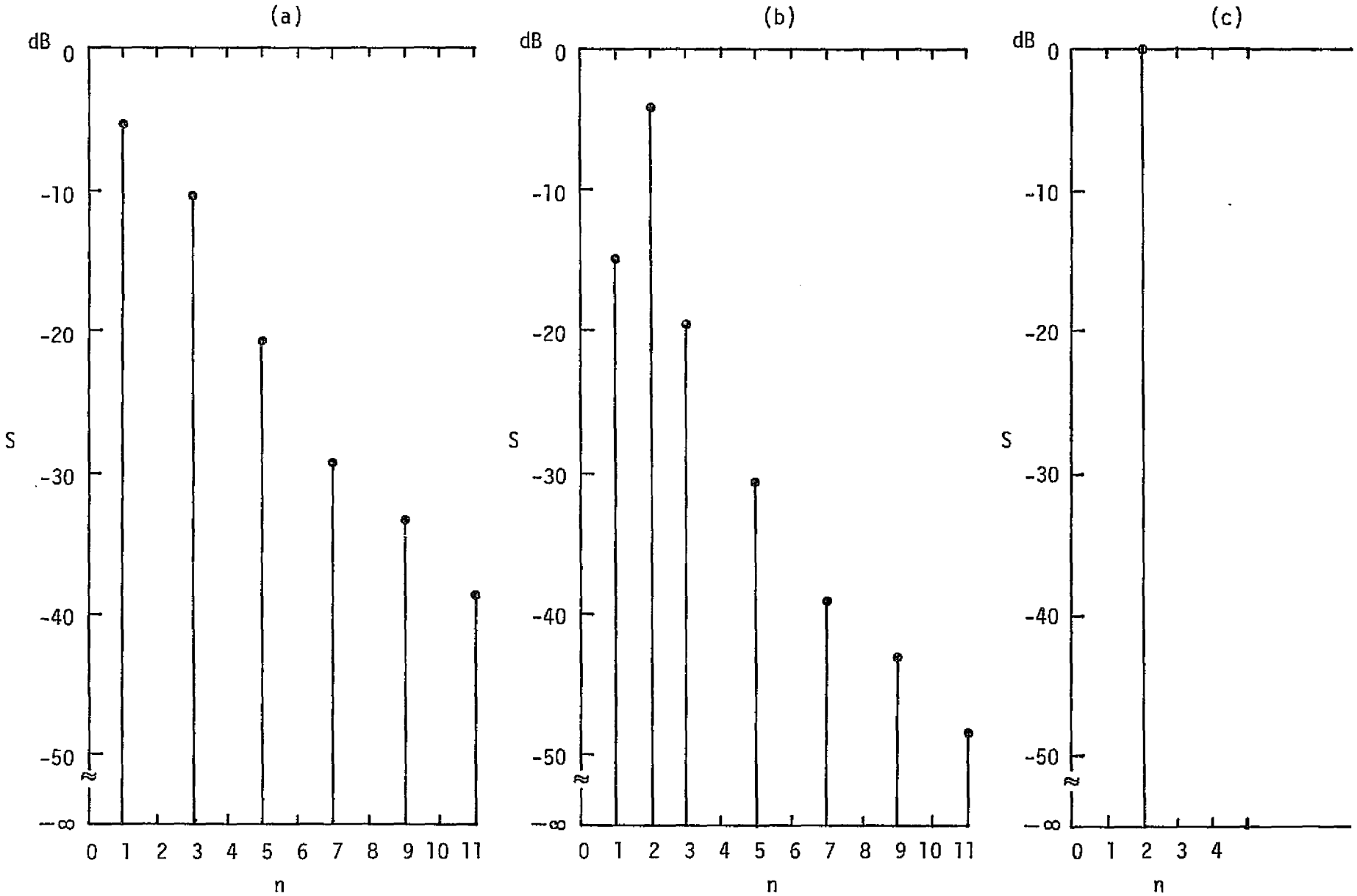

Figure 3. Power Spectrum of Beat Note Relative to Total Power, $\omega_B/\omega_m = 2$

d. $\theta_1 = 3\pi/2$, $\theta_2 = \pi/2$

$$|V_n| = \frac{V_B}{4}; \qquad n = 2 \tag{52}$$

$$|V_n| = 0; \qquad \text{otherwise}. \tag{53}$$

<u>Case 2</u>: $\omega_B/\omega_m = 5$

$$\theta_1 = 10\pi + 2\omega_m T\,\Delta f T - \omega_0 T$$

$$\theta_2 = -15\,\frac{\pi}{2} - 2\omega_m T\,\Delta f T - \omega_0 T \tag{54}$$

a. $\theta_1 = -\pi/4$, $\theta_2 = -3\pi/4$

$$|V_n| = \frac{V_B}{2}\left(\frac{n}{\pi}\right)\frac{1}{|n^2 - 25|}; \qquad n \text{ even} \tag{55}$$

$$|V_n| = \frac{V_B}{2}\,\frac{n^2}{|n^2 - 25|}\left|\frac{2}{\pi n} - \operatorname{sinc}^2(n/2)\right|;$$

$$n \text{ odd}, n \neq 5. \tag{56}$$

b. $\theta_1 = 2\pi$, $\theta_2 = -\pi/2$

$$|V_n| = \frac{V_B}{2}\sqrt{2}\left(\frac{n}{\pi}\right)\frac{1}{|n^2 - 25|}; \qquad n \text{ even} \tag{57}$$

$$|V_n| = \frac{V_B}{2}\sqrt{2}\,\frac{n^2}{|n^2 - 25|}\left|\frac{2}{\pi n} - \operatorname{sinc}^2(n/2)\right|;$$

$$n \text{ odd}, n \neq 5 \tag{58}$$

$$|V_n| = (0.707)\frac{V_B}{4}; \qquad n = 5. \tag{59}$$

c. $\theta_1 = 3\pi/4$, $\theta_2 = -3\pi/4$

$$|V_5| = \frac{V_B}{4} ; \qquad n = 5 \tag{60}$$

$$|V_n| \equiv 0 ; \qquad \text{otherwise} . \tag{61}$$

These three cases are presented in Figure 4 where $V_B = 1$ was assumed and the normalization used in Case 1 of Section 2.4 was also used.

3.0 CONCLUSION

We can see from Figures 3 and 4 that the discrete power spectrum of the beat note v_B goes through three distinct cycles as the target moves; the cycles are:

(1) All the power is in the fundamental component (i.e., $\omega_B/\omega_m = n$).

(2) The power is shared between the fundamental component and its harmonics.

(3) The power is distributed in the harmonics only.

We also note that the spectrum is nonsymmetric; this is due to the small values used for ω_B/ω_m (namely, 2 and 5). For large values of ω_B/ω_m, the spectrum will become symmetric.

REFERENCE:

1. M. Ismail. "A Study of the Double Modulated F.M. Radar," Mitteilungen aus dem Institut fur Hochfrequenztechnik and der Eidgenossischen Technischen Hochschule, Zurich, No. 21.

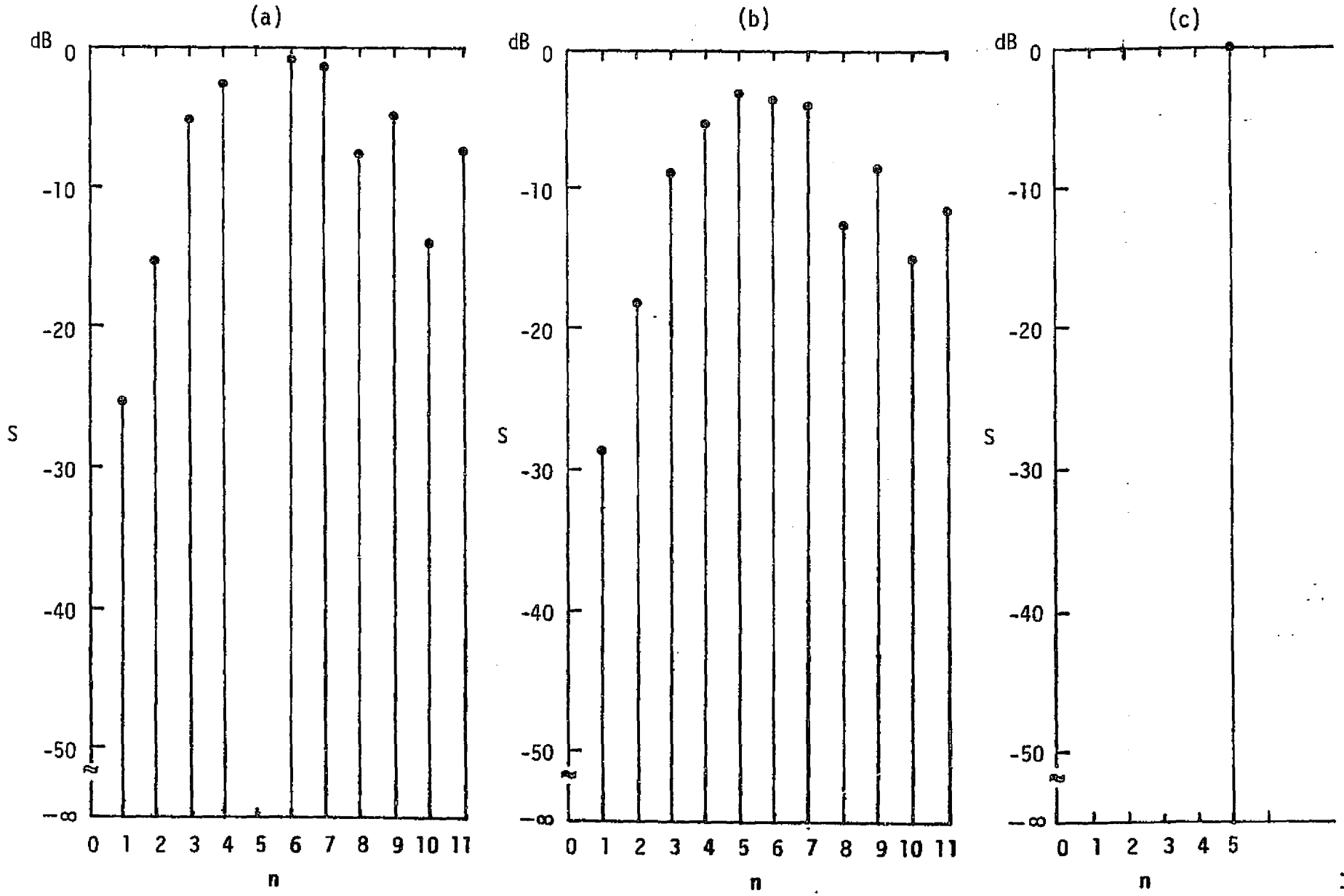

Figure 4. Power Spectrum of Beat Note Relative to Total Power, $\omega_B/\omega_m = 5$

APPENDIX C

TRANSIENT ANALYSIS OF PHASE LOCKED GUNN OSCILLATOR FREQUENCY SOURCE

PRECEDING PAGE BLANK NOT FILMED

APPENDIX C

TRANSIENT ANALYSIS OF PHASE LOCKED GUNN OSCILLATOR FREQUENCY SOURCE

by

Teferi Nessibou

1.0 INTRODUCTION

This appendix investigates the effects of switching a frequency divider on the transient phase error and the estimated frequency output of a Gunn VCO in a phase locked loop (PLL).

2.0 ANALYSIS

In the following analysis, we first consider a second-order loop with filter function

$$F(s) = \frac{1 + 2\zeta s/\omega_n}{1 + sK/\omega_n^2} \tag{1}$$

to derive the exact solution for the loop transient phase error.

The second part of this appendix utilizes the appropriate approximation for a high loop gain.

2.1 System Model

Figure 1 shows the diagram of the phase locked loop considered. The VCO output is mixed and filtered to drive the frequency divider (÷N); the output of the divider is then fed into the loop phase detector to close the loop. The frequency divider operates incrementally in steps of $\Delta\omega$ (which corresponds to a phase ramp).

The linear baseband equivalent model of this system is shown in Figure 2.

2.1.1 Definition of Terms Used

θ_J = loop phase error

θ_N = phase ramp due to divider

θ_T = estimated phase

K_1 = BPF gain

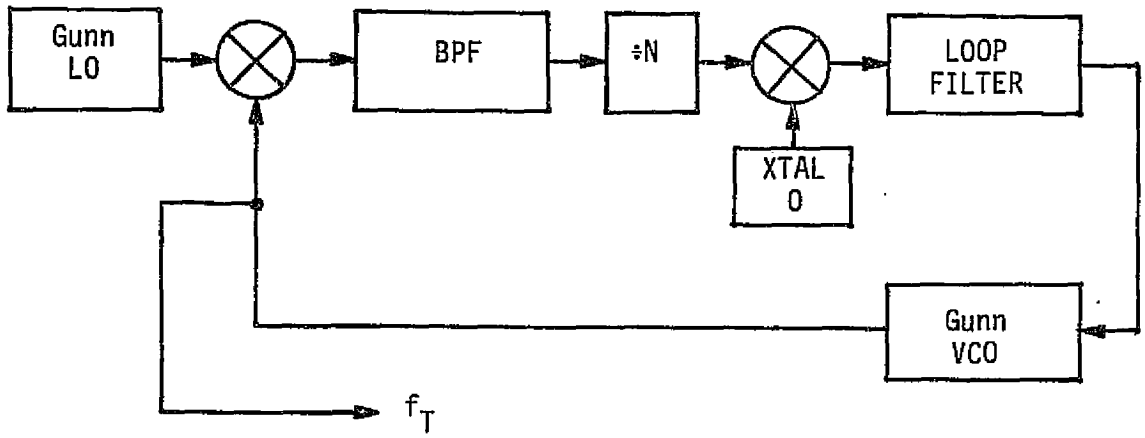

Figure 1. Phase Locked Frequency Source with Frequency Divider

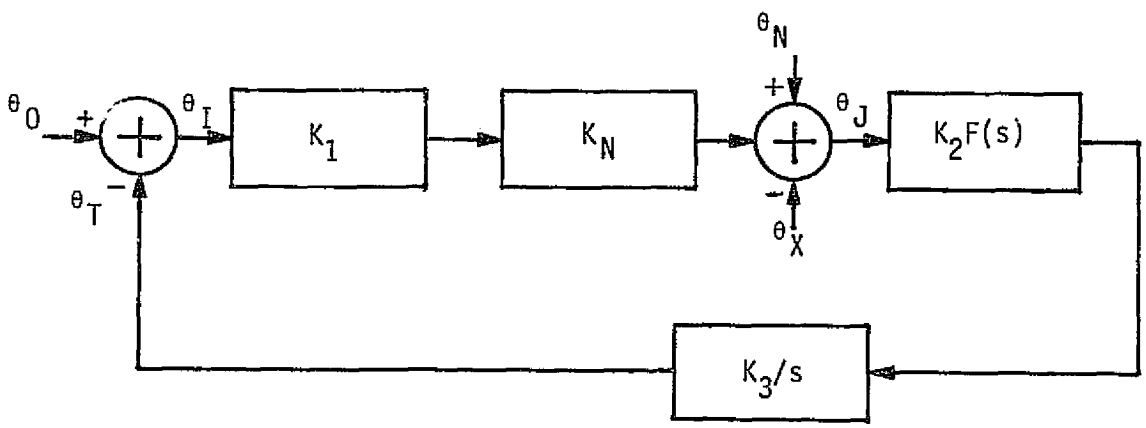

Figure 2. Linear Baseband Equivalent Model

K_N = frequency divider gain

K_2 = loop filter gain

K_3 = VCO gain

$K = K_1K_2K_3K_4$ = loop gain

$F(s)$ = loop filter transfer function

$1/s$ = VCO transfer function

$H(s)$ = closed loop transfer function

ω_n = loop natural frequency

ζ = damping factor

2.2 Transient Phase Error θ_J for a Frequency Step of $\theta_N = \Delta\omega$

Let $\Theta(s)$ be the Laplace transform of θ; then,

$$\frac{\Theta_J(s)}{\Theta_N(s)} = 1 - H(s) ; \tag{2}$$

$$\Theta_J(s) = [1 - H(s)]\,\Theta_N(s) ; \tag{3}$$

where

$$H(s) = \frac{(2\zeta\omega_n - \omega_n^2/K)\, s + \omega_n^2}{s^2 + 2\zeta\omega_n s + \omega_n^2} . \tag{4}$$

A frequency step $\Delta\omega$ can be expressed in operational notation as

$$\Theta_N(s) = \frac{\Delta\omega}{s^2} . \tag{5}$$

Consequently, the phase error becomes

$$\Theta_J(s) = [1 - H(s)]\,\frac{\Delta\omega}{s^2} \tag{6}$$

or, substituting for $H(s)$ and rearranging,

$$\Theta_J(s) = \frac{\Delta\omega}{s^2 + 2\zeta\omega_n s + \omega_n^2} + \left(\frac{\omega_n^2}{K}\right)\frac{\Delta\omega}{s\left(s^2 + 2\zeta\omega_n s + \omega_n^2\right)} \tag{7}$$

Taking the inverse Laplace transform of $\Theta_J(s)$, the transient response is found to be

$$\theta_J(t) = \frac{\Delta\omega}{K} + \frac{\Delta\omega}{\omega_n} e^{-\zeta\omega_n t}\left[\frac{1 - \zeta\omega_n/K}{\sqrt{\zeta^2 - 1}} \sinh\left(\omega_n\sqrt{\zeta^2 - 1}\right)t - \frac{\omega_n}{K}\cosh\left(\omega_n\sqrt{\zeta^2 - 1}\right)t\right]; \quad \zeta > 1 \tag{8}$$

$$\theta_J(t) = \frac{\Delta\omega}{K} + \frac{\Delta\omega}{\omega_n} e^{-\omega_n t}\left(\omega_n t - \frac{\omega_n^2}{K}t - \frac{\omega_n}{K}\right); \quad \zeta = 1 \tag{9}$$

$$\theta_J(t) = \frac{\Delta\omega}{K} + \frac{\Delta\omega}{\omega_n} e^{-\zeta\omega_n t}\left[\frac{1 - \zeta\omega_n/K}{\sqrt{1 - \zeta^2}} \sin\left(\omega_n\sqrt{1 - \zeta^2}\right)t - \frac{\omega_n}{K}\cos\left(\omega_n\sqrt{1 - \zeta^2}\right)t\right]; \quad \zeta < 1 \tag{10}$$

For high loop gain K, these expressions can be approximated by

$$\theta_J(t) = \frac{\Delta\omega}{\omega_n} e^{-\zeta\omega_n t}\left[\frac{\sinh\left(\omega_n\sqrt{\zeta^2 - 1}\right)t}{\sqrt{\zeta^2 - 1}}\right]; \quad \zeta > 1 \tag{11}$$

$$\theta_J(t) = \frac{\Delta\omega}{\omega_n} e^{-\omega_n t}\,\omega_n t; \quad \zeta = 1 \tag{12}$$

$$\theta_J(t) = \frac{\Delta\omega}{\omega_n} e^{-\zeta\omega_n t}\left[\frac{\sin\left(\omega_n\sqrt{1 - \zeta^2}\right)t}{\sqrt{1 - \zeta^2}}\right]; \quad \zeta < 1 \tag{13}$$

The curves representing $(\omega_n/\Delta\omega)\theta_J(t)$ for various values of the damping factor ζ are plotted in Figure 3.

2.3 Transient Frequency Response at the Output of the VCO for a Frequency Step of the Divider (÷N)

Because the loop gain K in our application is very high, we now approximate F(s) and H(s) by the expressions below and derive the time

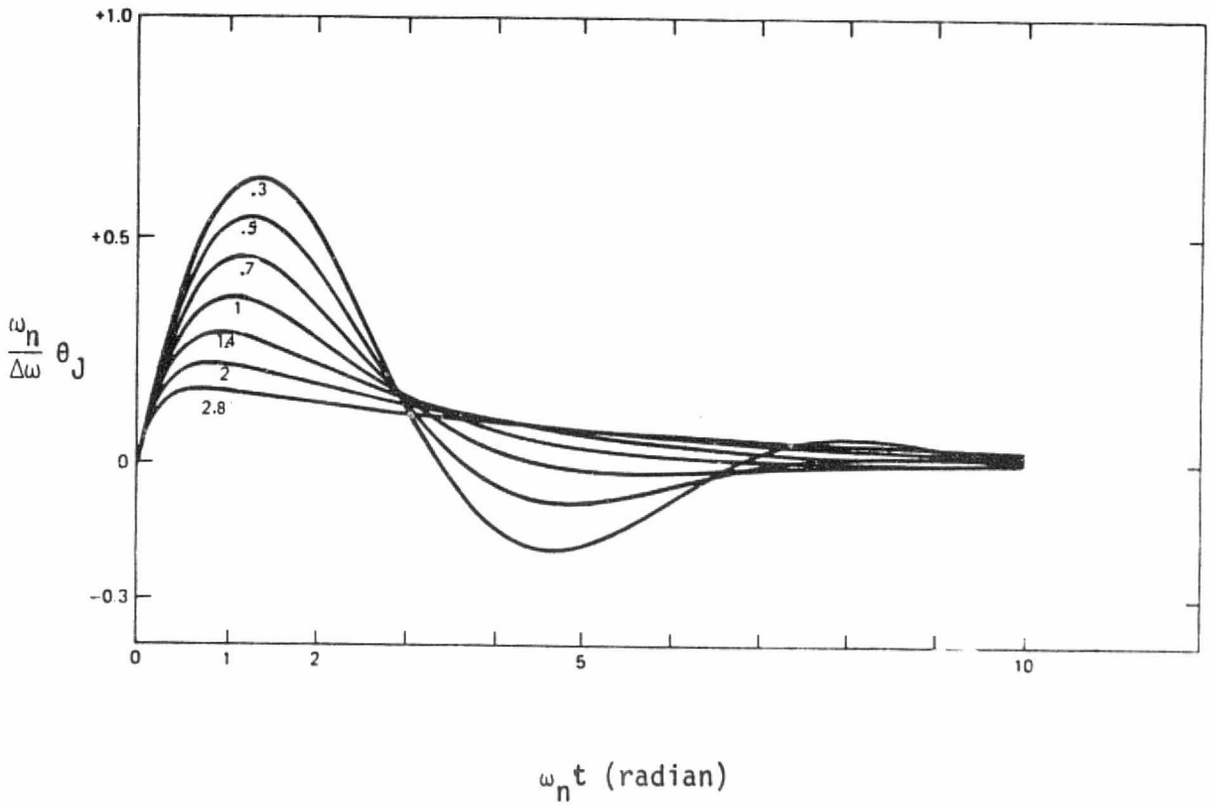

Figure 3. Phase Error for a Frequency Step of the Divider

response of the desired frequency f_T for the case where the damping factor is less than 1:

$$H(s) = \frac{2\zeta\omega_n s + \omega_n^2}{s^2 + 2\zeta\omega_n s + \omega_n^2}; \tag{14}$$

$$F(s) = \frac{1 + 2\zeta s/\omega_n}{sK/\omega_n^2}. \tag{15}$$

From the linear model in Figure 2, we see that

$$\Theta_T(s) = \left[K_2 K_3 \frac{F(s)}{s}\right] \Theta_J(s). \tag{16}$$

The effect of a frequency step on the phase of the desired signal θ_T can then be found by using

$$\Theta_J(s) = [1 - H(s)] \frac{\Delta\omega}{s^2} \tag{17}$$

in the expression of $\theta_T(s)$ above and taking the inverse Laplace transform; thus,

$$\Theta_T(s) = \left[K_2 K_3 \frac{F(s)}{s}\right][1 - H(s)] \frac{\Delta\omega}{s^2}. \tag{18}$$

Substituting for F(s) and H(s) and rearranging, we get

$$\Theta_T(s) = \frac{\Delta\omega}{K_1 K_N} \frac{\omega_n^2}{s^2(s^2 + 2\zeta\omega_n s + \omega_n^2)} + \frac{2\zeta\omega_n}{s(s^2 + 2\zeta\omega_n s + \omega_n^2)} \tag{19}$$

and taking the inverse transform

$$\theta_T(t) = \frac{\Delta\omega}{K_1 K_N}\left[t - \frac{e^{-\zeta\omega_n t}}{\omega_n} \frac{1}{\sqrt{1-\zeta^2}} \sin \omega_n\sqrt{1-\zeta^2}\, t\right]; \quad \zeta < 1. \tag{20}$$

The frequency variation of the transmitted signal is then simply obtained by taking the derivative of $\theta_T(t)$:

$$\frac{d\theta_T(t)}{dt} = f_T(t) ; \tag{21}$$

$$f_T(t) = \frac{\Delta\omega}{K_1 K_N}\left\{1 - e^{-\zeta\omega_n t}\left[\cos\left(\omega_n\sqrt{1-\zeta^2}\right)t - \frac{\zeta}{\sqrt{1-\zeta^2}}\sin\left(\omega_n\sqrt{1-\zeta^2}\right)t\right]\right\} . \tag{22}$$

For the particular value $\zeta = 0.707$, $f_T(t)$ is evaluated to be

$$f_T(t) = \frac{\Delta\omega}{K_1 K_N}\left\{1 - e^{-(0.707)\omega_n t}\left[\cos(0.707)\omega_n t - \sin(0.707)\omega_n t\right]\right\} . \tag{23}$$

Equation (23) normalized by $(K_1 K_N)/\Delta\omega$ is plotted in Figure 4.

3.0 CONCLUSION

An expression for the loop transient phase error for a frequency step of a frequency divider was derived and presented graphically for a second-order phase locked loop with two stages of down-conversion.

An expression for the transient frequency response at the output of the VCO for a frequency step of a frequency divider was also derived.

REFERENCE

1. A. Blanchard. Phase Locked Loops. Wiley, 1976.

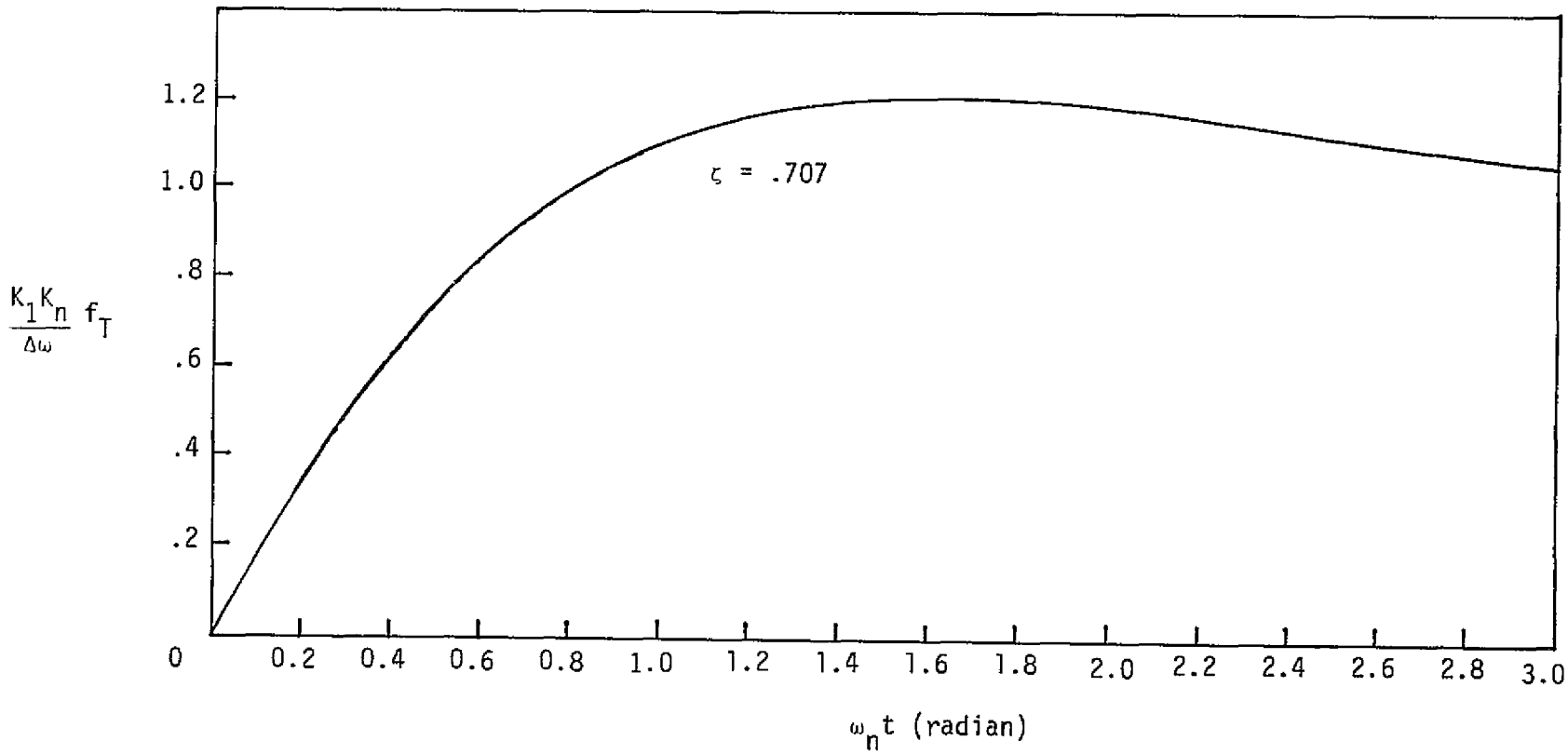

Figure 4. Frequency Change at the VCO Output for a Frequency Step of the Divider

APPENDIX D

THE FREQUENCY SWEEP LINEARITY REQUIREMENTS FOR A LINEARLY-MODULATED FM-CW RANGE MEASURING RADAR

PRECEDING PAGE BLANK NOT FILMED

APPENDIX D

THE FREQUENCY SWEEP LINEARITY REQUIREMENTS FOR A LINEARLY-MODULATED FM-CW RANGE MEASURING RADAR

by

Charles L. Weber

1.0 SUMMARY

The error in frequency estimation that is introduced due to a nonlinear frequency sweep is determined. The exact error is determined for an arbitrary nonlinear frequency sweep. A relatively tight and simple upper bound is also determined that applies to a very large class of nonlinear modulations. This class includes most nonlinear modulations that are of practical interest. Computations involving typical values show that the error that is introduced by a nonlinear frequency sweep is on the order of 0.13%.

Being more precise, the claim is that the average beat frequency is linearly proportional to range, independent of the shape of the instantaneous frequency modulation. In addition, the claim is that the slope is dependent only on the maximum frequency deviation and the observation time. In this appendix, we show the extent to which that is true. In particular, the above claim is true within an error of frequency estimation which is on the order of 0.13% for expected values of the system parameters. To within the same fractional error, the slope is dependent only on the maximum frequency deviation and the observation time.

In general, however, the above claim is not exactly true, but only approximately true, depending upon the extent of nonlinear modulation, averaging time, and range.

2.0 EVALUATION OF ERROR IN FREQUENCY ESTIMATION DUE TO NONLINEAR FREQUENCY SWEEP

The effect on frequency estimation due to thermal noise was determined in [1] for a CW radar, and the effect of phase noise was determined in Appendix A of this report. As a result, in this development, neither thermal noise nor phase noise is considered.

From (5), (7) and (8) of Appendix A, the accumulated phase due to the beat frequency which is proportional to the round-trip time, T_{RT},

to the target, is given by

$$\theta_b(t) \triangleq 2\pi \int_{t_0}^{t} f_i(\tau)\, d\tau - 2\pi \int_{t_0}^{t-T_{RT}} f_i(\tau)\, d\tau$$

$$= 2\pi \int_{t-T_{RT}}^{t} f_i(\tau)\, d\tau \,. \tag{1}$$

The round-trip time, T_{RT}, is assumed to be small with respect to the averaging time, T_{av}, so that the end effects at the beginning and end of the observation interval can be neglected.

The nonlinearities present in the frequency modulation which show up in the beat frequency can be determined from the instantaneous frequency of $\theta_b(t)$. In particular,

$$f_b(t) = \left(\frac{1}{2\pi}\right) \frac{d\theta_b(t)}{dt} = f_i(t) - f_i(t - T_{RT}) \,. \tag{2}$$

As discussed in Appendix A, the frequency counter essentially counts zero crossings for the observation period of T_{av}. This can be modeled analytically by saying that the frequency counter averages $f_b(t)$ for T_{av} sec [Appendix A, Eq. (23)].* Notationally,

$$\hat{f}_b = \frac{1}{T_{av}} \int_0^{T_{av}} [f_i(t) - f_i(t - T_{RT})]\, dt \,. \tag{3}$$

When the instantaneous frequency modulation is ideally linear, $\hat{f}_b$ in (3) reduces to

$$\hat{f}_b = f_b \,, \tag{4}$$

as shown in Appendix A, where the end effects have been neglected.

In order to determine the effects of nonlinear modulation on the estimate of the beat frequency, consider a power series expansion of $f_i(t)$ over the averaging period. In particular,

---

*The doppler frequency shift is neglected for reasons that are discussed in [1] and Appendix A.

$$f_i(t) = \sum_{k=1}^{\infty} a_k \left(\frac{t}{T_{av}}\right)^k ; \qquad 0 \le t \le T_{av} , \tag{5}$$

where

$$a_k = \left[\frac{T_{av}^2}{k!}\right] \left.\frac{d^k f_i(t)}{dt^i}\right|_{t=0}$$

and where the k=0 term is deleted since any constant contribution would be part of the carrier and, as such, would not contribute to any error in frequency estimation. Also, as shown in Figure 2b of Appendix A, the maximum instantaneous frequency deviation in the averaging interval T_{av} is taken to be ΔF. When that restriction is substituted into (5), we see that

$$F_i(T_{av}) = \sum_{k=1}^{\infty} a_k = \Delta F \quad \text{Hz} . \tag{6}$$

When examining the effects of nonlinear instantaneous frequency modulation, we shall consider the set of modulations which can be represented as a power series and whose maximum instantaneous frequency deviation is ΔF.

Upon substitution of the power series representation for $f_i(t)$ in (5) into the model for the frequency counter in (3) and carrying out the indicated integration, we have, after some algebraic simplification:

$$\hat{f}_b = \frac{1}{T_{av}} \int_0^{T_{av}} \sum_{k=1}^{\infty} a_k \left[\left(\frac{t}{T_{av}}\right)^k - \left(\frac{t - T_{RT}}{T_{av}}\right)^k\right] dt$$

$$= - \sum_{k=1}^{\infty} a_k \left[\sum_{\ell=0}^{k-1} \binom{k}{\ell} \left(\frac{1}{\ell+1}\right) \left(\frac{-T_{RT}}{T_{av}}\right)^{k-\ell}\right] . \tag{7}$$

In (7), all of the $\ell = k-1$ terms contribute to the part of $\hat{f}_b$ which is linear in T_{RT}. Removing all of the $\ell = k-1$ terms in the double sum in (7) and using (6),

$$\hat{f}_b = \left(\frac{\Delta F}{T_{RT}}\right)^{T_{RT}} - \sum_{k=2}^{\infty} a_k \left[\sum_{\ell=0}^{k-2} \binom{k}{\ell}\left(\frac{1}{\ell+1}\right)\left(\frac{-T_{RT}}{T_{av}}\right)^{k-\ell}\right]. \tag{8}$$

The contribution to $\hat{f}_b$ due to linear variation in T_{RT} has therefore been separated from the contribution which is nonlinear. Hence, the first term in (7) is considered the signal part or desired part, and the remaining double sum is the distortion due to the nonlinear modulation of $f_i(t)$.

The distortion or error due to the nonlinear modulation is defined as

$$N_F \triangleq -\sum_{k=2}^{\infty} a_k \left[\sum_{j=2}^{k} \binom{k}{j}\left(\frac{1}{k-j+1}\right)\left(\frac{-T_{RT}}{T_{av}}\right)^{j}\right], \tag{9}$$

where we have set $j = k-\ell$ in (8). The distortion varies as $(T_{RT}/T_{av})^2$. This is emphasized by setting $i = j-2$ with the result that

$$N_F = -\sum_{k=2}^{\infty} a_k \left[\left(\frac{T_{RT}}{T_{av}}\right)^2 \sum_{i=0}^{k-2} \binom{k}{i+2}\left(\frac{1}{k-i-1}\right)\left(\frac{-T_{RT}}{T_{av}}\right)^{i}\right]. \tag{10}$$

This can be simplified to

$$N_F = -\sum_{k=2}^{\infty} a_k \left[\left(\frac{T_{RT}}{T_{av}}\right)^2 \left(\frac{1}{k+1}\right) \sum_{i=0}^{k-2} \binom{k+1}{i+2}\left(\frac{-T_{RT}}{T_{av}}\right)^{i}\right]. \tag{11}$$

This is an exact expression for the effect of nonlinear modulation on $\hat{f}_b$. The fractional error can be written as

$$\text{Fractional Error} = \frac{|N_F|}{\left(\frac{\Delta F\ T_{RT}}{T_{av}}\right)}. \tag{12}$$

An approximation to N_F in (11) can be obtained for small (T_{RT}/T_{av}). The approximation is particularly good if the primary contribution of the nonlinear modulation is concentrated in the low values of k. For small T_{RT}/T_{av}, the sum on i in (11) can be approximated by

$$\sum_{i=0}^{k-2} \binom{k+1}{i+2}\left(\frac{-T_{RT}}{T_{av}}\right)^{i} = \binom{k+1}{2} - \binom{k+1}{3}\left(\frac{-T_{RT}}{T_{av}}\right) + \cdots + \binom{k+1}{k}\left(\frac{-T_{RT}}{T_{av}}\right)^{k-2}$$

$$\approx \binom{k+1}{2} \quad \text{for small } T_{RT}/T_{av} . \tag{13}$$

Then the effect of nonlinear modulation can be approximated by

$$N_F \approx \left(\frac{T_{RT}}{T_{av}}\right)^2 \sum_{k=2}^{\infty} \frac{k}{2} a_k . \tag{14}$$

For the applications envisioned in this CW radar, the approximation of N_F in (14) is most satisfactory.

Substituting (14) into (12), the fractional error is approximated by

$$\text{Fractional Error} \approx \left(\frac{T_{RT}}{T_{av}}\right) \frac{1}{2} \frac{\sum_{k=2}^{\infty} k\, a_k}{\Delta F} . \tag{15}$$

Because of the weighting by the factor k, it is seen that the error is more for a higher order nonlinear modulation.

<u>Example 1: Linear FM Only</u>

$$f_i(t) = a_1\left(\frac{t}{T_{av}}\right)$$

$$a_1 = \Delta F$$

$$a_k = 0 , \quad a_k \geq 2$$

$$\hat{f}_b = \Delta F\left(\frac{T_{RT}}{T_{av}}\right) \tag{16}$$

$$\text{Fractional Error} = 0 \tag{17}$$

Example 2: Pure Quadratic FM

$$f_i(t) = a_2\left(\frac{t}{T_{av}}\right)^2$$

$$a_2 = \Delta F$$

$$a_k = 0, \quad k \neq 2$$

$$\hat{f}_b = \Delta F\left(\frac{T_{RT}}{T_{av}}\right) - \Delta F\left(\frac{T_{RT}}{T_{av}}\right)^2 \tag{18}$$

$$\text{Fractional Error} = \frac{T_{RT}}{T_{av}} \tag{19}$$

At a range of $R = 200$ m, $T_{RT} = 13.3$ μsec. If the averaging time is $T_{av} = 10$ msec, then the Fractional Error is approximately 0.00133 or 0.133%. The approximation in (14) and (15) gives the exact answer for Pure Quadratic FM.

Example 3: Pure Fourth-Order FM

$$f_i(t) = (\Delta F)\left(\frac{t}{T_{av}}\right)^4. \tag{20}$$

From (15),

$$\text{Fractional Error} \approx 2\left(\frac{T_{RT}}{T_{av}}\right), \tag{21}$$

which is twice that of Pure Quadratic FM.

REFERENCE

1. "Ranging/Tracking System for Proximity Operations," Axiomatix Technical Proposal for RFP 9-BC73-38-8-48P, May 24, 1978.

APPENDIX E

PHASE NOISE OF A PHASE-LOCKED GUNN OSCILLATOR FREQUENCY SOURCE

PRECEDING PAGE BLANK NOT FILMED

APPENDIX E

PHASE NOISE OF A PHASE-LOCKED GUNN OSCILLATOR FREQUENCY SOURCE

by

Teferi Nessibou

1.0 INTRODUCTION

This appendix presents a relationship between phase noise due to oscillators and phase noise of the estimated phase error in a two-stage phase-locked loop (PLL). This noise is an important factor that affects the measurement accuracy of the reflected signal in the FM CW Radar.

2.0 ANALYSIS

The phase instabilities of the different oscillators are characterized by their respective power spectral density (psd), and the overall phase noise spectra is obtained by adding the individual contributions with appropriate weight (this is true because the phase noise is assumed to be a zero mean, stationary random process uncorrelated with the corresponding frequency output for each source; furthermore, the different noise sources are assumed to be independent). A convenience of this method is that the spectrum is directly measurable.

Consider the system of Figure 1. The system consists of a Gunn local oscillator (LO) with frequency output f_0, a low-frequency stable crystal oscillator (XTAL OSC) with center frequency f_X, a voltage controlled Gunn oscillator (VCO) whose output f_T is the desired frequency for transmission complemented by a bandpass IF filter (BPF) and a loop filter in a PLL configuration.

The three main sources of phase noise in this system are:

1. The LO with phase noise ϕ_{LO} of psd $S_{\phi_{LO}}(f)$.
2. The XTAL OSC with phase noise ϕ_X of psd $S_{\phi_X}(f)$.
3. The VCO with phase noise ϕ_{VCO} of psd $S_{\phi_{VCO}}(f)$.

The noise contributions of the phase detectors are assumed to be negligible.

The analysis begins with the linearized baseband model of Figure 2.

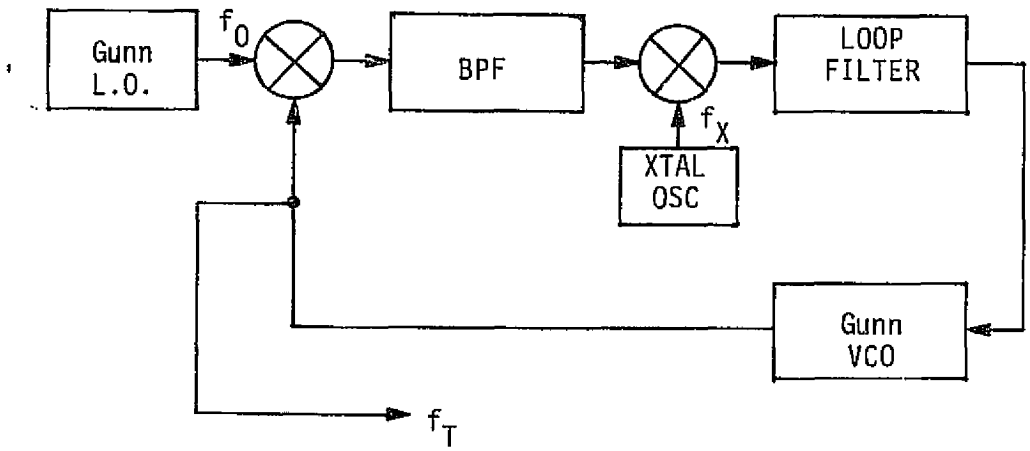

Figure 1. Block Diagram of P. L. Frequency Source

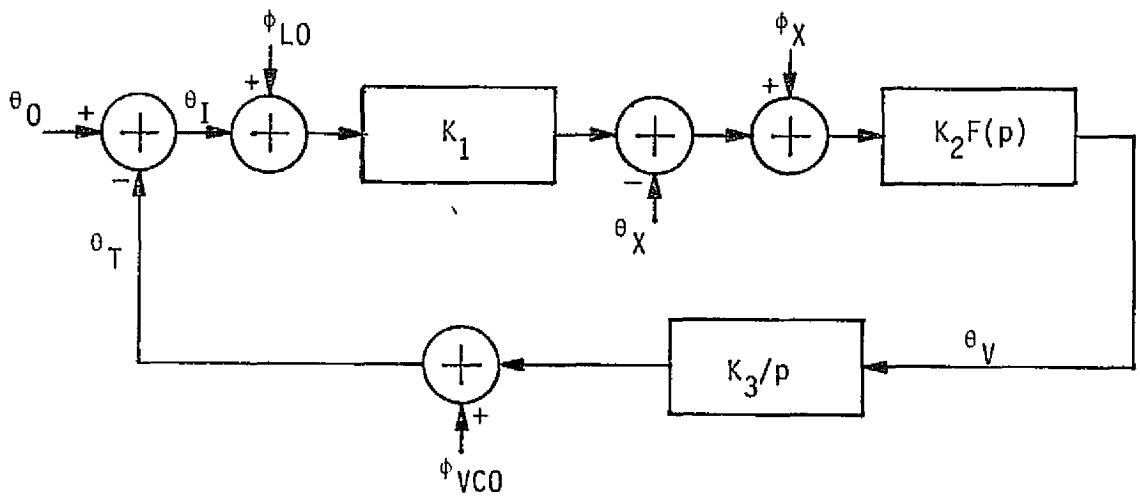

Figure 2. Baseband Equivalent Model

Definition of terms:

θ_0 = phase error due to LO

θ_T = estimated phase error

$\theta_I = \theta_0 - \theta_T$ = 1st IF phase error

θ_X = phase error due to XTAL OSC

θ_V = phase error at VCO input

K_1 = BPF gain

K_2 = Loop Filter gain

K_3 = VCO gain

$F(p)$ = Loop Filter transfer function

$\frac{1}{p}$ = VCO transfer function

Let $\Theta(p)$ and $\Phi(p)$ denote the transform of the corresponding θ and ϕ processes obtained by applying the Heaviside operator $p = d/dt$.

We then have,

$$\Theta_I(p) = \Theta_0(p) - \Theta_T(p) \tag{1}$$

$$\Theta_V(p) = \left\{\left[\Theta_0(p) - \Theta_T(p) + \Phi_{LO}(p)\right]K_1 - \Theta_X(p) + \Phi_X(p)\right\} K_2\, F(p) \tag{2}$$

$$\Theta_T(p) = \Theta_V(p)\,\frac{K_3}{p} + \Phi_{VCO}(p) \tag{3}$$

Substituting for $\Theta_V(p)$ in (3), we get

$$\Theta_T(p) = \left\{\left[\Phi_0(p) - \Theta_T(p) + \Phi_{LO}(p)\right]K_1 - \Theta_X(p) + \Phi_X(p)\right\} K_2K_3F(p) + \Phi_{VCO}(p) \tag{4}$$

Expanding the right-hand side of the above equation, we have

$$\begin{aligned}\Theta_T(p) = {} & \Theta_0(p)\, K_1K_2K_3\,\frac{F(p)}{p} - \Theta_T(p)\, K_1K_2K_3\,\frac{F(p)}{p} \\ & + \Phi_{LO}(p)\, K_1K_2K_3\,\frac{F(p)}{p} - \Theta_X(p)\, K_2K_3\,\frac{F(p)}{p} \\ & + \Phi_X(p)\, K_2K_3\,\frac{F(p)}{p} + \Phi_{VCO}(p)\end{aligned} \tag{5}$$

Solving for $\Theta_T(p)$, we get

$$\Theta_T(p) = \frac{\left[\Theta_0(p) + \Phi_{LO}(p)\right] K_1K_2K_3 \frac{F(p)}{p} + \left[\Theta_X(p) - \Phi_X(p)\right] K_2K_3 \frac{F(p)}{p} + \Phi_{VCO}(p)}{1 + K_1K_2K_3 \frac{F(p)}{p}} \tag{6}$$

Letting $p = j\omega$ and $K_1K_2K_3 = K$

$$\Theta_T(j\omega) = \frac{\left[\Theta_0(j\omega) + \Phi_{LO}(j\omega)\right] \frac{KF(j\omega)}{j\omega} + \left[\Phi_X(j\omega) - \Theta_X(j\omega)\right] K_2K_3 \frac{F(j\omega)}{j\omega} + \Phi_{VCO}(j\omega)}{1 + K \frac{F(j\omega)}{j\omega}} \tag{7}$$

The power spectral density of the process θ_T is given by

$$S_{\theta_T}(f) = \frac{1}{2\pi}\left|\Theta_T(j\omega)\right|^2 \tag{8}$$

Therefore, evaluating $S_{\theta_T}(f)$ for (7) will yield the desired relationship between the psd's.

Taking the magnitude squared of the right-hand side of (7) and dividing by 2π, we get

$$\frac{1}{2\pi}\left|\left[\Theta_0(j\omega) + \Phi_{LO}(j\omega)\right] \frac{KF(j\omega)}{j\omega+KF(j\omega)} + \left[\Phi_X(j\omega) - \Theta_X(j\omega)\right] \frac{K_2K_3F(j\omega)}{j\omega+KF(j\omega)} + \Phi_{VCO}(j\omega) \frac{j\omega}{j\omega+KF(j\omega)}\right|^2 \tag{9}$$

Let's consider the first term of (9) in the form

$$\frac{1}{2\pi}\left|\left[\Theta_0(j\omega) + \Phi_{LO}(j\omega)\right] \frac{KF(j\omega)}{j\omega+KF(j\omega)}\right|^2 \tag{10}$$

The expression inside the absolute values can be regarded as the transform of a signal plus noise $Z(j\omega)$ passed through a filter with transfer function

$$G_1(j\omega)$$

such that

$$Z(j\omega)\ G_1(j\omega) = Y_1(j\omega)$$

where

$$Z(j\omega) = \Theta_0(j\omega) + \Phi_{LO}(j\omega)$$

and

$$G_1(j\omega) = \frac{KF(j\omega)}{j\omega + KF(j\omega)}$$

Therefore, (10) can be written from (8)

$$\frac{1}{2\pi}\left|Y_1(j\omega)\right|^2 = S_{Y_1}(f)$$

We also know that

$$S_{Y_1}(f) = \left|G_1(j\omega)\right|^2 S_Z(f)$$

Since θ_0 and ϕ_0 are uncorrelated processes, the cross-spectral densities are zero. Thus,

$$S_Z(f) = S_{\theta_0}(f) + S_{\phi_{LO}}(f)$$

and

$$S_{Y_1}(f) = \left|G_1(j\omega)\right|^2 \left[S_{\theta_0}(f) + S_{\Phi_{LO}}(f)\right] \tag{11}$$

Similarly, the second term of (9) will have a psd

$$S_{Y_2}(f) = \left|G_2(j\omega)\right|^2 \left[S_{\theta_X}(f) + S_{\phi_X}(f)\right] \tag{12}$$

where

$$G_2(j\omega) = \frac{K_2K_3\ F(j\omega)}{j\omega + KF(j\omega)}$$

and the third term of (9) has a psd

$$S_{Y_3}(f) = \left|G_3(j\omega)\right|^2 S_{\phi_{VCO}}(f) \tag{13}$$

with

$$G_3(j\omega) = \frac{j\omega}{j\omega + KF(j\omega)}$$

Since the three noise sources are assumed to be independent, the cross-products of (9) have no contribution to the overall phase noise. The psd of the θ_T process is then the sum of (11), (12) and (13).

$$S_{\phi_T}(f) = S_{Y_1}(f) + S_{Y_2}(f) + S_{Y_3}(f) \tag{14}$$

The phase noise psd due to the three oscillators is therefore

$$S_{\phi_T}(f) = S_{\phi_{LO}}(f) \left|G_1(j\omega)\right|^2 + S_{\phi_X}(f) \left|G_2(j\omega)\right|^2 + S_{\phi_{VCO}}(f) \left|G_3(j\omega)\right|^2 \tag{15}$$

The closed loop transfer function of the system in Figure 1 is given by

$$H(j\omega) = \frac{KF(j\omega)}{j\omega + KF(j\omega)} \tag{16}$$

This function is related to the loop noise bandwidth by

$$2B_L = \frac{1}{2\pi} \int_{-\infty}^{\infty} |H(j\omega)|^2 \, d\omega \tag{17}$$

Noting that $G_1(j\omega) = H(j\omega)$

$$G_1(j\omega) = \frac{1}{K_1} H(j\omega)$$

and

$$G_3(j\omega) = 1 - H(j\omega)$$

(15) can be rewritten as

$$S_{\phi_T}(f) = S_{\phi_{LO}}(f) \left|H(j\omega)\right|^2 + S_{\phi_X}(f) \left|\frac{1}{K_1} H(j\omega)\right|^2 + S_{\phi_{VCO}}(f) \left|1 - H(j\omega)\right|^2 \tag{18}$$

From (18), we see that, while the phase noise contributions of the reference oscillators to the overall phase noise of the transmitted signal are lowpass filtered, that of the VCO is highpass filtered. This implies that, since the VCO is a low Q device and thus relatively noisy,

the low-frequency content of its noise spectrum will be filtered out and the phase noise performance of the system will be primarily controlled by the noise of the fixed oscillators. Since the Gunn local oscillator is fixed frequency, it can be high Q and thus contribute less noise. Figure 3 shows a typical phase noise spectra.

3.0 CONCLUSION

The effects of oscillators (fixed and variable) phase noise on the phase noise of the estimated phase in a PLL configuration and the relationship of the spectra of this noise process to the loop noise bandwidth was hown.

Since

$$\sigma^2_{\phi_T} = \frac{1}{2\pi}\int_{-\infty}^{\infty} S_{\phi_T}(j\omega)\, d\omega ,$$

the mean-squared phase error can also be determined from the phase noise psd of (18).

REFERENCES

1. W. C. Lindsey. Synchronization Systems in Communication and Control, Prentice Hall, 1972.

2. A. Papoulis. Probability, Random Variables and Stochastic Processes, McGraw Hill, 1965.

3. G. K. Huth. "Effects of Phase Noise on the Performance of 2-Way Coherent Communication Links," Appendix D, Axiomatix Report No. R7607-3, July 31, 1976.

4. W. C. Lindsey and J. L. Lewis. "Modeling, Characterization and Measurement of Oscillator Instabilities," CDRL Item No. 5020, Lincom Corp., Pasadena, California, and TRW, Redondo Beach, California, June 14, 1974.

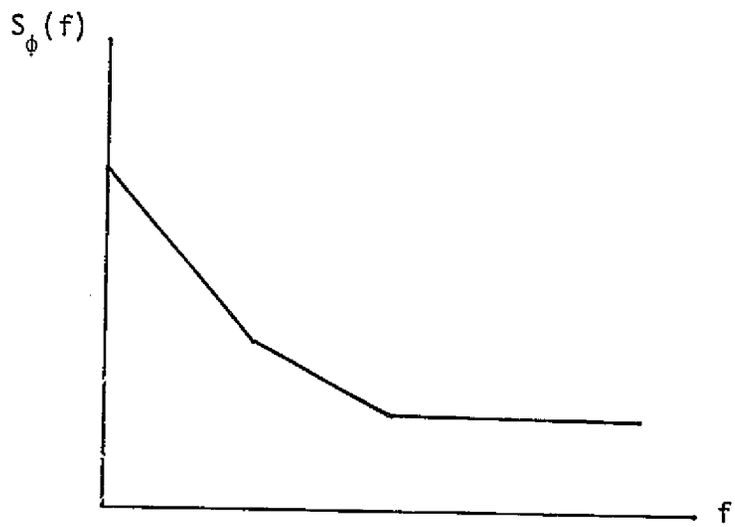

Figure 3. Typical Transmitter Phase Noise Spectra

APPENDIX F

EXPERIMENTAL VERIFICATION OF LOW-VELOCITY MEASUREMENT WITH CW K-BAND RADAR

PRECEDING PAGE BLANK NOT FILMED

APPENDIX F

EXPERIMENTAL VERIFICATION OF LOW-VELOCITY MEASUREMENT WITH CW K-BAND RADAR

by

Peter Nilsen
Sergei Udalov

As part of the Phase I contractual effort, Axiomatix conducted laboratory tests to assess the potential of low-velocity measurement capability for CW K-band, homodyne radar. Kustom Electronics, under subcontract to Axiomatix, modified a hand-held police velocity radar so that it would measure velocities lower than those for which it was originally designed. The radar used for the experiment operates nominally at 24 GHz.

Figure 1 is a photograph of the laboratory setup and Figure 2 shows a functional block diagram of the setup. The radar target consisted of a 0.1 square meter (radar cross-section) corner reflector mounted on a linear motion carriage. The doppler frequency was measured with a counter, and an averaging time of 10 sec was used to provide a frequency resolution of 0.1 Hz. The quality of the doppler data was determined by monitoring the doppler waveform on the oscilloscope.

Table 1 shows the measured doppler data for three typical runs. The experimental average measured velocity was 0.02 m/sec (0.06 ft/sec) and the experimental standard deviation was 0.001 m/sec (0.003 ft/sec). The actual velocity of the carriage, as measured independently of the radar, was 0.063 ft/sec, which is consistent with $\sigma = 0.003$ ft/sec.

The lowest velocity measured by Axiomatix was 0.06 ft/sec. Below this, erratic readings were obtained. This was attributed to multipath effects and the fact that the radar amplifier gains were not tailored for low frequencies and, therefore, their roll-off severely attenuated the very low frequencies. The Phase II breadboard will be designed to avoid this problem.

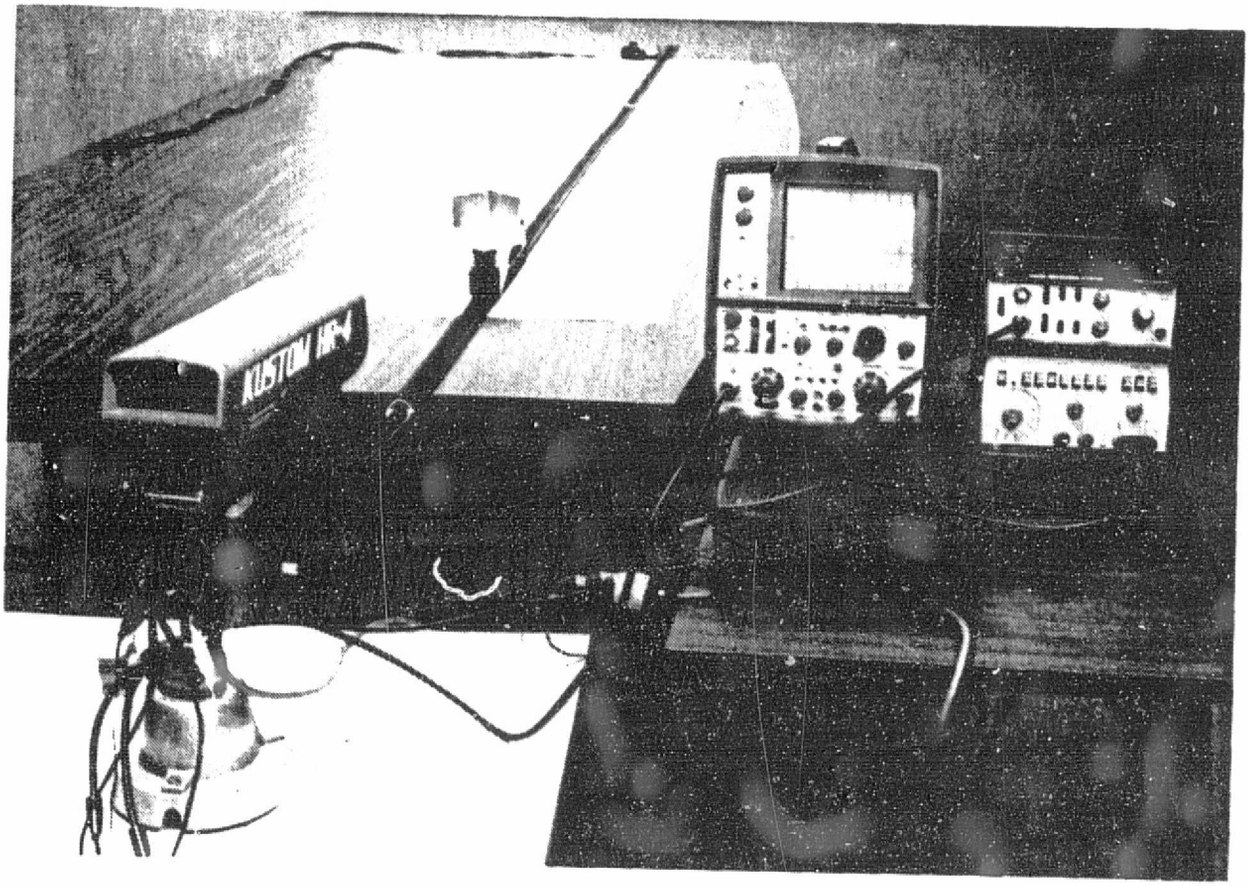

Figure 1. Experimental Test Laboratory Setup

ORIGINAL PAGE IS
OF POOR QUALITY

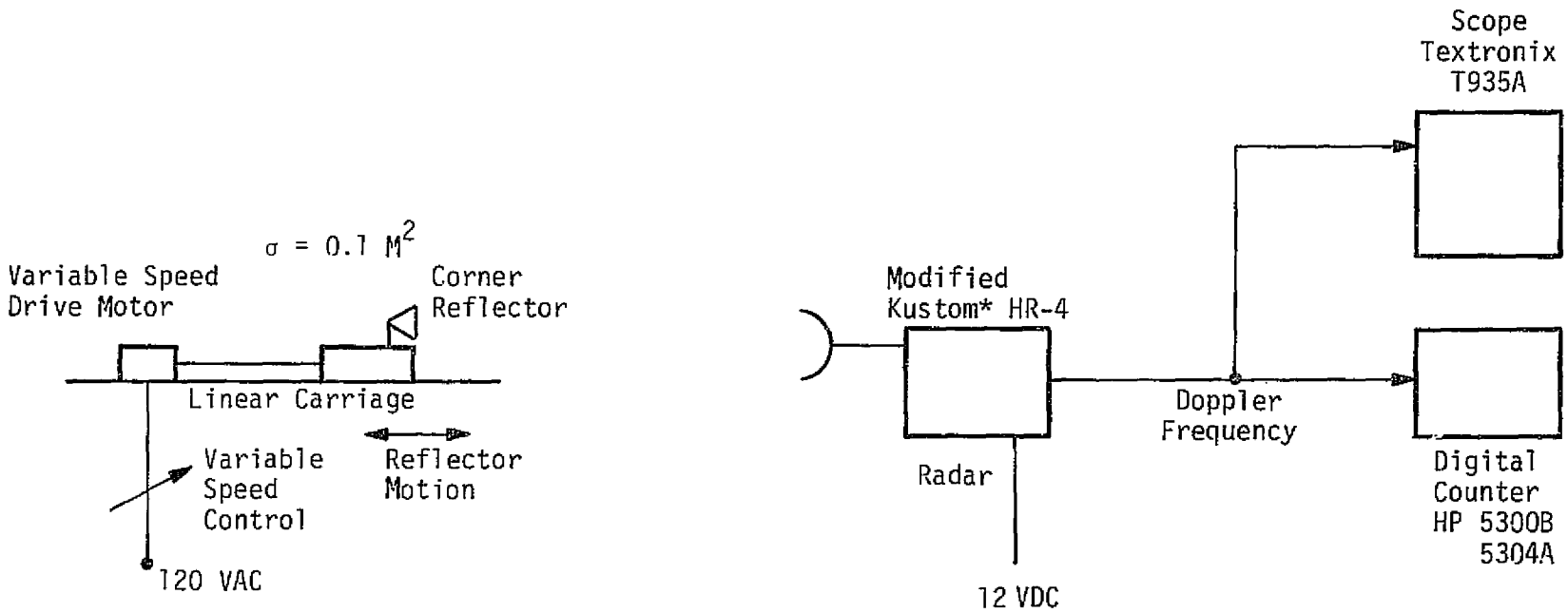

Figure 2. Experimental Test Block Diagram

*Kustom Electronics

Table 1. Experimental Test Data*

Measured Doppler (Hz)		
Run 1	Run 2	Run 3
3.2	3.0	3.5
3.5	3.3	3.3
3.2	3.6	3.0

$$\overline{V} = 0.06 \text{ ft/sec*}$$

$$\sigma_V = 0.003 \text{ ft/sec}$$

$$V_{actual} = 0.063 \text{ ft/sec}$$

*Radar frequency, f_0 = 24.150 GHz

APPENDIX G

PERFORMANCE GOAL SPECIFICATION FOR PHASE II BREADBOARD

PRECEDING PAGE BLANK NOT FILMED

APPENDIX G

PERFORMANCE GOAL SPECIFICATION FOR PHASE II BREADBOARD

The following specifications are performance goals for the Phase II breadboard. It is expected that, at the conclusion of Phase II testing, a specification for an engineering prototype will be generated.

1.0 Target Size: The radar shall meet the performance goals specified herein with a point target having a radar cross-section of 10 square meters.

2.0 Acquisition Performance: The acquisition performance shall be met for a target size given in Section 1.0 and over a range and velocity given in Sections 3.0 and 4.0.

2.1 Probability of Detection within acquisition time specified in Section 2.3: $P_d = 0.90$.

2.2 False Alarm Rate: Not greater than once every 15 minutes.

2.3 Acquisition Time: $T_{acq} < 30$ seconds.

3.0 Range: The performance specified herein shall be met over the range of 0.2 meters (2/3 ft) to 1850 meters (6000 ft).

4.0 Velocity: The performance specified herein shall be met over the velocity range of -0.01 m/sec (-0.03 ft/sec) to -6.1 m/sec (-20 ft/sec) and +0.01 m/sec (+0.03 ft/sec) to +6.1 m/sec (+20 ft/sec).

5.0 Acceleration: The accuracies specified in Section 6.0 shall be met for target accelerations up to ± 1.0 m/sec^2 (3.28 ft/sec^2).

6.0 Measurement Accuracy

6.1 Range Accuracy: $3\sigma = 1$ m (3.28 ft) at the range specified in Section 3.0 and $3\sigma = 0.61$ m (2 ft) at a maximum range of 1200 m (3936 ft).

6.2 Velocity: $3\sigma = 0.03$ cm/sec (1.0 ft/sec)

7.0 Pointing Accuracy: The performance specified herein shall be met with the radar pointed to within $\pm 1/2$ degree of the target.

8.0 Data Output

8.1 Update Interval: Normal mode, once per second. Station-keeping mode, once per 10 seconds.

8.2 Data Display: Range--The display characters shall be in tenths of feet, units of feet, tens of feet, hundreds of feet, and thousands of feet. Range Rate--The display characters shall be in

hundredths of feet per second, tenths of feet per second, units of feet per second, and tens of feet per second. A plus sign shall indicate closing relative target motion, and a minus sign shall indicate opening relative target motion.

8.3 Data Good Signal: A data good signal shall be provided for each measurement of each parameter. The signal shall indicate that the quality of the parameter is suitable for use.

9.0 System Characteristics

9.1 Operating Frequency--24 GHz.

9.2 Polarization--Circular.

9.3 Antenna--Type: Horn; Beamwidth (conical angle, 3 dB): 12°; Gain: 25 dB; Scan: Manual.

9.4 Transmitter Characteristics--Average Power: 200 mW.

9.5 Frequency Stability--(Long-term and temperature): $\pm 2.5 \times 10^3$, ($\Delta f = \pm 50$ MHz at 24 GHz).

9.6 Receiver Characteristics--Receiver type: Homodyne (zero IF); Receiver noise figure: 22 dB at 1 kHz (for details, see Figure 10 of Section 2.1).

10.0 Frequency Modulation Program

10.1 Modulation Format--Linear FM-CW.

10.2 Deviation (ΔF)--100 MHz p-p.

10.3 Repetition Frequency--$R < 500$ m: 12 Hz; $500 \text{ m} < R < 1850$ m: 3 Hz.

10.4 Modulation Slope--$R < 500$ m: 2400 MHz/sec; $500 \text{ m} < R < 1850$ m: 600 MHz/sec.

APPENDIX H

BIBLIOGRAPHY

PRECEDING PAGE BLANK NOT FILMED

APPENDIX H

BIBLIOGRAPHY

by

Sergei Udalov

In carrying out Phase I of the study to define a design for a Ranging and Tracking System for Proximity Operations, Axiomatix personnel conducted a literature search to determine if any of the existing and latest techniques could be applied to the implementation of the system. Presented below are the references considered. These references are organized according to the appropriate categories.

A. FM RADAR MODULATION AND RELATED SUBJECTS

1. S. R. J. Axelson. "Area Target Response of Triangularly Frequency-Modulated Continuous-Wave Radar," IEEE Transactions on Aerospace and Electronics, Vol. AES-14, No. 2, March 1978, pp. 266-277.

2. R. D. Davies and J. D. Meidl. "Delay Generation Offset: A Direction Sensitive Pulse-Coherent Doppler Detection Technique," IEEE Transactions on Aerospace and Electronics, Vol. AES-13, No. 4, July 1977, pp. 430-433.

3. B. G. Mattox and L. W. Couch. "Synthesis of Short-Range FM Radars With General Modulations," IEEE Transactions on Communications, Vol. COM-24, No. 1, January 1976, pp. 11-19.

4. L. W. Couch. "Effect of Modulation Nonlinearity on the Response of FM Radars," IEEE Transactions on Aerospace and Electronics, Vol. AES-9, July 1973, pp. 598-606.

5. G. A. McAlpine, J. F. Damman, and J. C. Highfill. "Post Mixer Spectra of Periodic FM Altimeters With Area Returns," IEEE Transactions on Aerospace and Electronic Systems, Vol. A, September 1971, pp. 932-940.

6. A. J. Hymans and J. Lait. "Analysis of a Frequency-Modulated Continuous-Wave Ranging System," Proceedings of the IEEE, Paper No. 3264E, July 1960, pp. 365-372.

7. A. W. Rihaczek and R. L. Mitchell. "Design of Zigzag FM Signals," IEEE Transactions on Aerospace and Electronic Systems, Vol. AES-4, No. 5, September 1968, pp. 680-692.

8. W. Fishein and O. E. Rittenbach. "Modulation Waveforms for Continuous Wave Radar," The Record of the IEEE 1975 International Radar Conference, Arlington, Virginia, April 21-23, 1975, pp. 192-197.

B. FM-CW RADAR DOPPLER TECHNIQUES

1. M. A. W. Ismail. "A Study of the Double Modulated F.M. Radar," Inst. Hochfrequenztech. an der E.T.H. Rept. 21, Verlag Leeman, Zurich, 1955.

2. M. A. W. Ismail. "A Precise New System of FM Radar," Proceedings of the IRE, Vol. 44, September 1956, pp. 1140-1145.

3. K. C. M. Glegg. "A Low Noise CW Doppler Technique," National Conference on Aeronautical Electronics (Dayton, Ohio), 1958, pp. 133-144.

4. N. D. Wallace. "Performance Prediction Method for a Class of FM-CW Radars," IEEE Transactions on Aerospace and Naval Electronics, Vol. AES-2, March 1964, pp. 36-44.

5. M. J. Withers. "Matched Filter for Frequency-Modulated Continuous-Wave Radar Systems," Proceedings of the IEEE, Vol. 113, No. 3, March 1966.

6. B. S. Rao. "Extending the Range of a Frequency-Modulated Altimeter," IEEE Transactions on Aerospace and Electronic Systems, Vol. AES-5, No. 5, May 1967, pp. 579-580.

C. DOPPLER VELOCITY MEASUREMENT AND NAVIGATION SYSTEMS

1. F. B. Berger. "The Nature of Doppler Velocity Measurement," IRE Transactions on Aeronautics and Navigation Electronics, Vol. ANE-4, September 1957, pp. 103-112.

2. F. B. Berger. "The Design of Airborne Doppler Velocity Measuring Systems," IRE Transactions on Aeronautics and Navigation Electronics, Vol. ANE-4, December 1957, pp. 157-175.

3. W. R. Freed. "Principles and Performance Analysis of Doppler Navigation Systems," IRE Transactions on Aeronautics and Navigation Electronics, Vol. ANE-4, December 1957, pp. 176-196.

4. M. A. Condie. "Basic Design Considerations - Automatic Navigator AN/APN-67," IRE Transactions on Aeronautics and Navigation Electronics, Vol. ANE-4, December 1957, pp. 197-201.

5. F. A. McMahon. "The AN/APN-81 Doppler Navigation Sytem," IRE Transactions on Aeronautics and Navigation Electronics, Vol. ANE-4, December 1957, pp. 202-211.

D. FREQUENCY MEASUREMENT AND TRACKING

1. W. W. H. Clarke and R. F. Nikkel. "Mean Frequency Determination of Narrow-Band Noise Spectra," Proceedings of the IEEE, Paper N-. 1836M, May 1955, pp. 364-370.

2. L. Ehrman. "Analysis of Zero-Crossing Frequency Discriminator with Random Inputs," IEEE Transactions on Aerospace and Navigation Electronics, Vol. ANE-12, No. 2, June 1965, pp. 113-119.

3. B. E. Keiser. "Digital Counter Techniques Increase Doppler Uses," Electronics, May 22, 1959, pp. 46-50.

4. J. A. Develet, Jr. "Fundamental Accuracy Limitations in a Two-Way Coherent Doppler Measurement System," IRE Transactions on Space Electronics and Telemetry, September 1961, pp. 80-85.

E. SPECIAL RADAR TECHNIQUES

1. F. J. O'Hara and G. M. Moore. "A High Performance CW Receiver Using Feed-Through Nulling," Microwave Journal, Vol. 6, September 1965, pp. 63-71.

2. S. E. Craig, W. Fishbein, and O. E. Rittenback. "Continuous-Wave Radar with High Range Resolution and Unambiguous Velocity Determination," IRE Transactions, Vol. MIL-6, April 1962, pp. 153-161.

3. O. K. Nilssen and W. D. Boyer. "Amplitude Modulated CW Radar," IRE Transactions, Vol. ANE-9, December 1962, pp. 250-254.

4. O. K. Nilssen. "New Methods of Range Measuring Doppler Radar," IRE Transactions, Vol. ANE-9, December 1962, pp. 255-265.

F. VELOCITY DIRECTION SENSING

1. H. P. Kalmus. "Direction Sensitive Doppler Device," Proceedings of the IRE, Vol. 45, June 1955, pp. 689-700.

2. S. H. Logue. "Rate-of-Climb Meter Uses Doppler Radar," Electronics, June 1, 1957, pp. 150-152.

G. CRYSTAL MIXER NOISE AND RELATED PHENOMENA

1. J. C. Greene and J. F. Lyons. "Receivers with Zero Intermediate Frequency," Proceedings of the IRE, Vol. 47, February 1959, pp. 335-336.

2. C. B. Andrews and H. A. Bazydlo. "Crystal Noise Effects on Zero IF Receiver," Proceedings of the IRE, Vol. 47, February 1959, pp. 2018-2019.

3. Hewlett-Packard. "X-Band Doppler Radar Modules," HP Technical Data Brochure, November 1971.

H. GENERAL BACKGROUND

1. W. K. Saunders. "Post-War Developments in Continuous-Wave and Frequency Modulated Radar," IRE Transactions, Vol. ANE-8, March 1961, pp. 7-19; October 1961, p. 105.

2. News Release. "FM, CW Radar Tested for Use in Space Link-Up," Electronic Design, December 20, 1963.

3. D. Mennie. "Helping Speeders Beat the Radar Rap," IEEE Spectrum, August 1978, pp. 38-42.

4. D. M. Grimes and T. O. Jones. "Automotive Radar: A Brief Review," Proceedings of the IEEE, Vol. 62, No. 6, June 1974, pp. 804-822.

I. BOOKS

1. M. I. Skolnik. Radar Design Principles. New York: McGraw-Hill, 1969.

2. M. I. Skolnik. Radar Handbook. New York: McGraw-Hill, 1970.

3. A. Blanchard. Phase-Locked Loops: Application to Coherent Receiver Design. New York: John Wiley & Sons, Inc., 1976.

4. F. M. Gardner. Phaselock Techniques. New York: John Wiley & Sons, Inc., 1966.

5. D. G. C. Luck. Frequency Modulated Radar. New York: McGraw-Hill, 1959.

6. L. N. Ridenour (ed.). Radar System Engineering. MIT Radiation Laboratory Series, Vol. 1. New York: McGraw-Hill, 1947.

7. D. K. Barton. Radar System Analysis. New York: Prentice-Hall, 1964.

8. D. K. Barton and H. R. Ward. Handbook of Radar Measurement. New York: Prentice-Hall, 1969.

9. R. S. Berkowitz. Modern Radar. New York: John Wiley & Sons, 1965.

10. S. A. Haronessian. Radar Detection and Tracking Systems. Dendham, Mass.: Artech House, Inc., 1973.

11. F. E. Nathanson. Radar Design Principles. New York: McGraw-Hill, 1969.